MARTIN MARIETTA ENERGY SYSTEMS LIBRARIES
3 4456 0361550 4

CENTRAL RESEARCH LIBRARY
DOCUMENT COLLECTION

1 of 6

ORNL-3011
UC-20 - Controlled Thermonuclear Processes

THERMONUCLEAR PROJECT

SEMIANNUAL PROGRESS REPORT

FOR PERIOD ENDING JULY 31, 1960

CENTRAL RESEARCH LIBRARY
DOCUMENT COLLECTION
LIBRARY LOAN COPY
DO NOT TRANSFER TO ANOTHER PERSON
If you wish someone else to see this document, send in name with document and the library will arrange a loan.

OAK RIDGE NATIONAL LABORATORY
operated by
UNION CARBIDE CORPORATION
for the
U.S. ATOMIC ENERGY COMMISSION

Printed in USA. Price $2.75. Available from the

Office of Technical Services
Department of Commerce
Washington 25, D.C.

LEGAL NOTICE

This report was prepared as an account of Government sponsored work. Neither the United States, nor the Commission, nor any person acting on behalf of the Commission:

A. Makes any warranty or representation, expressed or implied, with respect to the accuracy, completeness, or usefulness of the information contained in this report, or that the use of any information, apparatus, method, or process disclosed in this report may not infringe privately owned rights; or

B. Assumes any liabilities with respect to the use of, or for damages resulting from the use of any information, apparatus, method, or process disclosed in this report.

As used in the above, "person acting on behalf of the Commission" includes any employee or contractor of the Commission, or employee of such contractor, to the extent that such employee or contractor of the Commission, or employee of such contractor prepares, disseminates, or provides access to, any information pursuant to his employment or contract with the Commission, or his employment with such contractor.

ORNL-3011
ERRATA

THERMONUCLEAR PROJECT SEMIANNUAL PROGRESS REPORT FOR PERIOD ENDING JULY 31, 1960

Page	Line	Errata
4	12–13	*for* the pressure difference between the inner and outer system was 5 to 10 mm Hg *read* the pressure in the outer system was 5 to 10 times higher than the liner pressure.
4	18	*for* lines *read* liner
5	9	*for* 40-kev *read* 40-kw
5	21	*for* 9 ft horizontally and 16 ft vertically *read* 9 minutes horizontally and 16 minutes vertically.
93	ref 14	*for* UCRL-5648 *read* UCRL-5698
129	8	*for* 600 liters/sec *read* 6000 liters/sec

corrected - June 26, 1961. NB

ORNL-3011

Contract No. W-7405-eng-26

THERMONUCLEAR PROJECT SEMIANNUAL PROGRESS REPORT

for Period Ending July 31, 1960

DATE ISSUED

JAN 5 1961

OAK RIDGE NATIONAL LABORATORY
Oak Ridge, Tennessee
operated by
UNION CARBIDE CORPORATION
for the
U.S. ATOMIC ENERGY COMMISSION

MARTIN MARIETTA ENERGY SYSTEMS LIBRARIES

3 4456 0361550 4

CONTENTS

INTRODUCTION vii

ABSTRACTING SUMMARY ix

1. DCX-1 OPERATION AND PERFORMANCE 1
   1.1 Relocation and Engineering Modifications 1
   1.2 Gas Arc Operation 4
   1.3 Energy Loss Measurements 5
   1.4 Gas Dissociation and Mass Spectrometer Runs 9

2. DCX-2 DESIGN 13
   2.1 Introduction 13
   2.2 Theory 15
   2.3 Injection Considerations 17
   2.4 Present Status of Design 21
      2.4.1 Magnet 21
      2.4.2 Injection 24
      2.4.3 Vacuum 26

3. DCX-EP-B DESIGN AND SUPPORTING WORK (Not included, this report, see page 30.)

4. VACUUM ARC RESEARCH 31
   4.1 The Carbon Arc 31
      4.1.1 Microscopic Properties of the Carbon Arc (University of Chicago Laboratories for Applied Sciences) 31
      4.1.2 Ion Drifts in the Carbon Arc 34
      4.1.3 Effect of Arc Current Variations on the Doppler Width of C^{++} Lines in the Long Solenoid 37
      4.1.4 Density of Ions Outside a Magnetically Confined Vacuum Arc 38
      4.1.5 Randomizing of Electrons in the Carbon Arc 40
      4.1.6 A Simple Multigroup Treatment of Energy Degradation Due to Electron Heating in the Carbon Arc 42
   4.2 The Lithium Arc 46
      4.2.1 Lithium Vapor Arc. Preliminary Experiments 46
      4.2.2 Spectroscopy of Lithium Arcs 48
      4.2.3 Mass Spectrometry of the Lithium Arc 48
   4.3 The Deuterium Arc 50
      4.3.1 Introduction 50
      4.3.2 Adaptation of Deuterium Arc to DCX 51
      4.3.3 Spectroscopic Investigation 51
      4.3.4 Anode Properties 52

4.4 Arc Studies Pertinent to DCX-EP-B..... 53
4.4.1 Cooperative Neutralization of High Energy Ions and Energetic Electrons..... 53
4.4.2 Electron Burnout..... 54

4.5 Titanium Evaporation in an Arc..... 55

5. ION SOURCE AND ACCELERATOR DEVELOPMENT..... 57

5.1 Development of the von Ardenne Source..... 57

5.2 High-Current Ion Beam Injection System..... 61

6. THEORY AND COMPUTATION..... 65

6.1 Fokker-Planck Coefficients for a Plasma Including Radiation..... 65

6.2 Ion Energy Distributions, Ion Energy Degradation, and DCX-Type Critical Calculations..... 66

6.3 DCX Plasma Potential Before Burnout..... 70

6.4 Electron Capture Cross Section in H_2^+..... 72

6.5 Containment Zones..... 72

6.6 Particle Distribution in the DCX Ion Ring..... 75

7. INSTRUMENTATION..... 78

7.1 Energy Measurements with Solid State Detectors..... 78

8. MAGNETIC FIELD CALCULATION, ION TRAJECTORIES, AND MAGNETIC COIL DESIGN..... 80

8.1 Design of Magnetic Mirror Fields with Extremely Homogeneous Central Zones..... 80

8.2 Magnetic Field Codes..... 83

8.3 Properties of Infinite, Lumped Solenoids..... 84

8.4 Simulation of Axially Symmetric Magnetic Fields..... 85

8.5 Design of an Ion Injection Snout..... 93

8.6 Connection of Water Cooled Conductors..... 97

9. SPECTROSCOPIC INSTRUMENTATION..... 102

9.1 The Transmission Grating as a Diagnostic Tool..... 102

9.2 Grating Calibration Spectrometer..... 104

10. H_2^+ CROSS-SECTION MEASUREMENTS..... 105

10.1 Development of Crossed Beam Apparatus..... 105

10.2 Dissociation of H_2^+ by Hydrogen..... 106
10.2.1 Introduction..... 106
10.2.2 Apparatus..... 106

10.2.3 Experimental Procedure..... 108
10.2.4 Results..... 110

11. VACUUM SYSTEMS AND TECHNIQUES..... 114

11.1 Introduction..... 114

11.2 Diffusion Pumps..... 114
11.2.1 Tests of National Research Corporation 32-in. Diffusion Pump..... 114
11.2.2 Exposed Diffusion Pump Jets..... 115
11.2.3 Liquid Metal Diffusion Pumps..... 116

11.3 Evaporative Pumping..... 117
11.3.1 Introduction..... 117
11.3.2 Large-Scale Pump Test..... 118
11.3.3 Bakable Pump Test..... 120
11.3.4 Techniques for the Evaporation of Titanium..... 122
11.3.5 A Test of Titanium Pumping..... 125

11.4 Test of Large VacIon Pump..... 128
11.4.1 Startup Procedure..... 128
11.4.2 Ultimate Pressure..... 128
11.4.3 Pumping Characteristics for H_2..... 128
11.4.4 Reliability Experience..... 129

11.5 Gage Test Facility..... 129

11.6 Mass Spectrometry..... 132

11.7 Zeolite Trapping of Oil Diffusion Pumps..... 132

11.8 Permeability and Outgassing..... 133

12. PRELIMINARY SURVEY ON BALL LIGHTNING OBSERVATIONS..... 134

13. DESIGN AND ENGINEERING..... 137

PUBLICATIONS..... 139

ORNL REPORTS..... 141

OPEN LITERATURE PUBLICATIONS..... 142

INTRODUCTION

A. H. Snell

The present semiannual progress report introduces more active consideration than has been given in the past (by us, at least) to the importance of energy degradation in DCX-like devices. By energy degradation, we mean the cooling of the circulating proton beam by collisions with cold electrons, particularly in the arc. Such a cooling would quickly decrease the ion residence time, because of the sensitivity to energy of the charge-exchange cross sections. The subject has forced itself into prominence because of new measurements made with DCX (Sec 1.3), and so far it has been given only rather preliminary evaluation (Sec 6.2). It may have practical importance in compelling us to consider (a) whether to use an arc or not; (b) if an arc is used, how to generate one in which the mean energy of the electrons is increased far above the few electron volts that we have in the ordinary carbon vacuum arc; (c) the programming of starting with an arc and then shutting it off, in which so far we have ignored any effect upon the energy of the trapped circulating beam.

The following pages introduce also a new major apparatus designated as DCX-2. This will involve multiple passes through an arc, instead of the single pass used in DCX-1. Indeed in principle it can be operated without an arc. DCX-2 will comprise a carefully calculated, straightforward engineering approach to the multiple-pass geometry and will be quite flexible so far as magnetic configuration and vacuum pumping are concerned. Another apparatus in the design stage is designated as DCX-EP-B. This unit is more experimental, and is designed to employ some new concepts now under development. Some of these concepts cannot as yet be released publicly and therefore Chap. 3 of this report, covering the DCX-EP-B design, is being issued separately, with restricted distribution, as ORNL-3044.

During the interval March 1 to April 15, DCX-1 was dismantled, moved, reassembled with modifications, and placed again into operation (Sec 1.1). The modifications consisted primarily of the addition of four 32-in. diffusion pumps to facilitate operation with a hydrogen arc. Unfortunately, the vacuum conditions under hydrogen arc operation have so far been too

poor to yield any significant new observations; the vacuum extrapolation from a trial of hydrogen-arc operation with the old pumps has failed to be realized, and the reasons have yet to be understood (Sec 1.2). Meanwhile, further work has been done toward the understanding of the slopes of the $1/\tau$-vs-pressure curves obtained in the absence of an arc, using now a mass spectrometer to follow the composition of the background gas (Sec 1.4). There are unexplained features in these observations too, but in view of the increasing slope of the $1/\tau$ curve at the low-pressure end, there is still no certain evidence in these curves for the presence of loss mechanisms other than charge exchange. Background pressures considerably lower than 10^{-6} mm Hg are still required to permit other loss mechanisms to come into recognizable prominence.

In vacuum arc research, attempts are described in Sec 4.4.2 to ionize the background gas by the use of the so-called "reflux" arc, and further development of lithium and deuterium arc technology is described in Secs 4.2 and 4.3. In the former, there is a preliminary mass-spectrometric indication (Sec 4.2.3) that under certain conditions the lithium arc may consist largely of Li^{+++}. This would be exciting if borne out by further investigation, but there is a counter-observation by optical spectrometry that in the short arc at least the ion population is disappointingly mostly Li^{+} (Sec 4.2.2).

In the last progress report we left unexplained a certain anomaly associated with the C^{++} drift motion in the carbon arc, whereby a longitudinal drift velocity of 8×10^5 cm/sec apparently vanished near the cathode, without evidence of pile-up of ions. In Sec 4.1.2 evidence is adduced for an explanation in terms of a divergence or splaying-out of the C^{++} ion current outward from the luminous arc column, which combines with the stronger longitudinal motion; the C^{++} ions in the bright part of the arc near the cathode probably are locally generated. Spectroscopy of the dimmer light shows the drift of C^{++} outside of the central column, and indeed this is probably part of the ion current known to miss the cathode proper, and to cause structural damage to cathode supports if not properly shielded against.

A new feature in these reports is a concise summary of the microscopic properties of the carbon arc, extracted from the report of a subcontractor, the University of Chicago Laboratories for Applied Science (Sec 4.1.1).

Theoretical activities (Sec 6) include progress in formal plasma theory as well as calculations of more restricted applicability to immediate experimental problems.

Although our main difficulty in the d-c injection approach to the accumulation of a hot plasma is at present still the phenomenon of charge exchange, some thought penetrates to the coming problems of containment.

Section 10.2 describes results on the cross section for dissociation of H_2^+ by hydrogen in the energy range 200–600 kev. The lower end of this energy range is the site of the famous discrepancy by a factor of 3 between the United States and the Russian results. The measurements herein resolve the discrepancy in favor of the United Kingdom! At the higher end of the energy range, the old United States results are confirmed.

In vacuum technology, Sec 11.2 shows a continuation of routine testing of diffusion pumps, and Sec 11.3 shows growing local familiarity and experience with the production of vacua in the 10^{-9} mm Hg range.

ABSTRACTING SUMMARY

1. DCX-1 OPERATION AND PERFORMANCE

DCX-1 has been relocated and modified by the addition of vacuum pumps fast enough to accommodate operation with a deuterium arc. The new pumps have given about the expected pressure improvement in the outer vacuum system, but for reasons not fully understood, the vacuum in the inner system (liner) has not fallen below about 10^{-5} mm Hg with the deuterium arc in operation. Further work on the deuterium arc will be required to improve the situation.

Measurements of the energy distribution of the H^0 particles that emerge from the trapped circulating "300-kev" H^+ beam have been made. The H^0 particles are allowed to charge themselves by passing through a gas cell, and the resulting H^+ ions are energy-analyzed electrostatically.

By correcting for the charge-exchange cross section, the energy spectrum of the neutrals can be made to yield the energy spectrum of the trapped "300-kev" protons. In the median plane, using gas breakup, the trapped protons show little energy degradation, but when the carbon arc is used for breakup, the energy spectrum spreads both upward and downward. The spread seems to be accentuated off the median plane.

Efforts have been made to correlate the mean containment times τ of the circulating protons with the composition of the residual gas in the DCX-1 liner. A mass spectrometer is used to measure the composition. There is some qualitative correlation, the $1/\tau$-vs-pressure curves showing increased slope at the low end of the pressure range, where gases other than H_2 predominate.

2. DCX-2 DESIGN

A description is given for a projected apparatus in which a 600- or 900-kev molecular ion beam (H_2^+, H_3^+, D_2^+, or D_3^+) is injected into a magnetic mirror containment volume and is made to pass repeatedly through a dissociative arc. Conditions are calculated under which, after an initial buildup of a trapped atomic-ion population, the arc could be turned off, and dissociation of the molecular ions could continue upon the atomic ions. The simultaneous requirements of injected H_2^+ beam current, beam collimation, vacuum conditions, and magnetic field shaping are discussed, and it is concluded that they are attainable.

3. DCX-EP-B DESIGN AND SUPPORTING WORK

This material is covered in a separate report, Thermonuclear Project Semiann. Rep. July 31, 1960, Chap. 3, ORNL-3044 (OUO).

4. VACUUM ARC RESEARCH

Carbon Arc

Spectroscopic Doppler shift measurements in the carbon arc show longitudinal motion of C^{++} in the peripheral region of the arc column near the cathode, while inside the column there is little longitudinal motion there, suggesting a local origin for the latter ions. Line broadening for C^{+++} ions suggests a temperature comparable to that of the C^{++} ions,

viz., 800,000°K. A decrease of line width has been observed with an increase of arc current — possibly a consequence of a secondary pressure change. A theoretical treatment of the distribution of C ions outside of the carbon arc gives a magnetic field dependence in agreement with experiment, but the relative behavior of C^+ and C^{++} is unexplained. A summary of the microscopic properties of the carbon arc is given.

Lithium Arc

Lithium vacuum arcs can be successfully operated using vapor feed at the anode. They are brilliant green in color, because of the 5485 A line group of Li^+. The ionic composition of the arc is uncertain.

Deuterium Arc

A deuterium arc was operated in DCX-1. A 200-amp, 185-v arc gave about 2% dissociation of 600 kev H_2^+ ions, but since pumping was inadequate, the lowest liner pressure was only 1.5×10^{-5} mm Hg. The presence of the Balmer lines in the spectrum of the deuterium arc is thought to arise from the background gas rather than from recombination in the arc column. The anode of the deuterium arc dissipates about 2/3 of the input power.

In other work on gas arcs (e.g., deuterium) some gas is fed into the cathode. After establishment of an arc, reduction of cathode gas feed can cause the electron stream to "blow up" into a hollow cone. The possibility of using such an electron stream to burn out the background gas in a DCX-like device is discussed.

5. ION SOURCE AND ACCELERATOR DEVELOPMENT

Von Ardenne Source

Attempts are described to maximize the output of molecular ions (H_2^+). In the current range 20–50 ma, 70–80% of the output of hydrogen ions are H_2^+; at 50–100 ma, the H_2^+ current comprises 60–70% of the total. A sensitivity of the H_2^+ ratio to source pressure and to the spacing between intermediate electrode and anode has been established, but several other factors have been shown not to affect the H_2^+ ratio appreciably.

Injection System

A description is given of an accelerator tube now under test, which is designed for the acceleration of an ion beam of a few tenths of an ampere (d-c) into DCX-2.

6. THEORY AND COMPUTATION

Fokker-Planck Coefficients for a Plasma Including Radiation

A generalization of the Rostoker-Rosenbluth expansion of the Liouville equation has been used to obtain a set of coupled integral equations for the pair distribution functions of particles and radiation. These equations have been solved exactly for the case of a static spatially homogeneous plasma with no external fields. The method is a generalization of that of Lenard. The result yields the Fokker-Planck coefficients including transverse interactions.

DCX Plasma Potential Before Burnout

An estimate of the plasma potential to be expected in DCX-like devices shows that so long as the positive ion density remains less than that of the neutrals, the potential cannot be expected to exceed a few volts.

Electron Capture Cross Section in H_2^+

A Brinkman-Kramers calculation of the electron capture cross section of H_2^+ gives values ranging from $< 8.6 \times 10^{-16}$ cm^2 at 30 kev to $< 2.1 \times 10^{-18}$ cm^2 at 225 kev.

Containment Zones

Graphic results of further computation are given concerning the containment zones and particle distributions in DCX-1.

7. INSTRUMENTATION

Silicon surface-barrier detectors have been made to operate successfully in DCX-1. They give good resolution of the 600-kev H_2^0 particle peak from that of the 300-kev H^0 particles. The energy response is linear.

8. MAGNETIC FIELD CALCULATION, ION TRAJECTORIES, AND MAGNETIC COIL DESIGN

Design of Magnetic Mirror Fields with Extremely Homogeneous Central Zones

The design of magnetic mirror fields with central zones homogeneous to about 0.1% in field strength is described, and computational codes have been evolved for this and related purposes. A Fourier treatment is given for evaluation of the ripples produced in a long solenoid by lumping of the coils. A "model" is described which with four coils simulated closely the external field to be expected from a long device such as DCX-2. Preliminary consideration is given to the design of an injection snout for DCX-2, and tests of a model are described with a calculation of the effect of the end perturbation on ion orbits.

Connection of Water-Cooled Electrical Conductors

An engineering investigation of various methods of connecting heavy, water-cooled electrical conductors is reported, leading to the conclusion that soft solder is good for joints that need not be broken, and suggesting favorable choices for detachable joints.

9. SPECTROSCOPIC INSTRUMENTATION

Inexpensive transmission gratings are found to be useful in simple slitless spectroscopes, provided that high resolution is not required. They can be used either visually or photographically, they give a stigmatic image, and can have apertures of f/1 or higher.

10. CROSS-SECTION MEASUREMENTS

The cross section for H_2^+ attenuation in H_2 gas and the cross section for proton production by H_2^+ in H_2 gas have been remeasured in the energy range 200 to 600 kev. The results agree well with those of Sweetman at the lower end of the energy range, and with the earlier results of Barnett at the high energy end.

11. VACUUM SYSTEMS AND TECHNIQUES

Pump Testing

The speed of the National Research Corporation 32-in. diffusion pump is found to be about 14,000 liters/sec for air and 21,000 liters/sec for hydrogen, at the valve inlet. Other performance characteristics of this pump are described.

Two systems for the testing of evaporative pumping are described, together with the results of speed and saturation tests. Various methods of evaporation are compared; one that looks promising is titanium evaporation from a titanium-tantalum alloy; another is evaporation from a titanium-niobium alloy.

Calibration of Ion Gages

The comparative response of various ionization gages has been measured on a common system, relative to an absolute pressure response obtained from a leak. The results are expressed in terms of emission curents to be used with different makes of gages in order to give the same pressure readings.

1. DCX-1 OPERATION AND PERFORMANCE

C. F. Barnett
J. L. Dunlap
R. S. Edwards
G. R. Haste
L. A. Kendig
J. A. Ray
R. G. Reinhardt
W. J. Schill
E. R. Wells

1.1 RELOCATION AND ENGINEERING MODIFICATIONS

The relocation of DCX to Building 9201-2 occupied at least half of the period covered by this report. The major changes incorporated during the move have been (1) raising DCX an additional 5-1/2 ft in order that the underside be more accessible, (2) adding four 32-in. oil diffusion pumps to provide the pumping speed required for gas arc operation, and (3) redesigning and placing of monitoring and diagnostic equipment for greater convenience in data taking. A photograph of DCX in the new location is shown in Fig. 1.1.

The 32-in. diffusion pumps were installed at the cathode and anode regions to provide high pumping speeds in the vicinity of the arc electrodes. At first, the pumps lacked baffles for the suppression of backstreaming of oil vapor, and an excessive amount of oil was soon detected in the vacuum tank. Water cooled baffles were then installed on the two pumps on the anode end of DCX. This change resulted in a net reduction of 50% in pumping speeds for the two pumps. The pumps at the cathode end are still untrapped, but these are open to the vacuum system only when the gas arcs are being operated.

During the present period, major emphasis has been placed on engineering and fabrication of components for securing lower operating pressures and larger H_2^+ beam currents. A new system involving differential pumping has been designed, and all components are already fabricated and will be installed in September. The system will then consist of three regions: (1) the inner liner region, in which batch evaporation from four titanium-clad-tantalum filaments will provide hydrogen pumping speeds of 50,000 to 100,000 liters/sec; (2) the intermediate region, which will be pumped by eight titanium evaporative pumps and the two 14-in. Leybold diffusion pumps already in place; and (3) the outer region to be pumped by the four 32-in. diffusion pumps. Isolation between the regions will be achieved by passing the arc through suitably placed apertures. With a

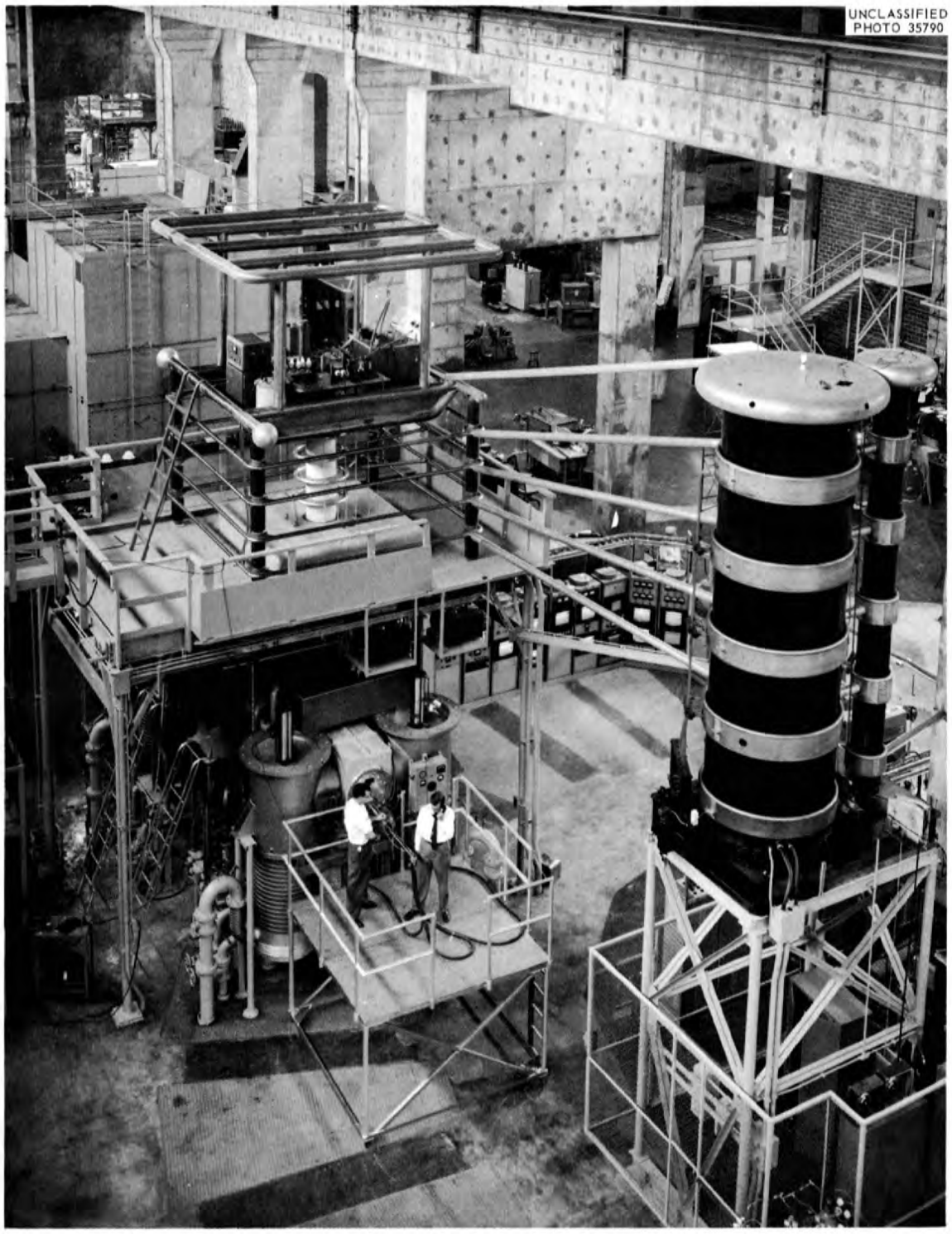

Fig. 1.1. Photograph of DCX-1 Facility.

deuterium arc in operation, it is anticipated that pressures of 5×10^{-7}, 5×10^{-6}, and 5×10^{-5} mm Hg can be maintained in the liner, intermediate, and outer regions, respectively. An ion pump of the VacIon variety similar to that described in a previous report[1] is being constructed by Varian Associates for use as an alternative method of evacuating the innermost region. This pump will be capable of speeds of 50,000 liters/sec (for hydrogen) and will be placed in the magnetic volume of the liner region.

In trials on a test stand, an unexpected difficulty has been encountered in the operation of this type of ion pump. Both a VacIon pump (250 liters/sec) and a diffusion pump (4 in.) have been connected to a system equipped with an omegatron mass spectrometer. It was found that with both pumps operating, the admission of a test gas resulted in an increase in the partial pressure of the background gas components. This was also true if only the VacIon pump was operating. If, however, only the diffusion pump was allowed to pump, this behavior was no longer observed. Instead, the background gas partial pressure remained relatively constant as the ion gage pressure was varied by an order of magnitude by the admission of the test gas.

The inference made from this observation is that, in the process of pumping the test gas, the VacIon pump re-emits previously pumped gas molecules from its cathodes. The test has recently been repeated with the addition of a preliminary bakeout in a vacuum furnace to see if the reemission could be reduced or eliminated, but results are not yet at hand.

As regards the projected increase in injected H_2^+ current, a contract has been negotiated with High Voltage Engineering Corporation for the construction of an ion source in which mass analysis will be accomplished at the high-voltage terminal of the accelerator tube. The source, to be delivered in September, will be capable of supplying a minimum of 25 ma of H_2^+ to DCX. The unused beam will be removed from the plasma region by passing the beam through apertures into a 10,000-liters/sec VacIon pump.

---

[1] Thermonuclear Project Semiann. Rep. Jan. 31, 1960, ORNL-2926, sec 1.2.2.

1.2 GAS ARC OPERATION

In conjunction with the Exploratory Physics Group, some preliminary gas arc runs were made in DCX before moving to the new location. The cathode used for all gas arcs was a hollow (3/8 in. ID, 0.700 in. OD) tungsten cylinder. In the PIG-type arc, the anode was a copper tube 10 in. long and 2-1/8 in. OD into which gas was bled. This tube was mounted on an eccentric arm so that it could be rotated out of the arc path. Behind the gas anode was a carbon electrode which could be floated for use with the PIG arc or could be grounded to produce a d-c-type arc. The lowest (corrected) pressures obtained in the liner were 4×10^{-5} mm Hg with a deuterium arc in operation. The associated decay times of the trapped proton population were 1 to 1.5 msec at this pressure. By using standard six-element carbon baffles, the pressure in the outer system was 5 to 10 times higher than the inner pressure. ~~difference between the inner and outer system was 5 to 10 mm Hg~~. The dissociation efficiency varied between 1 and 2% for deuterium arcs and was approximately 8% for argon arcs.

Electrode and baffle geometries such as used in the PIG Plate Facility were also employed. The anode was a copper cylinder, approximately 3 in. ID and 12 in. long, with tungsten baffles at 1-in. intervals. The baffles between liner and outer vacuum region were water cooled copper tubes 12 in. long and 2-7/8 in. ID. The lowest liner pressures obtained were 1.4×10^{-5} with a pressure differential of approximately 100 between the inner and outer vacuum systems. The dissociation efficiency was between 2 and 3%, and maximum decay times of 3.3 msec were recorded. In all runs involving these gas arcs there was considerable electrode deterioration, a fact implying contamination in the arcs.

In moving to the present building, the 32-in. pumps were installed and it was anticipated that considerably lower pressures would be forthcoming. As yet these lower pressures have not been achieved. Failure of the anode to withstand the arc bombardment has been our principal problem. The use of arcs of the geometry described above but with increased cooling on the anode has not produced an arc free of contaminants. The lowest liner pressure for deuterium arcs has been 1.5×10^{-5} mm Hg with pressure differentials of only a factor of 10. The reason for the low differential is not at present understood; however, with an argon arc, minimum pressures of 8×10^{-7} mm Hg and pressure differentials of 100 have been observed.

Operation with a reflecting-type (PIG) arc has been disappointing since this arc is unstable under certain conditions. It has been determined that when either the gas flow is reduced from 4–5 cc/sec or the arc current is increased above 70 amp, the arc diameter increases. For example, in the center of the anode extension coils, the arc diameter increases from about 3/4 in. to 1-1/2 to 2 in. when the arc current is increased from 70 to 90 amp.

Preliminary results indicate that a rotating, water cooled copper anode will withstand a 40-Kw arc without serious deterioration.

1.3 ENERGY LOSS MEASUREMENTS

Preliminary measurements have been made of the steady state energy spectra of neutral particles escaping DCX as the result of charge-exchange collisions with the background gas. Briefly, the energy spectra were obtained by collimating a beam of escaping neutrals, passing this beam through a low-pressure differentially pumped argon gas cell, and electrostatically analyzing the resulting proton beam. The proton detectors were electron multipliers constructed from 9524-B EMI photomultipliers. Figure 1.2 is a schematic diagram of the neutral spectrometer. On the basis of geometric ray tracings and a monoenergetic beam, the apertures provided a beam spot at the detectors measuring 0.17 in. horizontally and 0.25 in. vertically. The total acceptance angles looking into the DCX plasma region were approximately 9 minutes horizontally and 16 minutes vertically. The collimation resulted in a resolution of approximately 3%. The spectrometer was calibrated by using protons from an auxilary 600-kev accelerator.

Measurements were made on particles escaping DCX under three different conditions:

1. spectrometer located on the median plane with hydrogen gas at a pressure of 1×10^{-5} mm Hg used as the dissociating mechanism,
2. spectrometer located on the median plane with carbon arc dissociation at a pressure of 1.5×10^{-6} mm Hg resulting in a τ of approximately 2 msec,
3. spectrometer located 1-1/4 in. on the anode side of median plane with carbon arc breakup and τ of approximately 2 msec.

In each case 1 ma of H_2^+ was injected and the pressure in the argon gas cell was about 10^{-4} mm Hg. The carbon arcs were 60 in. long, operated at

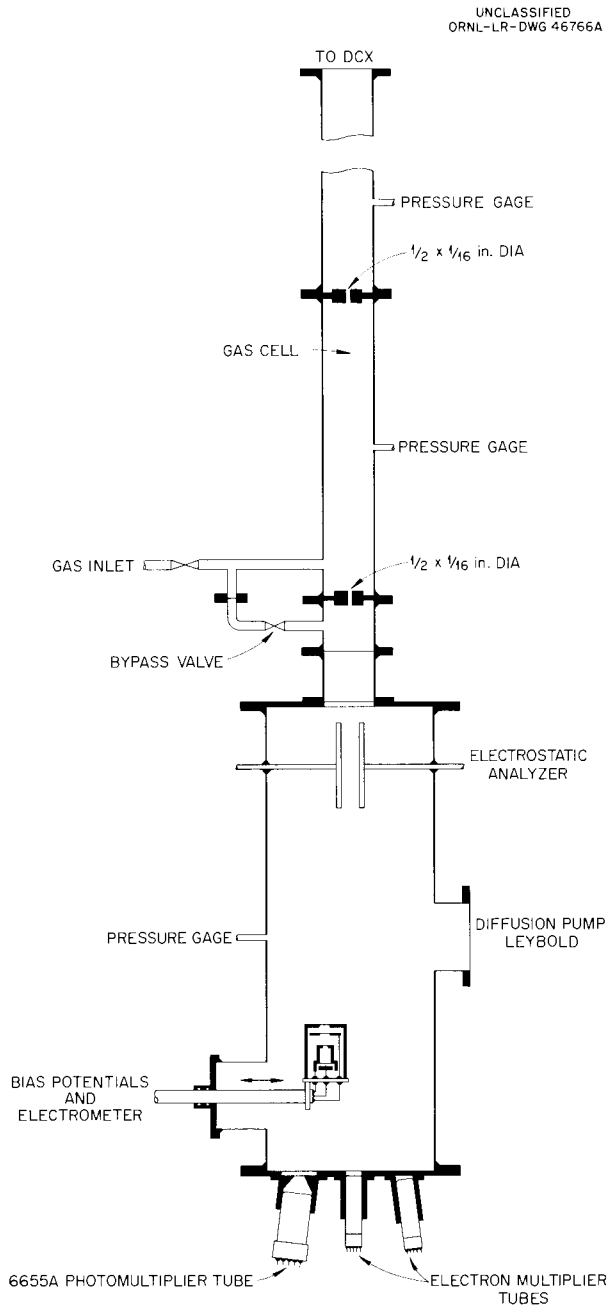

Fig. 1.2. Schematic Drawing of Neutral Spectrometer.

300 amp with standard electrodes and the standard 6-in. six-element baffle holders at the outer edge of the magnetic field coils. The typical density of arcs such as this is 10^{14} electrons/cc.

Figure 1.3 shows the spectra of the particles escaping DCX as the result of charge-exchange collisions with the background gas. The arc

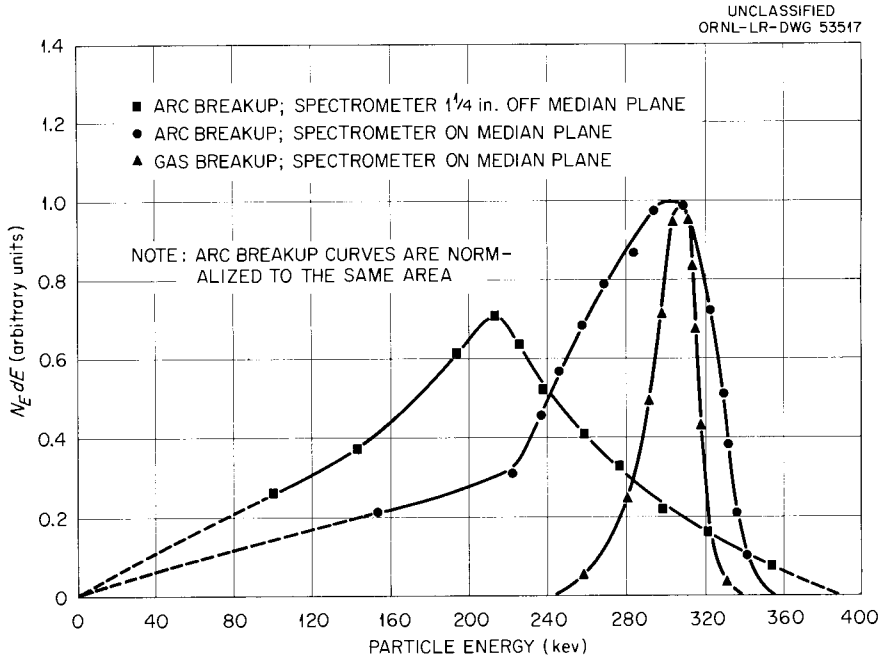

Fig. 1.3. Energy Distribution of Particles Escaping DCX.

breakup curves have been normalized to the same area, and the peak of the gas breakup curve has been normalized to unity. The high energy side of the gas dissociation curve matches very closely the shape of the calculated spectrometer response to a monoenergetic signal. The spectrometer signal at a particular energy E_1 is proportional to the charge-exchange reaction rate inside the plasma modified by the energy dependence in the spectrometer itself. This may be expressed by

$$S_1 \sim KN^{\circ}N^{+} \langle \sigma v \rangle \quad ,$$

where

K represents the energy correction factor for spectrometer efficiency,

N° is the neutral gas density,

N^{+} is the positive ion density,

$\langle \sigma v \rangle$ is the value of the product of the electron capture cross section and the particle velocity, averaged within the separate velocity intervals.

This equation permits conversion to the energy distribution of positive ions in the plasma of DCX in that region of space and angle that the spectrometer actually samples. The two energy-dependent corrections for spectrometer efficiency involve the electron loss cross section for the energetic neutrals in the gas cell and the secondary emission coefficient for

protons on the cesium-antimony surface of the electron multiplier first dynode. In the transposition of the energy distribution the σv factor predominates because of the steep energy dependence of the electron capture cross section.

The energy distribution of the protons in the plasma is shown in Fig. 1.4. The mean and most probable energies for each curve are shown in Table 1.1. An examination of the curves and the table reveals not only an energy loss to the cold electrons of the arc, but also a large number of the particles in the plasma with energy in excess of the injection

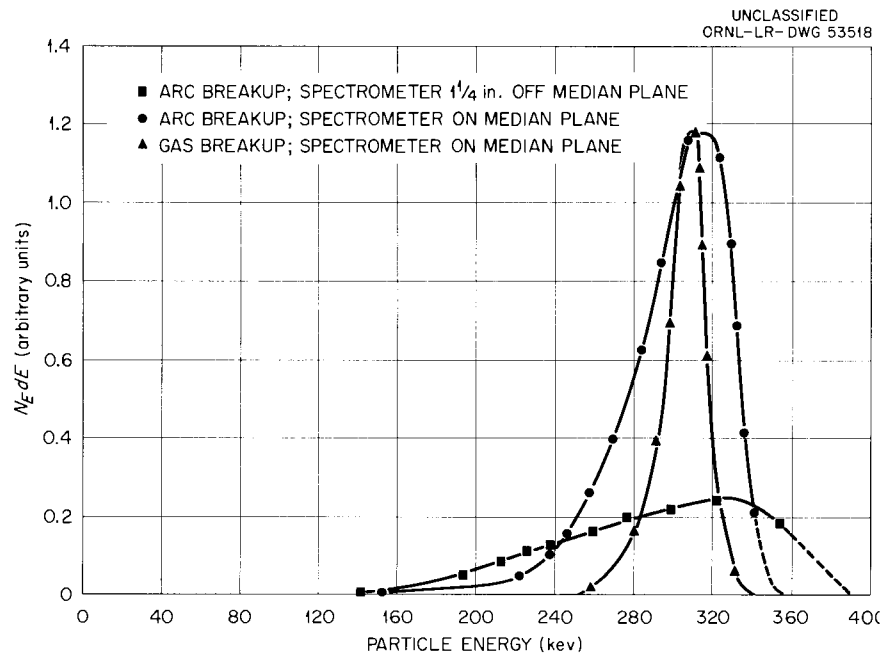

Fig. 1.4. Energy Distribution of Particles Inside DCX.

Table 1.1. Mean and Most Probable Energies (kev)

Operational Mode	Particles Escaping		Particles Inside	
	Mean E	Most Probable E	Mean E	Most Probable E
Gas dissociation	300	308	305	310
Arc, on midplane	245	302	300	315
Arc, 1-1/4 in. off midplane	195	215	295	330

energy of 300 kev. The assessment of the magnitude of the various phenomena is not possible with the present data; however, the curves of Fig. 1.4 are compatible with a model characterized by:

1. Some energy diffusion mechanism which, if operating alone, would result in a Gaussian distribution about the initial 300 kev and which can produce energies greater than 300 kev.
2. Energy loss in heating up cold electrons, with the result that the Gaussian produced by (1) is somewhat distorted and shifted toward lower energies.
3. A depletion of the lower energy population because of the energy dependence of the electron capture cross sections resulting in a shift of the mean energy of the distribution toward higher energies by an amount compensating the shift downward due to energy loss to the arc electrons.

At the present time the measurements are being repeated to determine if the sample of particles measured were representative of the true population and also to obtain the energy distribution as a function of time after the input proton beam is gated off.

1.4 GAS DISSOCIATION AND MASS SPECTROMETER RUNS

Recent gas dissociation runs which involved the simultaneous collection of neutral particle detector data and mass spectrometer analyses of the liner gas composition have resulted in a qualitative understanding of the variation of mean containment time with total pressure. A complete report[2] has been circulated, and only a portion will be repeated here.

Figure 1.5 shows the experimentally obtained $1/\tau$-vs-pressure curve for a run in which the liner pressure was varied with a hydrogen gas leak and, in addition, a curve calculated on the basis of a pure hydrogen background gas, using the cross sections of Barnett and Reynolds,[3] with an ion gage correction factor of two. Gross features of the experimental curve are: (1) the measured τ values are considerably shorter than would be expected on the basis of the charge-exchange cross section for 300-kev

---

[2]C. F. Barnett et al., DCX Gas Dissociation and Mass Spectrometer Runs of 7-1-60 and 7-5-60, internal technical memorandum No. 13 (Aug. 25, 1960).

[3]C. F. Barnett and H. K. Reynolds, Phys. Rev. 109, 355 (1958).

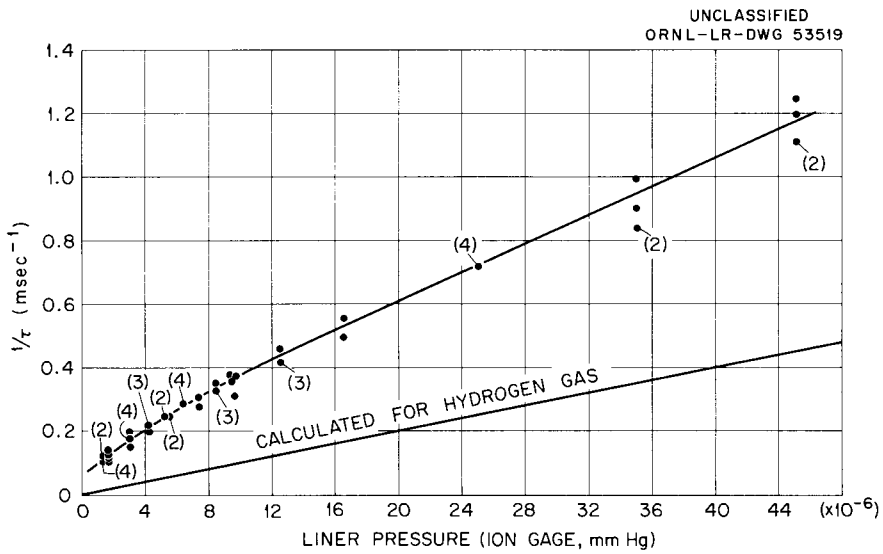

Fig. 1.5. Center Detector $1/\tau$ vs Pressure for Hydrogen Gas Breakup.

protons;[4] (2) at pressures above 14 to 16 $\times 10^{-6}$ mm Hg, the measured response is fairly linear, but with a slope a factor of 2 greater than the calculated slope; (3) the slope becomes steeper at progressively lower pressures; (4) with the present terminal slope, the low-pressure end of the curve fails to extrapolate through the origin.

Figure 1.6 is a pressure plot of the mass spectrometer data taken simultaneously with the $1/\tau$ data of Fig. 1.4. The sum of the impurity signals is expressed as a per cent of the total spectrometer response in Fig. 1.7. The presence of considerable quantities of impurities with (presumably) high proton charge-exchange cross sections results in τ values shorter than those expected on the basis of a pure hydrogen background. The relative amounts of the impurities remain nearly constant throughout the pressure range, but the absolute amounts increase gradually with pressure (see Fig. 1.6). As a result (see Fig. 1.7), the per cent total impurity decreases sharply with the initial increases in pressure (corresponding to initial decreases in the slope of the $1/\tau$-vs-pressure curve) but remains fairly constant at pressures greater than about 16 $\times 10^{-6}$ mm Hg (corresponding to the constant slope of the $1/\tau$ curve in this same pressure region).

[4]Note that with gas breakup, energy degradation is small (see Fig. 1.3).

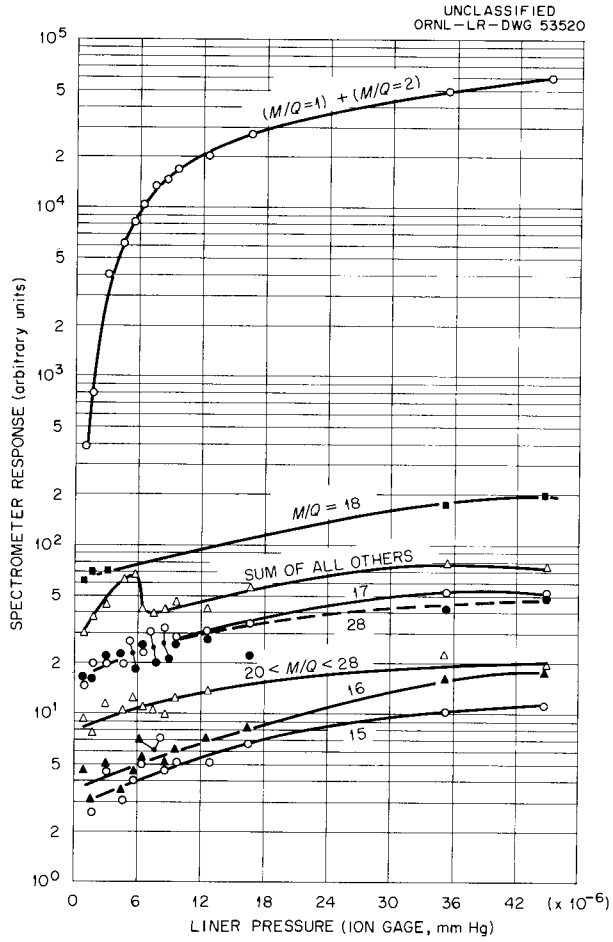

Fig. 1.6. Spectrometer Response vs Pressure (with H_2^+ Beam and Hydrogen Leak).

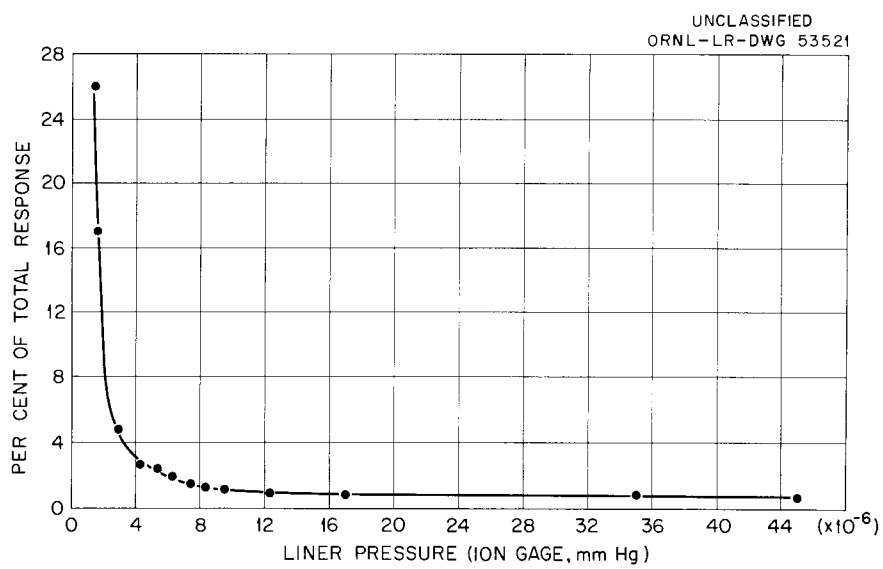

Fig. 1.7. Per Cent of Total Response Not Attributable to Hydrogen vs Pressure.

In another gas breakup experiment, $1/\tau$ data were obtained at two low pressures without using a hydrogen gas leak at the higher pressure. Data at the higher pressure were obtained by photographing the detector decay signals with the liner still hot from a steam bakeout. Then liquid nitrogen was forced through the liner cooling tubes and additional data taken at a considerably lower pressure. Figure 1.8 is a $1/\tau$-vs-pressure plot of these data, disregarding temperature corrections. The slope of this

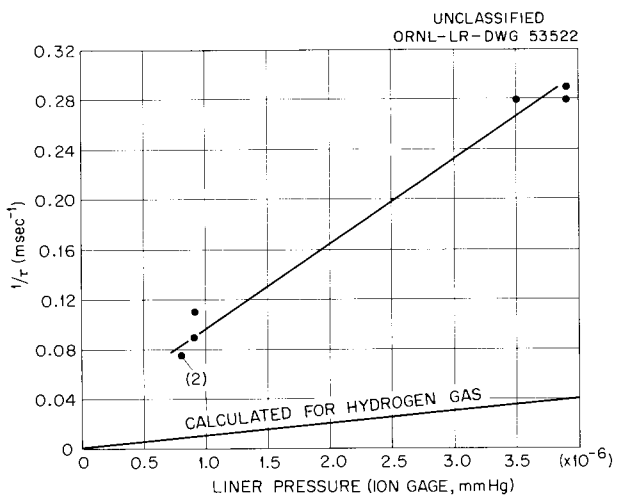

Fig. 1.8. Center Detector $1/\tau$ vs Pressure (Background Gas Dissociation).

curve is about six or seven times the calculated slope for hydrogen gas. By comparison, the low-pressure terminal slope of the $1/\tau$ curve of Fig. 1.5 is about 3-1/2 to 4 times the calculated slope. As one goes to lower pressures, the $1/\tau$ curves evidently become steeper and the extrapolation through the origin becomes more reasonable.

The previous report[5] presented $1/\tau$-vs-pressure curves for gas dissociation which showed unexpected irregularities in the low-pressure region. The explanation offered at that time, that the irregularities might arise from the stimulation of impurity gases by the presence of the added gas, is supported by the low-pressure irregularity shown in Fig. 1.6. Similar irregularities in mass spectrometer data were noted in scans made during argon gas dissociation experiments. In neither the argon nor the hydrogen experiments were these variations in the composition of the background gas pronounced enough to effect the regularity of the $1/\tau$ curves.

[5]Thermonuclear Project Semiann. Rep. Jan. 31, 1960, ORNL-2926, sec 1.3.1.

2. DCX-2 DESIGN

P. R. Bell
J. S. Culver
S. M. DeCamp
R. A. Dandl
J. C. Ezell
W. F. Gauster
G. G. Kelley
N. H. Lazar
R. J. Mackin, Jr.
J. R. McNally, Jr.
R. V. Neidigh
C. E. Normand
J. F. Potts
M. Rankin
E. D. Shipley
A. Simon

2.1 INTRODUCTION

Experience with DCX-1 during the past year has made its limitations fairly apparent.[1] These consist mainly of charge-exchange losses, energy and angle scattering, and energy losses in the trapping arc. We are now designing a machine to be called DCX-2, whose purpose is the achievement of burnout and a plasma density in the region of 10^{13} particles/cm^3 despite such arc losses. The main features which distinguish the new machine from its predecessor are:

1. An injection scheme which permits a long path length for molecular ions in the plasma region, and thus many passes through a trapping plasma.
2. Use of the ion-pumping effect of the trapped plasma, which is expected to yield pumping speeds approaching 10^6 liters/sec.
3. A magnetic field of such strength and scale as to make the mirror losses no more than those predicted by adiabatic theory.

In view of the dominant role of losses in the arc, it is a natural hope to be able to turn off the arc and continue to dissociate molecular ions in the already-accumulated plasma. A minimum design aim in DCX-2 is the achievement, with an initial carbon arc, of a sufficient density of trapped protons to make this feat possible. Also contemplated, of course, are experiments with more desirable arcs or other trapping plasmas, making use of the fact that comparatively low arc densities are permitted by the multipass feature. It appears even to be within the range of the expected machine parameters to achieve burnout and plasma buildup without an arc, as is being attempted in the Russian OGRA.

A major engineering aim is reliability and flexibility of operation. Provision is made for injection of all kinds of molecular ions from H_2^+ to D_3^+; for operation with several types of arc or without an arc; and

[1] C. F. Barnett *et al.*, Thermonuclear Project Semiann. Rep. Jan. 31, 1960, ORNL-2926, p 1.

for ready access and installation of various kinds of plasma-diagnostic equipment. Parameters for initial operation include: injection of H_2^+ at 600 kev in currents up to 0.5 amp (von Ardenne ion source); central magnetic field 12 kilogauss uniform over a 2-m length to a few parts in 10^4; mirror ratio 3.5; magnet power 10 Mw; chamber diameter 1 m; length between mirror centers 4 m; required upper limit of initial pressure, 4×10^{-7} mm Hg of hydrogen and 4×10^{-8} mm of other gases.

Figure 2.1 shows DCX-2 as it is envisioned at the present time. In Table 2.1, its major design parameters are compared with those of DCX-1.

The design is proceeding as a cooperative effort of those listed at the start of this chapter (and several members of their groups). Most

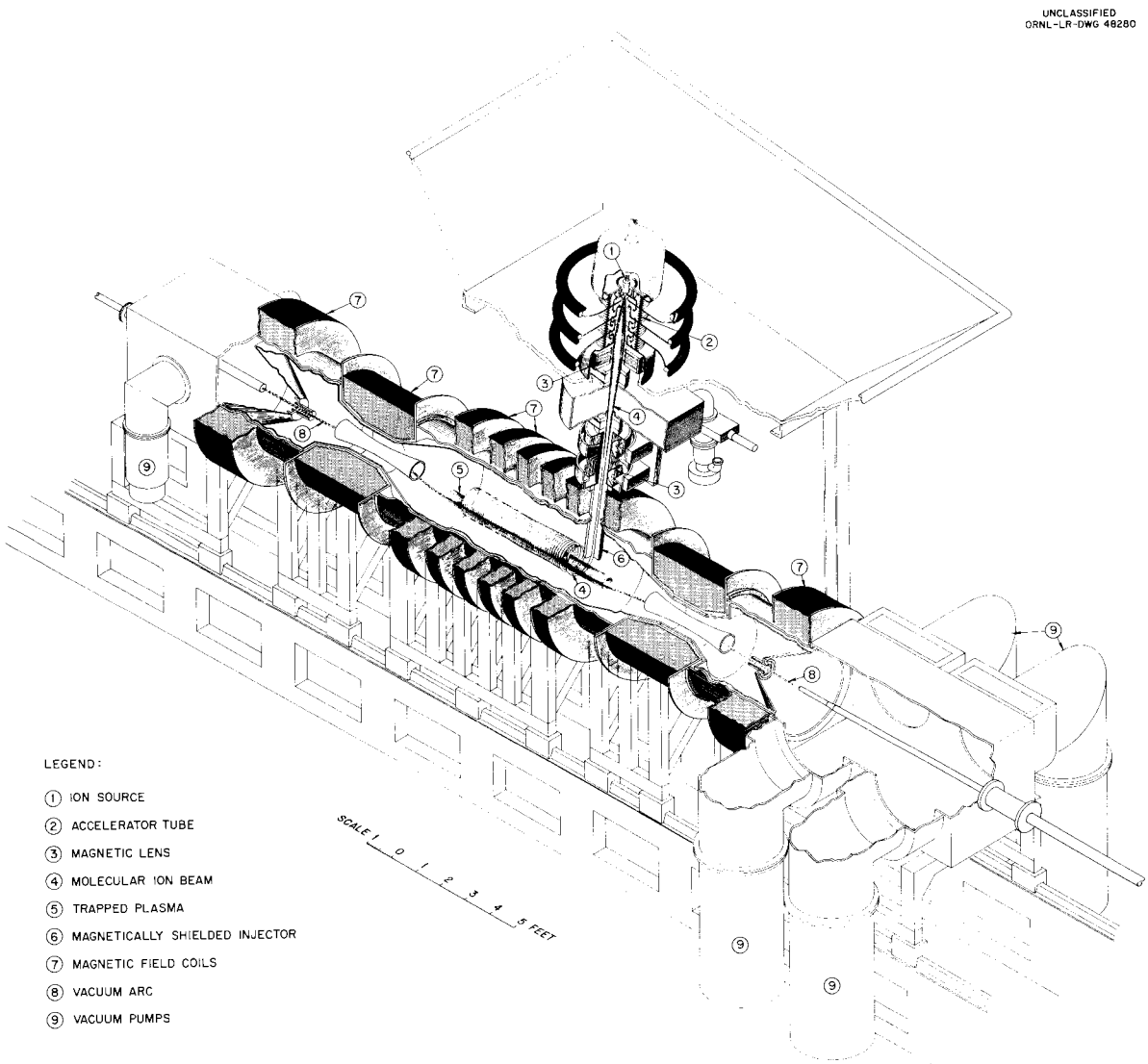

Fig. 2.1. DCX-2 Machine: Conceptual.

Table 2.1. Design Parameters of DCX-1 (Latest Configuration) vs DCX-2 H^+ trapping assumed for both

	DCX-1	DCX-2
Central field, kilogauss	10.0	12.0
Mirror ratio	2.1	3.5
Homogeneity of field	Very poor	Good
Adiabaticity of trapped orbits	(none) $\frac{2\pi\rho}{L} \approx 1$	(good) $\frac{2\pi\rho}{L} \approx 0.15$
Number of passes	1.0	60.0 nominal
Nominal maximum beam currents, ma	15.0	500.0
Trapped proton energy, kev	300.0	300.0
Magnet power, Mw	3.0	10.0
Distance between mirror coil centers, m	0.78	4.06
Distance between mirror coils, m	0.44	3.15
Inside diameter of liner, m	0.71	0.92
Inside diameter of mirror coil, m	0.46	0.41
Over-all length of vacuum tank, m	5.65	8.5

of the engineering is being performed by the Y-12 Engineering Division. In many respects the design resembles that of a similar machine by Gilbert et al.[2] We are indebted to the members of that group for several valuable discussions.

2.2 THEORY

The estimation of the plasma density that can be achieved in the presence of the carbon arc is performed by equating the total number of particles contained in the plasma volume (n_+V) to the product of the proton current being trapped and the mean residence time (τ) of the trapped particles in the volume:

$$n_+V = iB\tau \quad , \tag{1}$$

[2]F. C. Gilbert et al., High Energy Molecular Injection into a Mirror Machine, UCRL-5827 (1960).

where i is the molecular ion current (in ma) and B is the trapping efficiency. We take the mean residence time to be the arc-limited value observed in DCX-1.

In DCX-2 we hope to achieve a sufficient number of passes through the arc to give essentially 100 per cent breakup. Thus, we may expect

$$n_+ V = 6 \times 10^{13}\ i(\text{ma}) \quad . \tag{2}$$

A plausible value for the plasma volume in DCX-2 is 100 liters. For this volume,

$$n_+ = 6 \times 10^8\ i \quad . \tag{3}$$

After an initial period of trapping with the arc, we now suppose the arc to be turned off, the molecular-ion dissociation subsequently continuing upon the trapped H^+ ion population that had been established by the dissociation in the arc. Under these conditions, Simon's theory[3] of burnout in an OGRA-like device becomes directly applicable.

The results of the theory can be expressed as S-shaped curves for the relationship between the density n_+ of the fast trapped H^+ ions and the injected H_2^+ beam current. A parameter in which there is some uncertainty is L, the path length of the H_2^+ ions through the volume occupied by the trapped protons. Figure 2.2 shows S-curves for two values of L which lie in the expected range. Also shown in the figure is a dashed line representing the relationship between n_+ and i given above. (Another line gives the relationship for only 40 per cent dissociation, which would require 10 passes through DCX-1 arc.) If the input H_2^+ current exceeds the value given by the right-hand extremity of the lower bend, an OGRA-like buildup of density will be achieved, and an initiating arc is not necessary. Anywhere above the middle part of the S-curve, buildup will also ensue. So, in terms of these diagrams the procedure is to build up density by arc breakup following an appropriate dashed line upward until it crosses an appropriate S-curve. The point of crossing gives the current at which the dissociation of the trapped protons is sufficient to

---

[3]A. Simon, Critical Current for Burnout in an OGRA-Type Device, ORNL-2831 (1959).

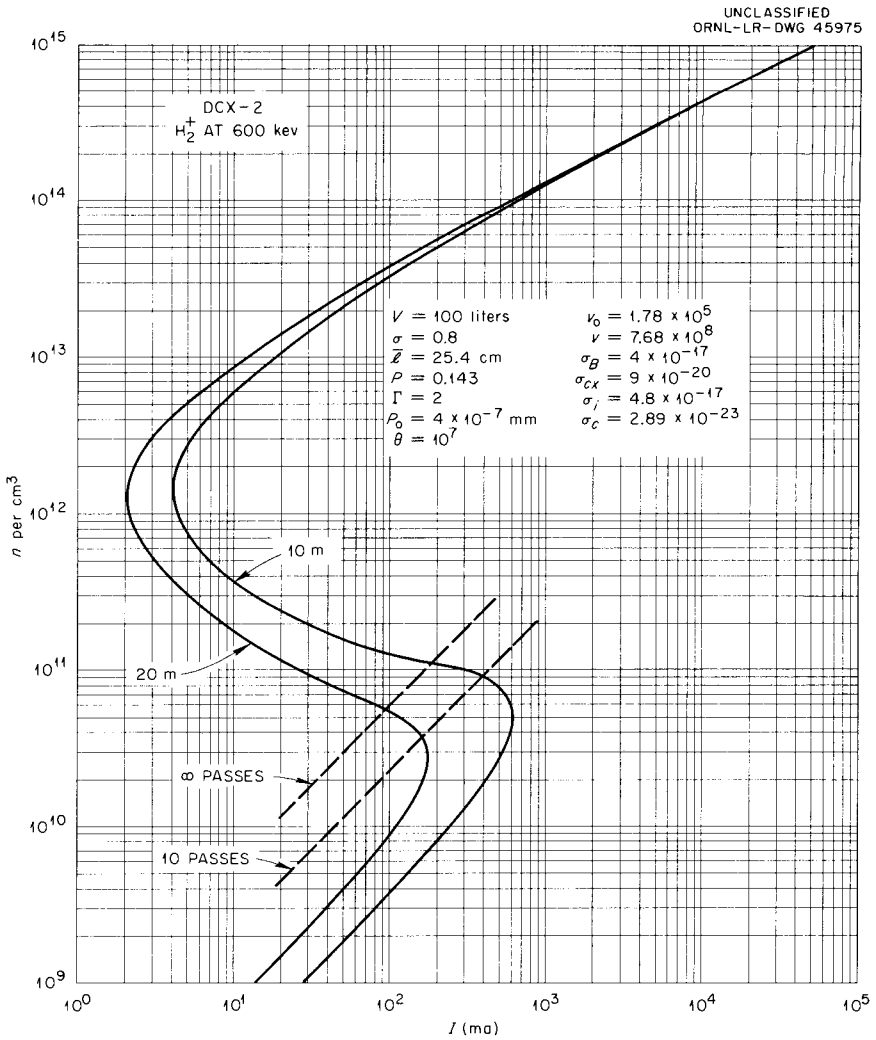

Fig. 2.2. Theoretical Plasma Buildup Curves for DCX-2 Derived over a Range of Assumptions as to Plasma Volume and Path Length of H_2^+ Ions in the H^+ Plasma.

cause further buildup in the absence of the arc. So, one can turn off the arc as slowly as he wishes after that density condition has been realized. According to Fig. 2.2, an estimated injected H_2^+ current required for buildup is of the order of 100 ma (L = 20 m). Operation with another kind of trapping plasma would move the dashed curve to the left by a factor corresponding to the ratio of the limiting time constant to 10 msec.

2.3 INJECTION CONSIDERATIONS

The injection scheme is built around the idea of leading molecular ions into DCX-2 through a magnetically shielded snout, directing them into

the tightest possible helical path. On this path they move down the machine, then back, and strike the snout. In OGRA a similar injection system is used; however, magnetic field gradients are established which cause the orbits to precess in azimuth, so that after their first reflection from the opposite mirror, the ions miss the snout. They are thereby permitted to travel the length of the machine several times before eventually being lost on the snout. In OGRA this precession is achieved at a considerable cost in adiabaticity,[4] which limits the ultimate ion density to a value considerably less than might otherwise be achieved. In DCX-2 the ratio of snout diameter (15 cm) to orbit diameter (25 cm) is great enough that magnetic precession of the beam to miss the snout after one reflection is almost out of the question. The suggestion has been made[5] that the application of a radial electric field will result in enough precession, at least in the crucial early stages, to increase the path length substantially. Quantitative analysis shows that this should require quite a modest applied voltage (about 25 kv).

The pitch of the beam helix as it leaves the snout must be such that all of the molecular ions miss the snout on the first revolution. This is to be achieved by inclining the snout along the magnet axis, ~7.5 degrees. This gives a 10-cm advance per turn of the molecular ions. Since the uniform field region is ~2 m long, ~40 rev may be expected. This figure can be improved markedly by slightly reducing the magnetic field at the point of injection. As the molecular ions move down the axis and out of the reduced field region, the pitch of the helix sharpens up and can be made as fine as is consistent with the beam's angular divergence. The required fractional field dip to reduce 7.5° pitch to zero is 1.6%.[6] The initial angular divergence, Δ_i, will be magnified as the beam moves out of the reduced field region, and it can be shown that the final divergence,

---

[4]A. Garren *et al.*, *Proc. U.N. Intern. Conf. Peaceful Uses Atomic Energy, 2nd, Geneva* **31**, 65 (1958).

[5]A. Ruark, private communication.

[6]The analysis that leads to this estimate and those which follow is based on the constancy of the magnetic moment, $\mu = m(v_\perp)^2/2B$, and the assumption of a small pitch angle.

Δ_f, is given by

$$\Delta_f \cong \sqrt{2\alpha_i \Delta_i} \quad , \tag{4}$$

where α_i is the initial pitch angle. For a conservative initial (total) divergence of 0.5° and an initial pitch angle of 7.5°, Δ_f = 2.7°, or nearly 40 per cent of the initial angle.

Estimating the dip's full effect on the path length requires an evaluation of the distortion which is produced in the beam's angular distribution. Figure 2.3 shows the projected distribution of an initially uniformly distributed cylindrical beam and the distribution in α_f, the final

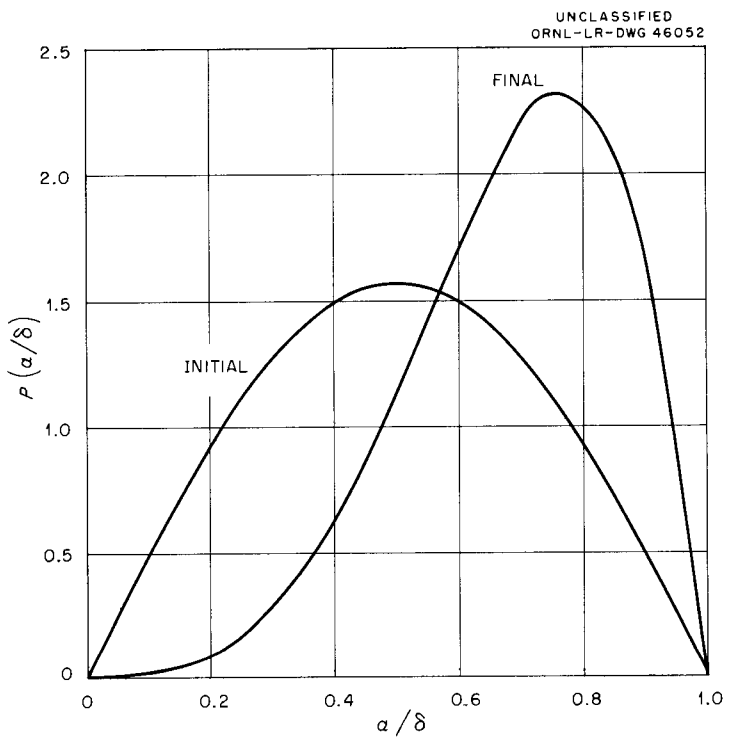

Fig. 2.3. Distribution of Axial Component of Ray Angles in an Ion Beam Which Is Initially Uniformly Distributed.

pitch angle, which results. The final distribution is peaked at

$$\alpha_f \cong 0.75\ \Delta_f \tag{5}$$

and has a full width at half maximum of 0.45 Δ_f. It follows that the use of the field dip results in a mean decrease in the pitch of the helix by

a factor of about 3, with a corresponding increase in mean path length. This figure improves as the initial divergence is decreased, but only as the square root.

If one injects into the uniform field region in such a way that pitch angles are distributed up to a maximum α_f (max), then

$$\frac{\Delta B}{B} \leq \alpha_f^2 \text{ (max)} \tag{6}$$

defines the extent of the uniform field region. For the example given above

$$\frac{\Delta B}{B} \leq 0.23\% \quad . \tag{7}$$

Not only must the uniform field meet this requirement, but also the field in the dip region must be accurate to this degree. For a given α_i, the required field precision scales directly as the initial beam divergence.

Where the shape of the "uniform" field is known, a more careful calculation of the path length, L', is possible. Estimates have been made for several simple field shapes, and the results all agree to within 20% of that computed for a constant pitch helix with the most probable α_f taken from Fig. 2.3

$$L' = \frac{2.7\mathcal{L}}{\Delta_f} \quad , \tag{8}$$

where $\mathcal{L}$ is the length of the uniform region. Clearly, comparatively little is to be gained by attempting to tailor the field shape in addition to specifying a certain degree of uniformity.

The length L' so computed must be multiplied by about one-third to give L, the actual path length in the plasma. For the beam with initial divergence one-half degree and $\mathcal{L}$ = 2 m, L = 33 m. If a smaller snout permits reduction in the initial pitch angle by a factor n, or if the angular divergence can be reduced by the same factor, L will be multiplied by $\sqrt{n}$. This would require a field homogeneous to (0.23/n)% over the uniform region. Note that the precision of the initial alignment is not critical, since adjusting the field dip can determine the range of α_f.

The H_2^+ orbit circumference is 0.8 m. The number of passes through an arc would then be 3L/0.8, or 125 for the example considered.

2.4 PRESENT STATUS OF DESIGN

2.4.1 Magnet

The calculations related to the synthesis of the required magnetic field are sufficiently advanced that it is fairly evident that homogeneity to within a few parts in 10^4 can be achieved over the entire "uniform" region. The "uniform" region is 0.5 m in diameter and 2 m long. With the coil configuration which has evolved, it has turned out – essentially by accident – that just outboard of the outermost booster coil is a narrow field dip of about 2%. This is quite a fortunate occurrence, inasmuch as other calculations have shown that it would be extremely difficult to produce such a narrow dip by means of currents in supplementary coils. Note that Fig. 2.1 is obsolete in that it shows the injector snout penetration between two of the booster coils, the point at which it was originally proposed to place the field dip.

Since DCX-2 is to be designed for D^+ and H^+ experiments, the electrical arrangement of the magnet coils has to be laid out for operation either with full flux density (and with a power not larger than the available total generator capacity of around 20 Mw) or with flux density $1/\sqrt{2}$ and with half total generator power. The H^+ operation is supposed to free about 10 Mw for other experiments.

The wiring diagram shown in Fig. 2.4 takes care of this requirement. Each coil or each symmetrical pair of coils is divided into six parts which can be connected in two different ways as indicated in the figure by "D operation" and "H operation." In the first case, two generators are operating in series; whereas, in the second case, only one generator is used. The voltages and currents which must be produced in these two modes of operation are indicated in Fig. 2.4. In order to achieve a flux density ratio of exactly $\sqrt{2}$ (i.e., when the energy of the ions is supposed to be exactly equal for D^+ and for H^+ experiments) voltages and currents must deviate slightly from the rated generator values. Keeping the power of the generators in both cases exactly at the rated level, it would be necessary to work during D^+ experiments with 3% over-voltage and 3% under-current; whereas, when operating for H^+ experiments, 3% under-voltage and 3% over-current would be required.

UNCLASSIFIED
ORNL-LR-DWG 46067

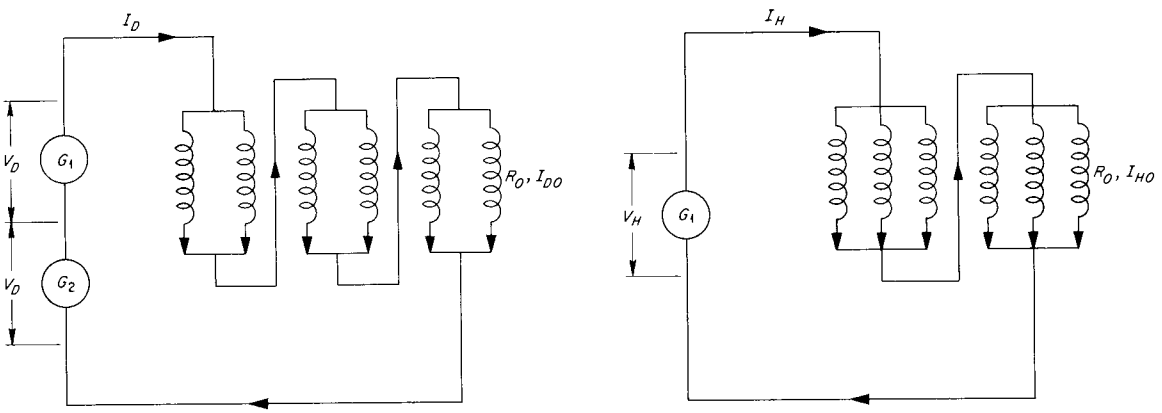

$$R_D = \tfrac{3}{2} R_O$$
$$I_D = 2\, V_D/R_O = \tfrac{4}{3}\, V_D/R_O$$
$$I_{DO} = I_D/2 = \tfrac{2}{3}\, V_D/R_O$$
$$2P_D = 2V_D \times I_D = \tfrac{8}{3}\, V_D^2/R_O$$

"D-OPERATION"

$$I_{DO}/I_{HO} = \sqrt{2} = \frac{\tfrac{2}{3}\, V_D/R_O}{\tfrac{1}{2}\, V_H/R_O} = \tfrac{4}{3}\, V_D/V_H$$
$$V_D/V_H = \tfrac{3}{4}\sqrt{2} = 1.061$$
$$I_D/I_H = \frac{2\sqrt{2}}{3} = 0.943$$
$$P_D = V_D I_D = V_H I_H = P_H$$

$$R_H = \tfrac{2}{3} R_O$$
$$I_H = V_H/R_H = \tfrac{3}{2}\, V_H/R_O$$
$$I_{HO} = I_H/3 = \tfrac{1}{2}\, V_H/R_O$$
$$P_H = V_H \times I_H = \tfrac{3}{2}\, V_H^2/R_O$$

"H-OPERATION"

Fig. 2.4. Coil Wiring Diagram for D^+ and H^+ Operation.

Three independent circuits will be involved; booster coils inboard of the mirror coils (5 Mw in D operation), mirror coils (12 Mw in D operation), and booster coils outboard of the mirrors (3.5 Mw in D operation). The current regulators now in use on the several generators have been found capable of maintaining the desired current ratios with adequate precision.

The coils will be made up of "pancakes" formed by the spiral winding of hollow copper conductors. In order to achieve relatively short tube lengths per coolant flow path, the technique of multiple parallel water channels has been adopted. Figure 2.5 shows a model for eightfold parallel water flow.[7] The first water circuit starts at (1) and spirals in the front plane to (2). Here, the conductor is bent to the rear plane of the pancake and spirals out to (3), which is a hydraulic exit point. The electric current, however, might be conducted over a short jumper back to the front plane to the second parallel water circuit. This circuit starts at

[7]The model uses a different color for each parallel water path.

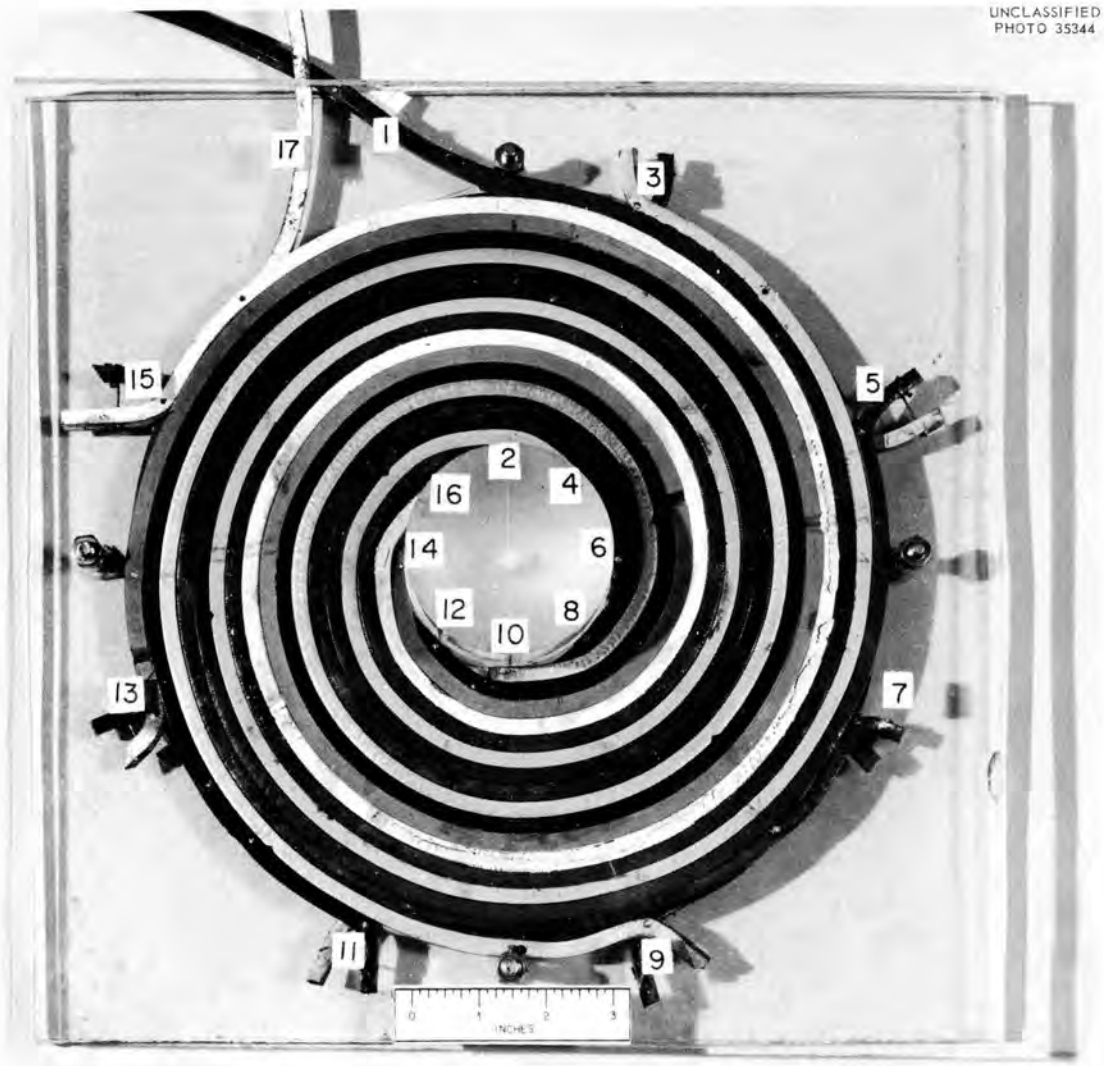

Fig. 2.5. Model for Eightfold Parallel Water Flow.

(3) in the front plane, spirals in to (4), is here bent to the rear plane, and comes out at (5). Altogether, there are eight parallel water paths, whereas the turns can be electrically connected either all in series or in 2, 4, or 8 parallel paths.

Providing the necessary current densities in the presence of the other requirements will require adjustable shunts on the individual coils. It is hoped that the shunt currents can be limited to 1% of the total.

Measurements are being made which will determine whether it will be necessary to compensate for the fields resulting from the polarization of the building's structural steel.

2.4.2 Injection

The initial experiments on high-current 600-kev beams are described elsewhere in this report. It is too soon to be able to say what angular divergence can be achieved.

The source for these high-current ion beams has been under development for nearly two years.[8] It employs the "duo-plasmatron" principle suggested by M. von Ardenne.[9] Currents up to 340 ma at 80 kev have been obtained. Mass analysis carried out at currents up to 100 ma has shown that at this range a 70% H_2^+ yield may be obtained. Details of the source at the present level of development are given elsewhere in this report.

The accelerator tube to be used with DCX-2 is described in a previous report.[10] It is being used now in the experiments on high-current 600-kev beams. This tube avoids the necessity of pre-acceleration focusing by use of high-voltage gradients and minimization of the drift regions, particularly at the low-energy end. By this means it is possible to provide sufficient bore to enable the beam to avoid striking the electrodes, in spite of beam divergence.

The acceleration takes place in four equal voltage steps. All gaps, considered as lenses, have focal lengths too long to be important to the ion optical properties of the tube.

The two magnetic solenoid lenses provided for convergence of the beam below the tube both have 6-in.-dia bores and minimum focal lengths of 16 in. for H_2^+ ions at 600 kev. Figure 2.6 shows a typical beam profile through the injection system.

No provision has been made for electromagnetic steering of the beam. Beam bending devices have the difficulty of being energy-dependent, and with the large power densities in the beam small energy changes may result in excessive heating of unprotected surfaces. To avoid the necessity for

---

[8] Thermonuclear Project Semiann. Reps. ORNL-2457, ORNL-2693, and ORNL-2802.

[9] M. von Ardenne, Tabellen der Electronenphysik, Ionenphysik, und Übermikroskopie, VEB Deutscher Verlag der Wissenschaften, Berlin, 1956.

[10] R. C. Davis et al., Thermonuclear Project Semiann. Rep. July 31, 1959, ORNL-2802, p 67.

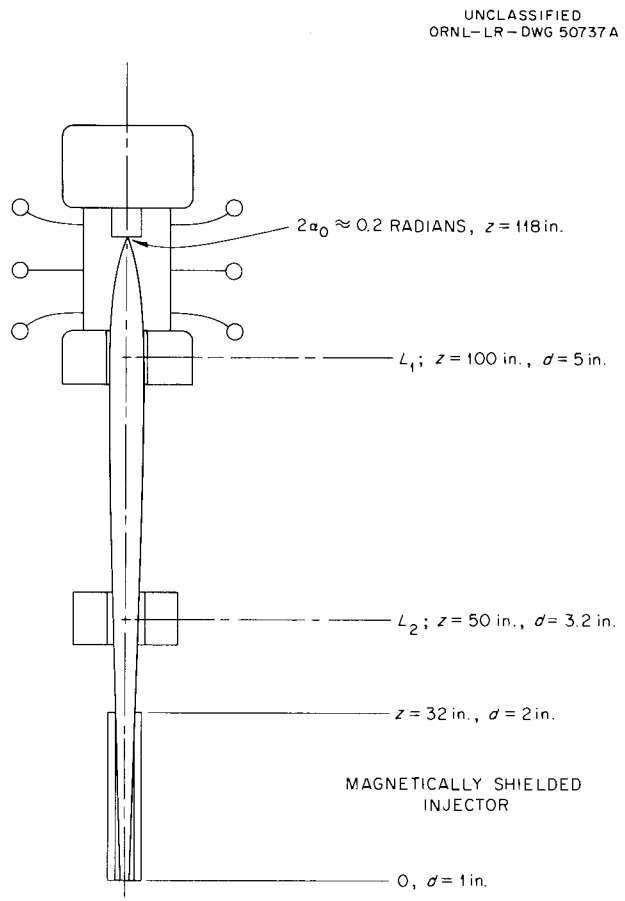

Fig. 2.6. Beam Profile Through Injector at Maximum Current (400 ma).

these devices, provision is being made for movement of the whole accelerator assembly for alignment. Stray magnetic fields (~150 gauss) will be shielded against in the tube.

The injector snout, which provides magnetic shielding for the molecular ion beam, is similar to a design described by Gilbert[11] based on an idea attributed to Christofilos[11] and Rabi.[12] It consists of two elements: The outermost is a set of current-carrying leads wound so as to produce within them a uniform field opposite in direction to the applied field. Coaxial within these leads is a set of high-permeability cylindrical shells. A schematic drawing appears in Fig. 2.7. In principle the field on the axis of such a device can be reduced to any desired value, and the arrangement can be made to produce no perturbation in the external field except

[11]F. C. Gilbert, A Beam Inflector, UCRL-5698 (1960).

[12]A. Ruark, private communication.

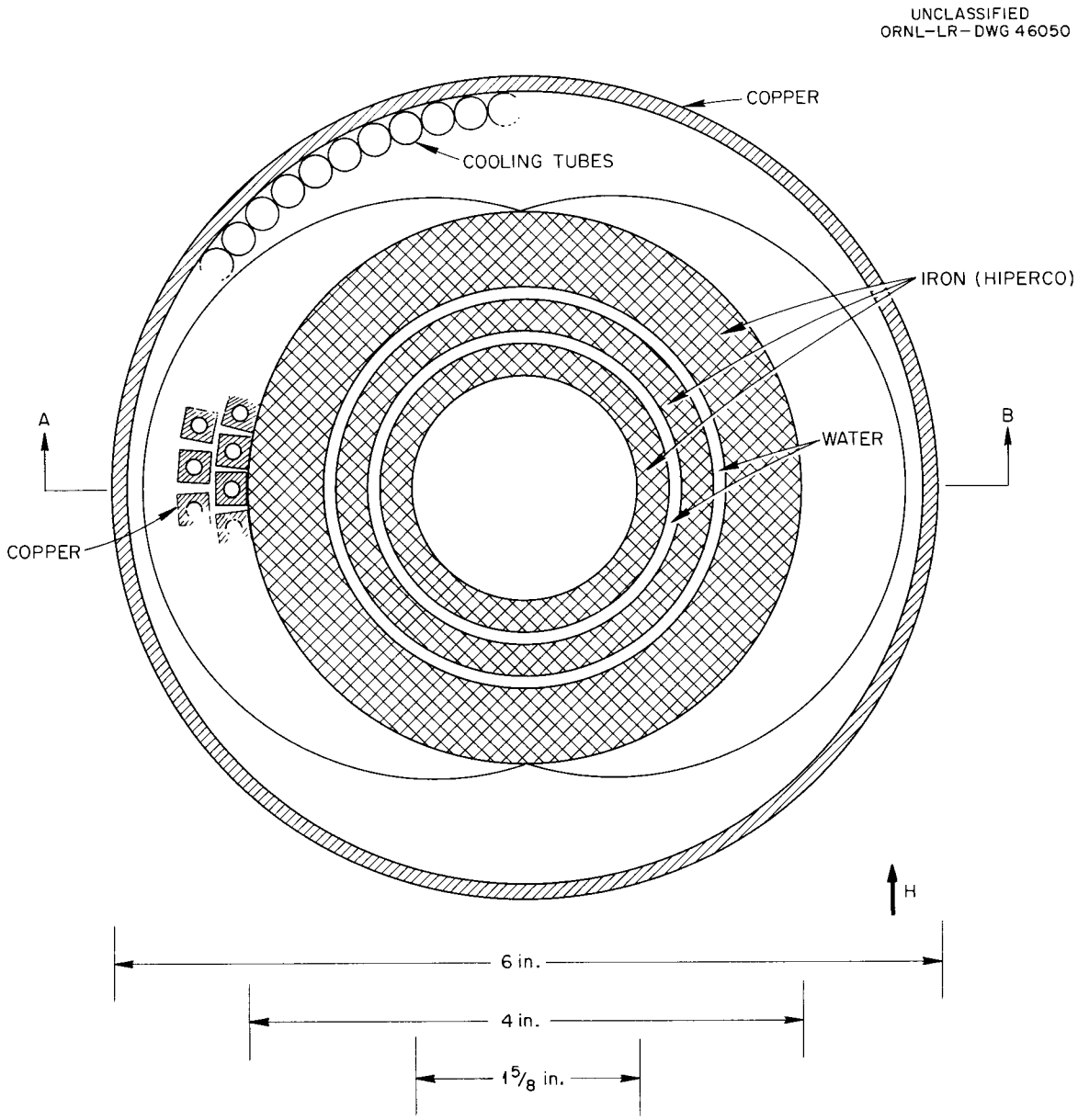

Fig. 2.7. Cross Section of Injection Snout.

for end effects. These have not yet been evaluated. The detailed design is proceeding and tests on a preliminary model are under way.[13]

2.4.3 Vacuum

There are two major features which determine the outlines of the vacuum system design. The first of these is the need to accommodate any one of several types of gas arc. The most stringent requirements are imposed

[13]This report, sec 8.5.

by a deuterium arc[14] which operates with 5 atmospheric cm^3 of deuterium per sec. To handle this gas and still provide a pressure near 10^{-7} mm Hg in the central region of the machine there will be two 32-in. diffusion pumps on the cathode end and two stages of differential pumping between the cathode and the central region.

In order to maintain 10^{-7} mm Hg in the central region in the presence of the beam's 1/2 amp of incoming molecular ions, all of which eventually get converted to hydrogen gas, a pumping speed of about 10^6 liters/sec is required. The ion pumping action of the trapped plasma is expected to accomplish this. Molecules which drift into the plasma region will be ionized. The ions so produced will be constrained to follow magnetic-field lines and will eventually drift outside the mirrors, where they will recombine. It is proposed to make the pumping speed in the region outboard of the mirrors approximately 10 times the conductance through the throat of the mirror coils, so that only 10% of the gas will return to the central region. A part of the motivation for the high mirror ratio (3.5) is the possibility of minimizing the gas conductance through the throats of the mirror coils. It appears that this conductance (on each end) can be limited to 2000 liters/sec for hydrogen gas without interfering with the flow of cold ions through the mirror throat. Accordingly, a pumping speed of 20,000 liters/sec is required in each "ballast" region immediately outside the mirror coils. The pressure which must be maintained there is 10^{-6} mm Hg; pumping will be by evaporated titanium. Experiments by Neidigh[15] and Clausing[16] have demonstrated that such pumping speeds are well within the range of capability of evaporators presently in use. The intermediate differential pumping region will be maintained at 10^{-5} mm Hg by similar titanium pumping, although only about 5000 liters/sec pumping speed is required. All titanium pumps will be supplemented by well-trapped oil diffusion pumps.

---

[14]R. A. Gibbons *et al.*, Thermonuclear Project Semiann. Rep. Jan. 31, 1960, ORNL-2926, p 47.

[15]R. V. Neidigh, personal communication.

[16]R. E. Clausing, personal communication. Also, this report, chap. 11.

Just as in DCX-1 the central vacuum region will be surrounded by a mechanically sealed water-cooled copper liner. The region outside the liner will be connected to the intermediate vacuum region for pumping purposes. A schematic diagram of the differential pumping system is given in Fig. 2.8.

The details of the multiple differential pumping arrangement are peculiar to the deuterium arc. They probably will not be necessary for the carbon or metal-vapor arcs which are also contemplated, and certainly not for OGRA-type operation.

It is proposed to clean the inner surface of the liner by operation of a strongly radiating argon arc. Provision is being made to allow the liner to come up to high temperatures during the cleanup process, although it has not yet been demonstrated that this is necessary.

UNCLASSIFIED
ORNL-LR-DWG 46144

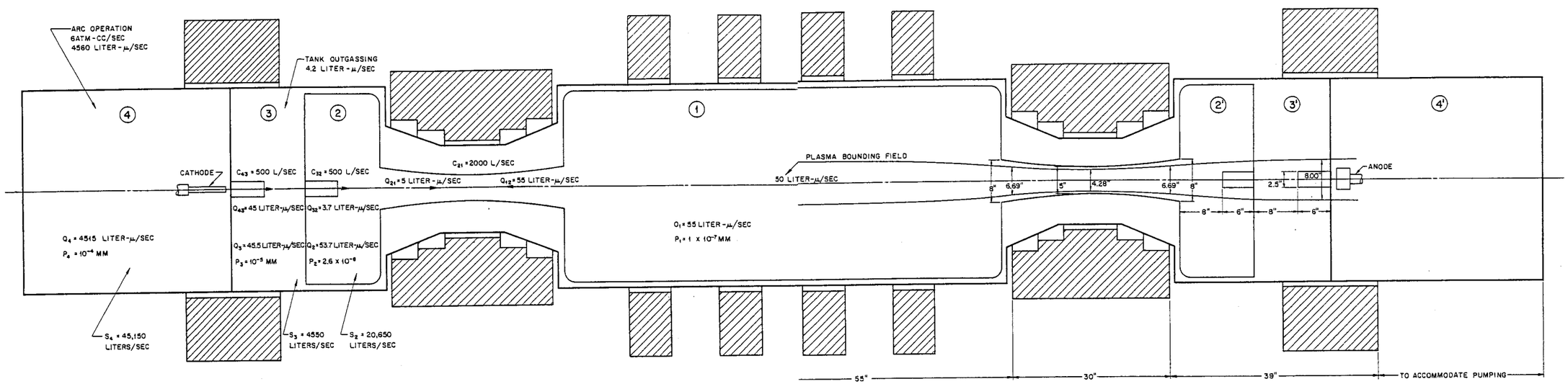

Fig. 2.8. Schematial Pumping System.

3. DCX-EP-B DESIGN AND SUPPORTING WORK

Since a portion of the work covered by the above title is in the "Official Use Only" category the entire chapter has been deleted. The chapter is being issued concurrently with this report but with an Official Use Only designation and is numbered ORNL-3044.

4. VACUUM ARC RESEARCH

4.1 THE CARBON ARC

4.1.1 Microscopic Properties of the Carbon Arc (University of Chicago Laboratories for Applied Sciences)

Editor's note: The Oak Ridge National Laboratory has a subcontractural arrangement with the University of Chicago Laboratories for Applied Sciences, to provide for experimental and theoretical work on vacuum arcs. The subcontract is administered under the direction of P. R. Bell. We have chosen an extract of their semiannual report[1] for reproduction here, because it gives a neat summary of knowledge of the vacuum carbon arc as developed at ORNL and at Chicago. The names associated with the Chicago report are as follows: M. Blidy, P. J. Dickerman, H. Halle, J. R. Hoenig, T. R. Hogness, J. C. Morris, S. J. Nicolosi, E. N. Parker, E. J. Pekol, C. F. Price, V. J. Raelson, F. F. Rieke, D. A. Tidman, and M. L. Weber.

Theoretical Considerations

"This section lists orders of magnitude for several microscopic parameters of the vacuum arc, using the atomic weight of carbon to characterize the ions. While most of them probably have been calculated previously and others make use of previously obtained experimental data, they are given here to illustrate values we shall use in interpreting any experimental data obtained during the remainder of the contract period.

"There are a number of elementary theoretical conclusions that can be reached from the gross observational data concerning the high-energy carbon arc.

"Typical values for the electron and ion temperatures are quoted as 4 ev and 50 ev, respectively, in the presence of fields of the order of 4000 gauss along the arc. The corresponding thermal velocities are 1.3×10^8 cm/sec for the electrons and 4.2×10^6 cm/sec for carbon ions. The

---

[1] Investigation of High-Current Arcs in Vacuum and Strong Magnetic Fields, Semiannual Report, Sept. 16, 1959–Mar. 31, 1960, LAS-SR-M181-5, p 21–24.

electron cyclotron frequency and radius are 6.4×10^{10} radians/sec and 2×10^{-3} cm. For a singly charged carbon ion, they are 3.33×10^{6} radians/sec and 1.26 cm. Clearly the arc radius cannot be smaller than the ion cyclotron radius. If we take the density in the arc to be $10^{14}/cm^3$, then the electron partial pressure (for singly ionized atoms) is 5.6×10^{2} dynes/cm^2, and the ion partial pressure is 7×10^{3} dynes/cm^2. Taking the ion-ion collision cross section to be of the order of 10^{-16} cm^2, the mean free path is 10^{2} cm, and the collision frequency is 4×10^{4} collisions/sec. A similar cross section for electron-ion collisions gives a collision frequency of 1.3×10^{6} collisions/sec, yielding an electron mean free path of about 10^{2} cm. Such collisions are important only for the electrons and have little effect on the ions. The electron-electron mean free path is of the order of 0.2 cm so that the collision frequency is 6×10^{8}/sec.

"It can be seen that the ions and the electrons both have a collision frequency which is low compared to their cyclotron frequency. To estimate their diffusion rates across the field, let us compute the time t required to random walk a distance L with one step of length ℓ every τ seconds. Obviously ℓ is of the order of the cyclotron radius and $1/\tau$ is the collision frequency ν. We have $t \cong L^2/\ell^2\nu$. Thus with L = 1 cm, we have $t \cong 4 \times 10^{-4}$ sec for the electrons, which is a mean diffusion velocity of 2.4×10^{4} cm/sec. For the ions $t = 1.6 \times 10^{-5}$ sec, for a mean drift velocity of 6×10^{4} cm/sec. It follows that the singly charged ions diffuse somewhat faster than the electrons by virtue of their larger cyclotron radius. Thus we expect the center of the arc to show a slight deficiency of ions, producing a radial electric field directed inward toward the axis of the arc. If ϕ is the potential difference between the axis and the edge of the arc, we expect that ϕ will grow to some value comparable to the thermal energy, $\phi = O(kT_i/e)$, where T_i is the ion temperature. Thus, presumably, if we can measure ϕ, we have a measure of T_i.

"If L is the radius of the arc, then ϕ results in a radial electric field, $E \cong -\phi/L$, which, in the presence of the field B along the arc, leads to an azimuthal velocity v_ϕ given by $v_\phi = cE/B = (c/B)(-\phi/L)$.

"If T_i has the observed value of about 50 volts, it follows immediately that $\phi = 50$ volts. With B = 4000 gauss, L = 1 cm, we have v_ϕ of the order of 12 km/sec.

"The electron conductivity is $\sigma \cong 10^7 T^{3/2}$ esu. If the electron temperature is 4 volts (4×10^4 °K), then $\sigma \cong 10^{14}$ esu. It follows that an electric field along the arc of, say, 0.5 volts/cm yields a current density of the order of 1.7×10^{11} esu, or 60 amps/cm^2, in rough agreement with the current density in the arc.

"The mean free path of an ion is comparable to the length of the arc, so that if E is the electric field along the arc, w the resulting ion velocity, t_i the mean time between ion-ion collisions, and M the ion mass, we have a mean ion drift of something like $\langle w \rangle = ZeEt_i/2M$ if we assume that the principal impediment is other ions. For singly charged carbon ions in 0.5 volts/cm, we have $\langle w \rangle = 5 \times 10^5$ cm/sec, so that the ion current density is 2.4×10^{10} esu or 10 amps/cm^2. Thus, if there were many doubly or triply charged ions, the ion current, being proportional to Z^2, could become comparable to the electron current. The mean free drift, between collisions, for an ion is $\langle w \rangle t_i$, which is 12 cm. The mean drift $\langle w \rangle$ should appear as a Doppler shift of the line center when the arc is viewed spectroscopically along its length.

"Now consider the characteristic frequencies of oscillation in the arc. The plasma frequency is $\nu_p = 10^4 N^{1/2}$ or about 10^{11} cps. The hydromagnetic wave velocity $B/(4\pi NM)^{1/2}$ is 250 km/sec for $B = 4 \times 10^3$ gauss. Thus the fundamental hydromagnetic frequency in an arc of length s is $B/2s(4\pi NM)^{1/2}$, or 0.25 megacycles for s = 1 meter. The characteristic hydromagnetic decay time is $r^2\sigma/c^2$, in terms of the characteristic length r. If r is 1 meter, this is 10^{-3} sec, whereas if r is comparable to the diameter of the plasma column, say $r \cong 1$ cm, we have 10^{-5} sec. Thus the hydromagnetic waves may be simply damped.

"Thus we expect disturbances with characteristic frequencies in the neighborhood of 1 megacycle as the result of hydromagnetic motions and as the result of the ion cyclotron frequency. We expect disturbances with characteristic frequencies in the neighborhood of 10^{10} to 10^{11} cps as the result of plasma oscillations and as the result of the electron cyclotron frequency. We expect coupling between hydromagnetic motions and ion cyclotron motions, and between plasma oscillations and electron cyclotron motions, so that there may be no pure hydromagnetic and plasma oscillation modes."

4.1.2 Ion Drifts in the Carbon Arc

M. R. Skidmore

Doppler shifts corresponding to ordered ion drifts along the carbon arc in a magnetic field have been reported.[2,3] These previous observations indicated that the drift velocity of the carbon ions was toward the cathode in the anode region but that it decreased essentially to zero as the ions approached the cathode. This suggested the existence of an important mechanism for ion loss from the arc column as the ions drifted toward the cathode.

A flat, beveled cathode was used to permit spectral study along the arc of the weak peripheral region of the arc column. This geometry eliminated the very strong spectral contribution from the core of the arc usually associated with a viewing direction within a few degrees of the arc axis. The results of such an observation are illustrated in Fig. 4.1, which corresponds to a stigmatic echelle spectrogram of the carbon arc in a magnetic field. The bright cathode surface is indicated by the vertical continuum of wavelengths. To the right of this vertical is the very broad C^{++} spectral triplet. To the left are seen the same spectral lines associated, however, with the peripheral portion of the arc column in the region of the cathode tip. It is observed that the Doppler shift given by atoms radiating in this outer region of the arc is to the red with respect to atoms radiating in the core. Thus, the radiating ions are moving away from the spectrograph and hence toward the cathode end of the system. It has been determined that the C^{++} ions have an average drift energy of about 27 ev toward the cathode in this peripheral region of the arc. Normally, the luminous core, having negligible drift, is so bright as to subdue spectral effects associated with the weak radiation in the peripheral region of the arc. This may account for the earlier apparent anomaly of no or little drift observed near the cathode. The

---

[2]M. R. Skidmore, J. R. McNally, Jr., and G. K. Werner, Bull. Am. Phys. Soc. 4, 388 (1959).

[3]J. R. McNally, Jr., et al., Thermonuclear Project Semiann. Rep. Jan. 31, 1960, ORNL-2926, p 34.

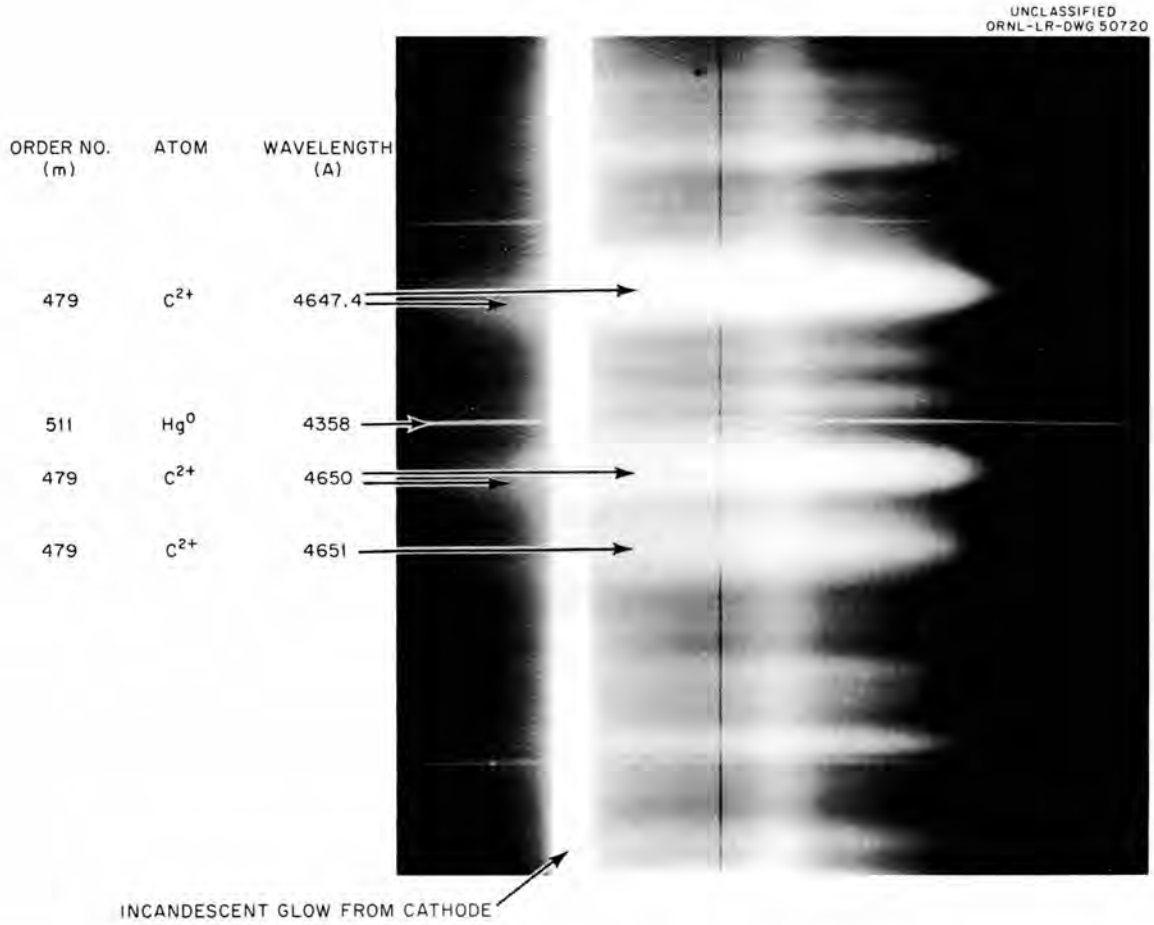

Fig. 4.1. Ion Drift in the Peripheral Region.

present interpretation also appears to be consistent with the asymmetry observed in comparing measured line profiles with theoretical Gaussian profiles reported earlier.[3] This asymmetry, being a tail on the high wavelength side of the line spectra of the arc core, is probably due to atoms radiating in the peripheral region of the arc.

Studies were made of the line profiles of different ionic species in the carbon arc in the Long Solenoid in order to ensure that the quantitative evaluation of the C^{++} 4650 A triplet in terms of a Gaussian profile, and hence temperature, was consistent for other lines of the same ion species as well as different ion species. Preliminary observations (see Fig. 4.2) of the 5812-A line of C^{+++} indicate line broadening of the same magnitude as the 4650-A line group measured previously.[2,3]

Inasmuch as the echelle dispersion is inversely proportional to the spectrum order number the actual line widths illustrated in Fig. 4.2 are somewhat less than in Fig. 4.1 and Fig. 4.3. Figure 4.3 is an almost-axial spectral view of the carbon arc but taken for a case involving a hollow cathode. The two long streaks across the spectrum lines are the continuum

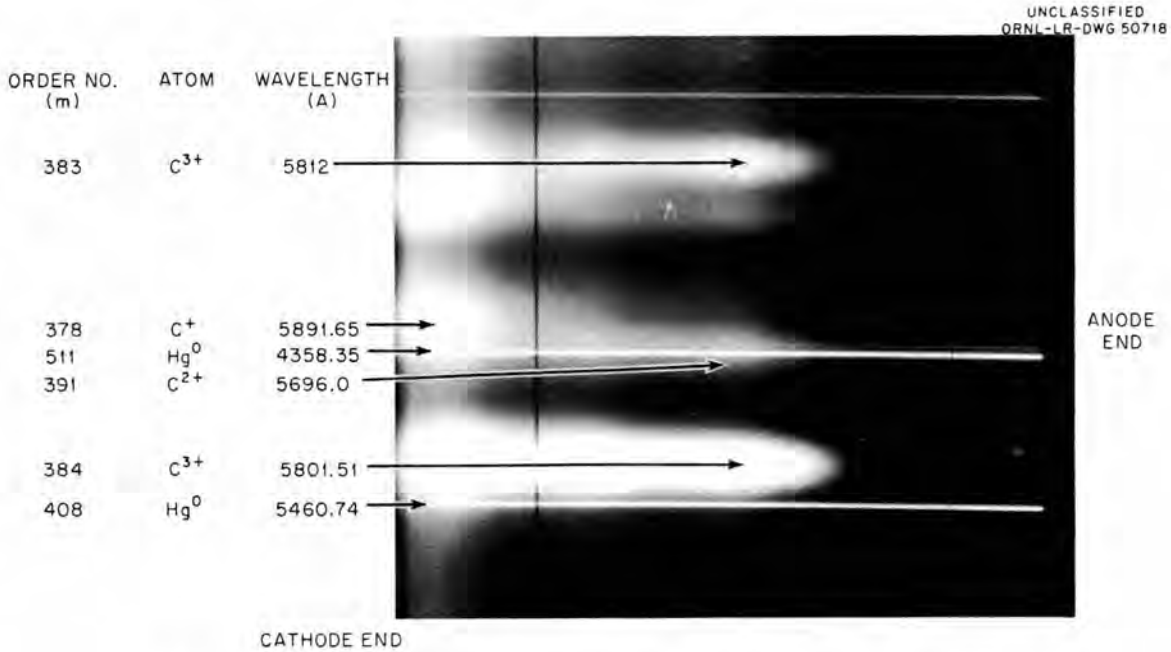

Fig. 4.2. Doppler Broadening of Various Ions of Carbon.

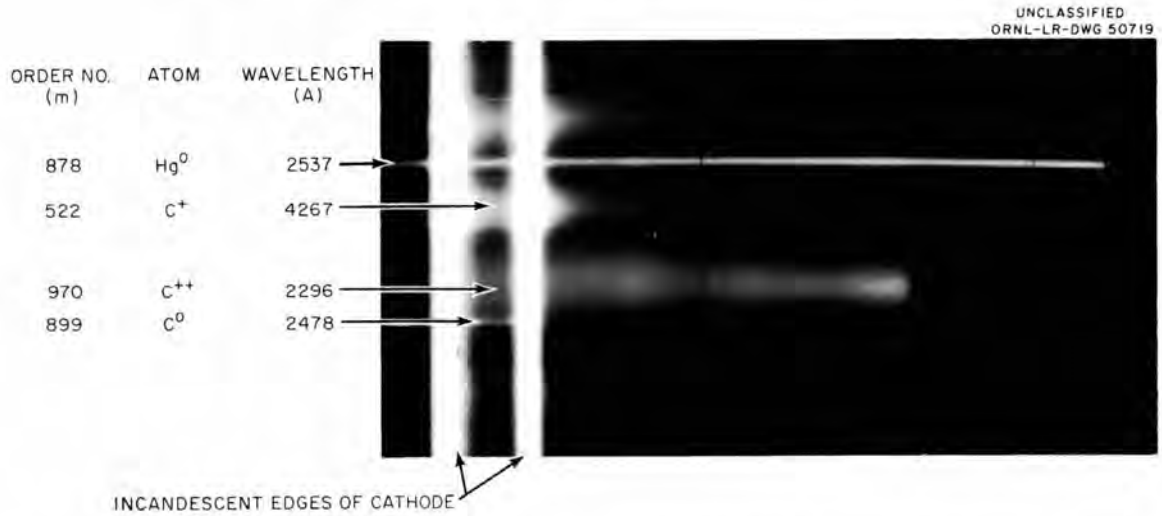

Fig. 4.3. Doppler Broadening and Spatial Distribution of Spectra in 5-ft Carbon Arc.

radiation from the incandescent edges of the hollow cathode, and the space between them represents the interior of the cathode. Note that the sharp 2478-A line of neutral C exists only inside the hollow cathode and shows the characteristic Zeeman doubling due to the σ polarization components. The intensity of C^+ (4267 A) is also high only in the region of the cathode but broadening is very marked indicating high ion velocities. The 2296-A line of C^{++} occurs all along the arc and, like the C^{++} 4650-A triplet group, reveals marked Doppler broadening. The temperatures estimated from the half-widths of C^{+++} lines and the 2296-A C^{++} line agree approximately with the earlier quantitative measurements[2,3] on the 4650-A C^{++} group (~800,000°K) and hence support the viewpoint that there is very probably a local thermodynamic equilibrium for the ions.

Quantitative studies will be made of ion drifts and line broadenings for all ion species at different axial and radial positions in the arc as soon as the new Long Solenoid Facility is in operation.

4.1.3 Effect of Arc Current Variations on the Doppler Width of C^{++} Lines in the Long Solenoid

P. M. Griffin G. K. Werner

A series of observations was made of the Doppler broadened line of C^{++} from a 54-in. carbon arc in the "old" Long Solenoid Facility.[4] Arc currents ranged from 150 to 500 amp. Care was taken to obtain exposures over the entire range of measurable densities so that photometric errors would be minimized. The half-width of the line λ 4647 A, as observed with a 1.8-m Bausch and Lomb echelle spectrograph, was determined for all exposures obtained. Experimentally predetermined weighting factors, based only on photometric considerations, were used in the averaging of results.

The width of the line at half the peak intensity decreased as the arc current was increased as shown in Fig. 4.4. However, other parameters of the system such as tank pressure, arc voltage, and the partial pressure of impurities in the arc also changed as the arc current was increased.

---

[4] J. F. Potts *et al.*, *Thermonuclear Project Semiann. Rep. Jan. 31, 1959*, ORNL-2693, p 41.

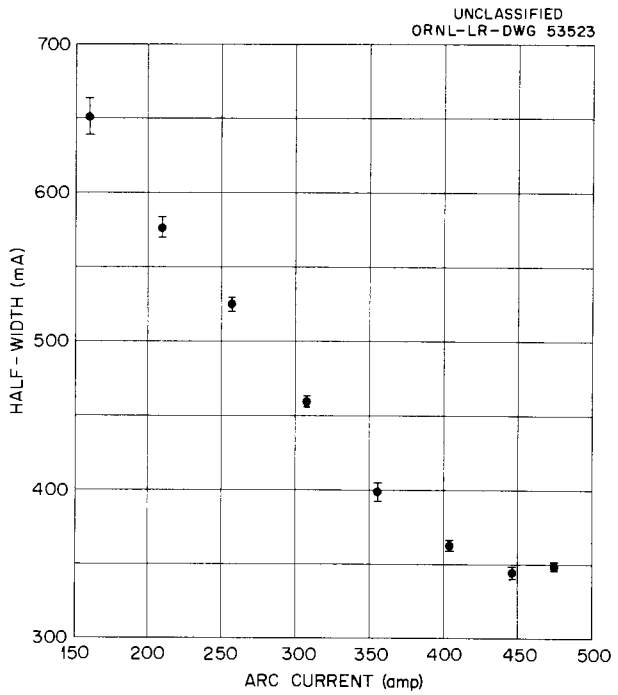

Fig. 4.4. Half-Width of λ 4647 A at Various Arc Currents.

It is thus possible that the decrease in line width was a consequence of these other changes; for example, analysis of the data in Table 4.1 indicates a good correlation of line width with tank pressure using the relationship $\omega = 61\ p^{-0.20}$; however, this correlation may be fortuitous.

Further investigation of this problem is continuing using data from the "old" facility plus anticipated experiments with the new and more powerful solenoid now under assembly. In addition, improved methods of intensity measurement and data reduction are being developed which will make feasible much more extensive investigations of this type.

4.1.4 Density of Ions Outside a Magnetically Confined Vacuum Arc

R. G. Alsmiller

The equations governing the density of a single ion species outside a magnetically confined arc have been extended to include the linear diffusion due to the residual vacuum as well as the nonlinear diffusion included previously.[5] The equations may be solved in the case of a linear

[5]R. G. Alsmiller, Jr., Thermonuclear Project Semiann. Rep. Jan. 31, 1960, ORNL-2926, p 64.

Table 4.1. Half-Width of the λ 4647 A C^{++} Line at Various Arc Currents

Arc length: 54 in.
Magnetic field: 2600 gauss
Point of observation: transverse view at midplane

Arc		Tank Pressure at Cathode End (mm Hg)	Number of Determinations of Half-Width, n	Average Half-Width and Probable Error* (mA)
Current (amp)	Voltage (v)			
		$\times 10^{-5}$		
158	97	0.9	7	651 ± 13
208	107	1.32	9	577 ± 7
256	112	1.85	12	525 ± 4
307	121	4.25	11	460 ± 3
355	127	9.75	9	399 ± 6
404	134	13.8	9	363 ± 3
447	140	16.0	9	345 ± 4
475	145	18.0	7	349 ± 2

$$*P.E. = t_{0.5,n}\sqrt{\frac{\Sigma w_i(\bar{\omega} - \omega_i)^2}{(n-1)\,\Sigma w_i}}\ , \text{ where } \bar{\omega} = \frac{\Sigma w_i \omega_i}{\Sigma w_i}\ .$$

geometry, but only approximate limiting solutions have been obtained in a cylindrical geometry. The primary effect of the linear diffusion is to make the particle density go to zero much more slowly than in the purely nonlinear case.

A comparison has been made between the calculated particle density and the experimental results of Neidigh.[6] Unfortunately the arc used by Neidigh contained several ion species, so the one species theory applies only in a very approximate way if at all. (The equations governing the diffusion of two ion species have been considered and it seems that collisions between the two ion species are not negligible, but the equations

[6]R. V. Neidigh, Thermonuclear Project Semiann. Rep. July 31, 1959, ORNL-2802, p 31.

are completely intractable so no quantitative results have been obtained.) On the basis of the one species theory the magnetic field dependence is approximately that obtained by Neidigh, but the behavior of the C^+ ions as compared to the C^{++} ions is not in agreement with the experimental results.

4.1.5 Randomizing of Electrons in the Carbon Arc

J. R. McNally, Jr.

The single particle and multiple small angle scattering theory of electrons gives[7]

$$\Delta\theta = \frac{2Z_1Z_2e^2}{bmv^2} \quad \text{(single particle scattering)} \quad ,$$

and

$$(\Delta\theta)^2 = 8\pi n\lambda\left(\frac{Z_1Z_2e^2}{mv^2}\right)^2 \ln\left(\frac{b_{max}}{b_{min}}\right) \quad \text{(multiple small angle scattering)} \quad ,$$

where $\Delta\theta$ is the angular deflection (in radians) of the electron ($Z_1 = 1$) per collision with an ion of charge Z_2 and at an impact parameter distance b; e, m, and v are the electron charge, mass, and velocity; b_{max} and b_{min} are the distances of maximum approach (the Debye distance, $\sqrt{KT/4\pi ne^2}$) and minimum approach ($2e^2/mv^2$ for electrons on electrons); n is the ion density; λ is the mean free path for a random walk through an angle of $\sqrt{(\Delta\theta)^2}$. The value of ln (b_{max}/b_{min}) is usually taken to be about 10 (ref 8). Choosing $n \cong 10^{14}$ cm^{-3}, $Z_{eff} \cong 3$, and various values of $\Delta\theta$ and $\sqrt{\Delta\theta^2}$, we compute Tables 4.2 and 4.3. Thus, one can conclude from these simple calculations that for electrons in the carbon arc and at a mean electron energy of about 5 ev ($v \cong 1.3 \times 10^8$), a single scattering event producing a 57° scatter angle has an effective cross section of about 8×10^{-14} cm^2 and will occur on the average in a distance of about 0.13 cm. This is the maximum Z distance on the average that an electron moves before such a single scattering

[7]A. Simon, An Introduction to Thermonuclear Research, Pergamon Press, London, 1959.

[8]L. Spitzer, Physics of Fully Ionized Gases, Interscience, New York, 1956.

Table 4.2. Impact Parameter, Effective Cross Section, and Mean Free Paths for Various Single Particle Scattering Angles

v, Electron Velocity (cm/sec)	$\Delta\theta$, Angle of Scatter (radians)	b, Impact Parameter Distance (cm)	$\sigma = \pi b^2$, Effective Cross Section (cm^2)	$\lambda = 1/n\sigma$, Mean Free Path (cm)
1×10^8	0.001	1.6×10^{-4}	8×10^{-8}	1.3×10^{-7}
1×10^8	0.01	1.6×10^{-5}	8×10^{-10}	1.3×10^{-5}
1×10^8	0.1	1.6×10^{-6}	8×10^{-12}	1.3×10^{-3}
1×10^8	1.0	1.6×10^{-7}	8×10^{-14}	1.3×10^{-1}
1×10^9	0.1	1.6×10^{-8}	8×10^{-16}	1.3×10^{1}
1×10^9	1.0	1.6×10^{-9}	8×10^{-18}	1.3×10^{3}

Table 4.3. Mean Free Path to Effect Multiple Scatter to Random Angles at Different Electron Velocities

v, Electron Velocity (cm/sec)	$\sqrt{(\Delta\theta)^2}$, Effective Angle of Scatter (radians)	λ, Mean Free Path (cm)
1×10^8	0.1	7×10^{-5}
1×10^8	1.0	7×10^{-3}
1×10^9	0.1	7×10^{-1}
1×10^9	1.0	7×10

event. For the energetic electrons far in the tail of the distribution ($v \cong 10^9$ cm/sec) single particle scattering is negligibly small.

Multiple small angle scattering leads to much shorter mean free paths; for example, at 57° it occurs on the average in 0.007 cm at $v \cong 10^8$ cm/sec and in 70 cm at $v \cong 10^9$ cm/sec. Thus, the possibility exists that only a very few runaway electrons can be found in the carbon arc and then only if randomization permits populating the distribution at $v = 10^9$ cm/sec (~400 ev) or if high frequency fields permit acceleration to these energies, since the d-c field in the present carbon arcs is too small to

permit attaining this energy directly. Practically all of the electrons are effectively randomized since in general the "maximum" distance traveled along the arc axis can be λ, yet λ is already quite small. Energy dumping in excitation processes of carbon ions also depletes the high energy tail of the electron distribution.

The essential point is that there are extremely strong randomizing processes for the electrons in the carbon arc. Thus, it is probably not unusual that the mean energy of electron drift toward the anode is only about 0.03 ev compared to the mean energy of random motion of about 5 ev (ref 9).

4.1.6 A Simple Multigroup Treatment of Energy Degradation Due to Electron Heating in the Carbon Arc

J. R. McNally, Jr.

The degradation of the energy of trapped protons in DCX results in a rapid increase in the charge-exchange cross section and decrease in the effective trapping times. Using a simple multigroup treatment analogous to the problem of radioactive decay with branching[10] the effect has been roughed out and comparison may be made with experimental results by Barnett *et al.*[11]

The calculation is based on the rate of energy loss of a hot ion to a sea of cold electrons[12] and is given by

$$\frac{dE}{dt} \cong \left[\frac{4\pi e^4 (n_e \alpha)}{m v_+}\right] \ln \Lambda \quad ,$$

for $v_+ > v_e$, where e is the electron charge, m the electron mass, v_+ the ion velocity, and v_e the electron velocity. The term $(n_e \alpha)$ is the effective electron density of the carbon arc distributed through the plasma

---

[9] M. R. Skidmore, J. R. McNally, Jr., and G. K. Werner, *Thermonuclear Project Semiann. Rep. Jan. 31, 1960*, ORNL-2926, p 38.

[10] G. Friedlander and J. W. Kennedy, *Nuclear and Radiochemistry*, Wiley, New York, 1949.

[11] C. F. Barnett *et al.*, this report sec 1.4.

[12] This differs by a factor of 2 from the expression given by F. C. Gilbert in UCRL-5697 (1959).

volume. The value of ln Λ is about 10 but is a quite insensitive parameter.[13] Thus, one obtains for a 300-kev proton

$$\frac{dE}{dt} \cong 6 \times 10^{-6}(n_e\alpha) \text{ ev/sec} \quad ,$$

and the time for the proton to lose 10% of its energy is about 2.5 msec for $n_e\alpha = 2 \times 10^{12}$. If we define the energy group limits as 300, 270, 243, 219, and 197 kev and particle decay constants as follows (see Fig. 4.5),

$$\lambda_i^* = \frac{1}{\tau_{eh,10\%}} = (n_e\alpha)(5 \times 10^{-9}) \left(\frac{v_o}{v_+}\right) \cong 400 \left(\frac{v_o}{v_+}\right) \quad ,$$

where $\tau_{eh,10\%}$ is the mean time for the proton to lose 10% of its energy, due to cold electron heating. For the decay constant associated with charge-exchange losses in the arc or in the gas,

---

[13] L. Spitzer, Physics of Fully Ionized Gases, Interscience, New York, 1956.

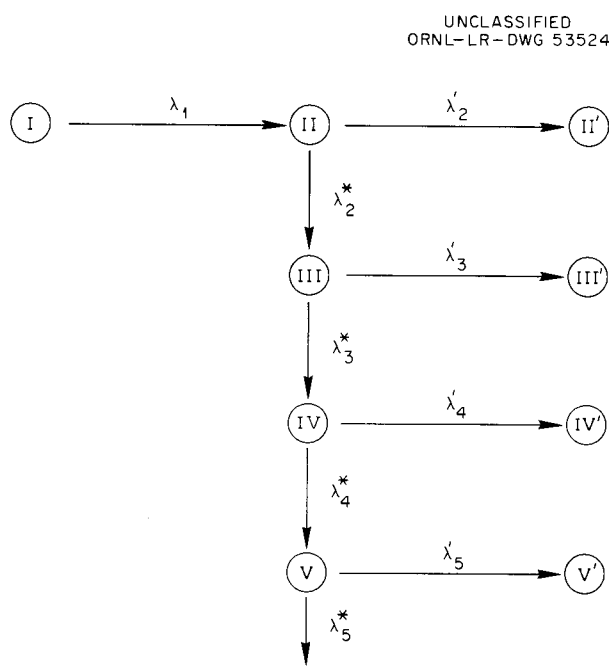

Fig. 4.5. Analogy of DCX Multigroup Method to Radioactive Decay with Branching. I is equivalent to a large source of abundance I and having decay constant λ_1 ($I\lambda_1 = I_2+\eta$ by analogy with DCX and represents the feed rate in particles/sec to the upper energy group of abundance II, etc.).

$$\lambda_i' = \lambda_{c\text{-}x\ arc} + \lambda_{c\text{-}x\ gas}$$

$$\cong (n_e\alpha)(1 \times 10^{-19}) \left(\frac{v_o}{v_+}\right)^6 (v_+) + n_o(1.5 \times 10^{-18}) \left(\frac{v_o}{v_+}\right)^8 (v_+) \quad ,$$

where n_o, the nitrogen density, is taken as 3×10^{10} nitrogen atoms/cm^3 ($p = 5 \times 10^{-7}$ mm Hg), and v_o, the initial energy of the proton, is taken as 7.6×10^8 cm/sec. The selection of parameters for nitrogen losses is only about one-fifth as sensitive as for the arc losses at this low pressure. The term $n_e\alpha$ is taken as 2×10^{12} ions/cm^3. Thus,

$$\lambda_i' = 152 \left(\frac{v_o}{v_+}\right)^5 + 34 \left(\frac{v_o}{v_+}\right)^7$$

and the total decay constant from group i is

$$\lambda_i = \lambda_i^* + \lambda_i' \quad .$$

Table 4.4 gives the decay constants of the selected energy groups (v_+ is arbitrarily chosen as the v at the upper limit of the ith energy group). The equilibrium abundances (at t = 0) as given by [10]

$$N_n = (I_2+\eta) \frac{\lambda_2^* \lambda_3^* \cdots \lambda_{n-1}^*}{\lambda_2 \lambda_3 \cdots \lambda_n} \quad ,$$

Table 4.4. Decay Constants Associated with Selected Energy Groups

Group	E_{upper}, Initial Energy (kev)	λ_i^*, Energy Group Decay Constant (sec^{-1})	λ_i', Particle Loss Decay Constant (sec^{-1})	λ_i, Total Decay Constant (sec^{-1})
II	300	400	186	586
III	270	421	247	668
IV	243	444	329	773
V	219	468	438	906

are for $I_{2+\eta} = 1.5 \times 10^{15}$ particles/sec:

$$II_{equil} = 2.56 \times 10^{12} \text{ particles} ,$$

$$III_{equil} = 1.60 \times 10^{12} \text{ particles} ,$$

$$IV_{equil} = 0.90 \times 10^{12} \text{ particles} ,$$

$$V_{equil} = 0.41 \times 10^{12} \text{ particles} ,$$

$$\Sigma = 5.47 \times 10^{12} \text{ particles} ,$$

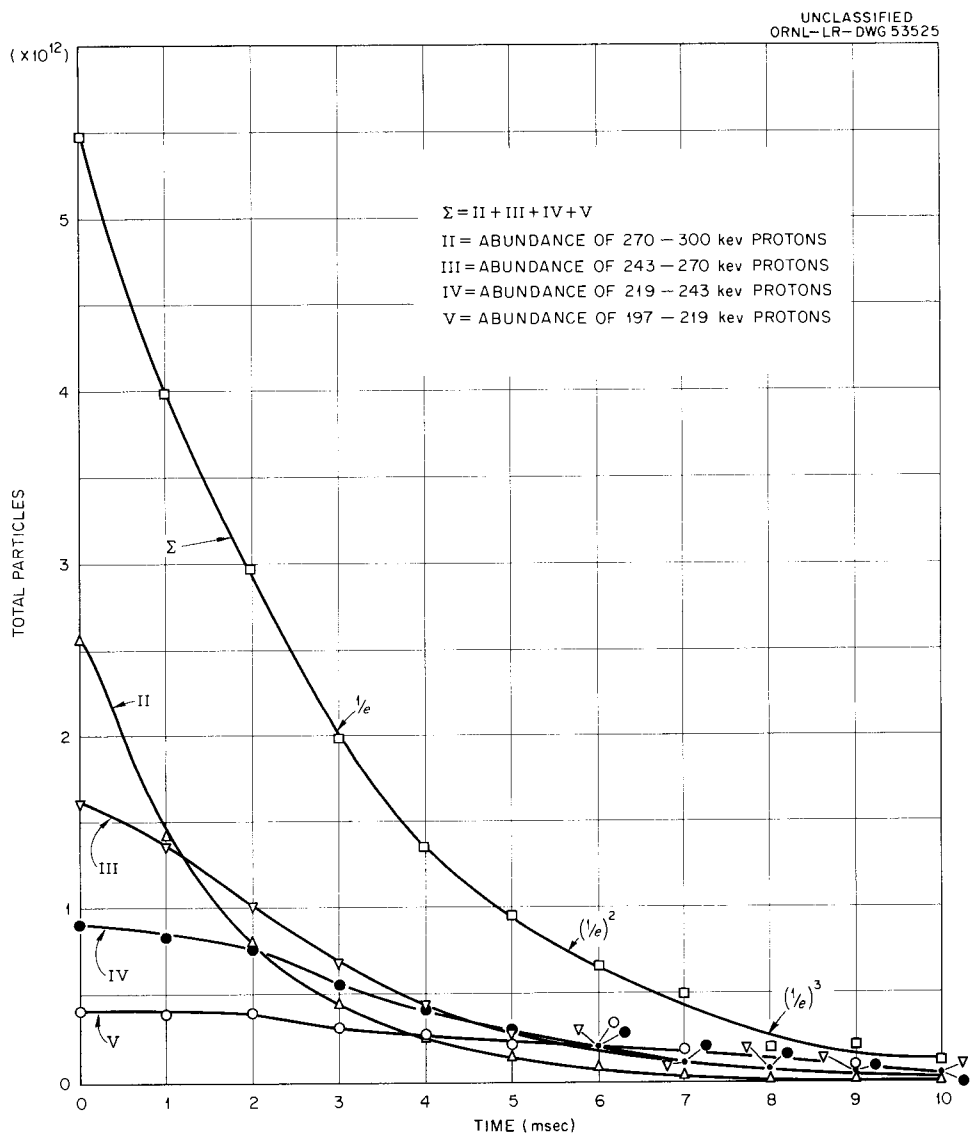

Fig. 4.6. Decay of Proton Groups in DCX-1.

corresponding respectively to 47%, 29%, 16%, and 8% of the total accounted for.

The results of the time-dependent solutions for beam gated-off are given in Fig. 4.6. The variation of the total particle density with time is the sum of the four groups and is denoted by Σ. The e-folding time for Σ is approximately 3.0 msec for the first e-fold τ, about 2.7 msec for the second e-fold τ, and about 2.3 msec for the third e-fold τ. The 3.0 msec value may be compared with the theoretical case for no energy degradation of $\tau = 1000/186 = 5.4$ msec (nitrogen-like background assumed) and compares favorably with the observed τ's reported by Barnett et al.[11]

4.2 THE LITHIUM ARC

4.2.1 Lithium Vapor Arc. Preliminary Experiments

J. S. Culver R. A. Gibbons R. J. Mackin, Jr.
R. F. Rayburn R. M. Warner C. W. Wright

During this period the group conducted preliminary experiments directed toward the application of the principles of the deuterium arc to the operation of an arc fed by lithium vapor. The first version of the arc was operated in a vertical magnetic field. A 1-cm-OD tubular tantalum cathode was used. The anode is shown in Fig. 4.7. The components are a water-cooled copper jacket, a tantalum liner, conical tantalum baffle plates strung on stainless steel support rods, a tantalum boiler cover, and a lithium-boiler pot. The following principles are embodied in the design: the arc runs through the baffles to the boiler cover; the cover radiates heat to the lithium in the pot beneath it and provides a vapor feed; the baffles impede the escape of neutral lithium and provide a high ionization efficiency; lithium which condenses on the baffles runs to the walls and thence back to the pot; the liner has only mechanical contact with the wall and therefore runs much hotter than the wall (however, adjusting the flow of the wall's cooling water provides some control of the liner temperature and hence of the vapor feed).

Vapor feed control was found to be effective and to lie in the desired range, that is, from a well-behaved arc down to extinction. Extreme values of voltage and current were 65 v, 100 amp, and 210 v, 40 amp. The

UNCLASSIFIED
ORNL-LR-DWG 50511

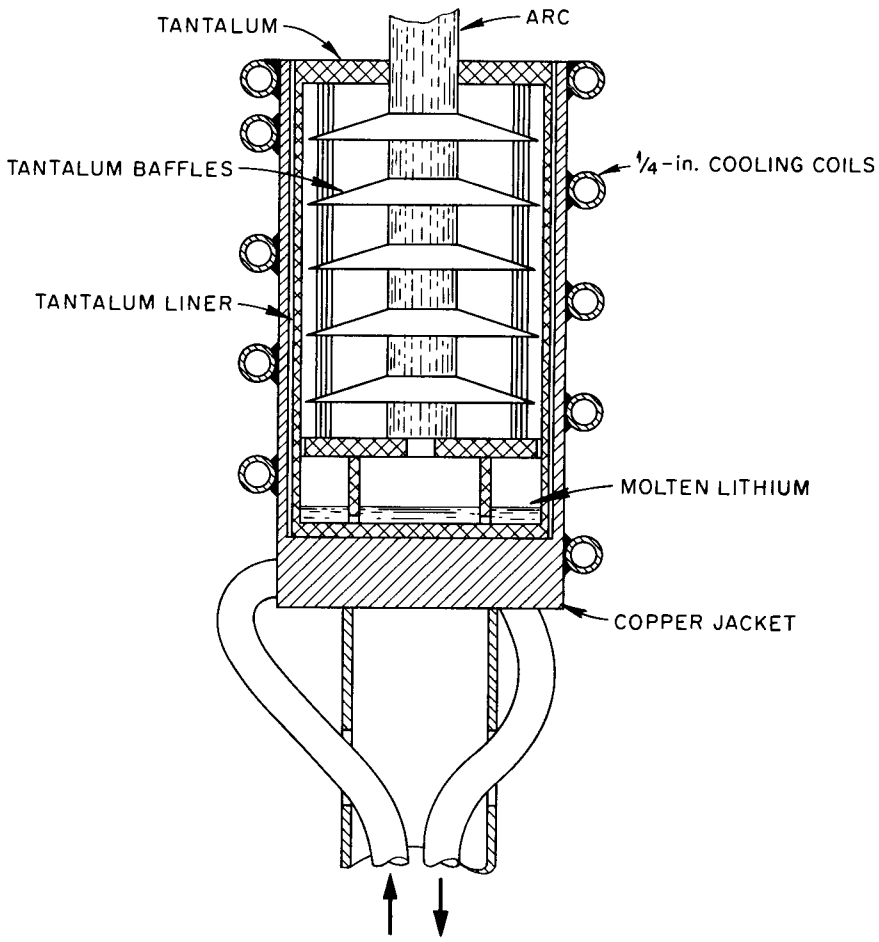

Fig. 4.7. Lithium Anode.

arc was found to act as a "chemical" pump, maintaining a pressure of 1×10^{-5} mm Hg with the diffusion pumps valved off. The pumping speed for deuterium gas was found to be 180 liters/sec, with a few hundred square centimeters of surface covered.

The principles were adapted to lithium arc operation in the PPF (PIG-Pump Facility) in the usual three-region geometry.[14] Again, satisfactory arc operation was achieved, and a base pressure of 4×10^{-7} mm Hg observed. In the central region, spectral lines of neutral lithium were too weak to

[14]R. A. Gibbons, Thermonuclear Project Semiann. Rep. Jan. 31, 1960, ORNL-2926, p 47.

be detected in a 0.5-m Ebert-type scanning spectrometer (Jaco 82,000). Line broadening of the 4672 A line of Li II indicated an ion temperature of 7 ev. The arc was a brilliant green color, being strongly dominated by the 5485 A line group. The total radiation was about 10% as intense as that from a carbon arc in the same apparatus.

All but one of the lines of Li III lie outside the range of the spectrometer. A line at 4500 A, expected from Li III, showed only instrumental broadening and was concluded to emanate from a neutral impurity.

We are indebted to P. R. Bell for stimulating our interest in this problem and for many helpful discussions. Another group, under his direction, is continuing this work.

4.2.2 Spectroscopy of Lithium Arcs

W. F. Peed

A number of spectrograms have been recorded of the short vertical solenoid with lithium arcs from 90 to 150 amp. Using low dispersion and wavelength coverage from 2000 A to 7000 A (Bausch and Lomb Cornu spectrograph), the predominant ion species is without exception Li^+ as evidenced by the line at 5486 A (E.P. = 61.3 ev). Neutral lithium is present in all cases with much lower apparent intensity in the main arc stream. The principal impurity observed is copper. Tungsten anodes, in general, yield a cleaner spectrum.

4.2.3 Mass Spectrometry of the Lithium Arc

R. V. Neidigh

The mass spectrometer work on the carbon arc reported previously[15] described a mass analyzer utilizing the velocity selector principle. This device has since been used with the lithium arc experiments conducted in the vertical solenoid.[16] Some preliminary information about the species of ions present and their abundance in the plasma surrounding

[15]R. V. Neidigh, Thermonuclear Project Semiann. Rep. Jan. 31, 1960, ORNL-2926, p 30.

[16]This report, sec 4.2.1.

the lithium arc may be obtained from the oscilloscope photographs in Fig. 4.8.

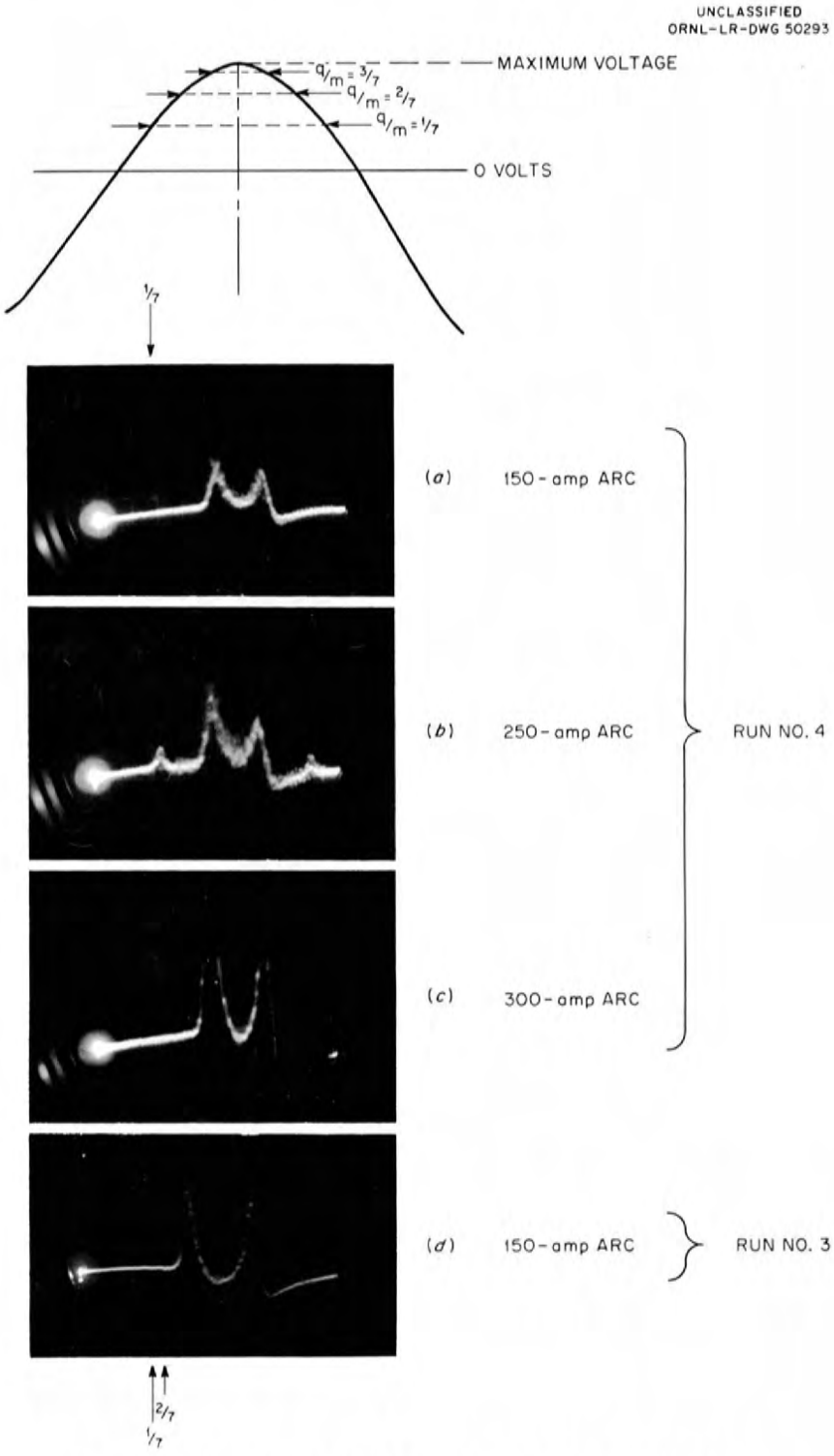

Fig. 4.8. Mass Spectrometric Arc Analysis.

The identity of the peaks (charge to mass ratio) observed in the photos was determined by raising the a-c modulating voltage on the velocity selecting channel until a peak appeared on the oscilloscope trace (an ion species arrived at the collector) and noting the voltage at which the peak appeared. As the voltage exceeds the critical value for a certain ion species the peak will separate into two peaks — one for the critical value on the upswing of the a-c cycle and another on the downswing. By this technique very small peaks, otherwise obscured in the noise, may be seen to move back and forth on the scope trace as the voltage is raised and lowered.

In most of the lithium arc runs fairly steady operation with pressures in the range of 10^{-6} to 10^{-5} mm Hg was obtained a few minutes after startup. The analyzer would not hold voltage until this steady operational state had been reached. Then the $q/m \approx 1/2$ ion was the dominant one as can be seen in the photographs of Fig. 4.8. The peaks at $q/m \approx 1/7$ and $\approx 2/7$ could be seen by visual observation at the time Fig. 4.8 (d) was made. These small peaks were identified by the technique described above. The $q/m \approx 1/7$ peak seen in Fig. 4.8 (b) appeared only briefly as the arc current was being raised.

The prominent peak seen by the analyzer which "looked" at the plasma 1/4 in. from the main arc column corresponds to a q/m of about 3/7. The identity of this peak may be accurately determined, but has not yet been, by comparing with the peaks of a hydrogen or deuterium arc. It may be that the peak is hydrogen from water vapor, although this seems unlikely since the vacuum was not correspondingly poor.

4.3 THE DEUTERIUM ARC

J. S. Culver R. J. Mackin, Jr.
R. A. Gibbons T. F. Rayburn
R. M. Warner

4.3.1 Introduction

The previously described high-vacuum deuterium arc development work is continuing in the PPF (PIG-Pump Facility).[17] The objective is a dissociating arc which is free from charge exchange for use in DCX. There

[17]R. A. Gibbons *et al.*, *Thermonuclear Project Semiann. Rep. Jan. 31, 1960*, ORNL-2926, p 47.

has been, however, both a change in the facility location (from Building 9204-3 to Building 9201-2) and a shift in the emphasis of the work (from vacuum studies to plasma properties).

Since there is in preparation a separate report covering the deuterium-arc work to date, only three major topics will be covered briefly here. These are: (1) operation of a deuterium arc in DCX, (2) spectroscopic investigation of the arc radiation, and (3) anode properties.

There has been only one major alteration in the facility. New magnet coils have been installed which permit arc operation in a mirror field whose strength is 7 kilogauss in the center and 14 kilogauss maximum.

4.3.2 Adaptation of Deuterium Arc to DCX[18]

After developing and proving the anode and differential vacuum baffle configurations in the PPF, the deuterium arc was installed and operated in DCX. The high magnetic field in DCX effected quite stable arc operation, both electrically and in the vacuum properties.

The major achievements were as follows:

1. The minimum pressure achieved in the DCX liner was 1.4×10^{-5} mm Hg (corrected reading) with a 200-amp, 185-v arc. The limit was set by gas influx from the ends, which were at a 100 times greater pressure.
2. The molecular ion beam breakup measurements indicated a dissociation efficiency of about 2%. Generally, the efficiency went down as the anode gas-flow rate was decreased.
3. The plasma decay times were 2 to 3 msec in the best of the three arc runs in DCX. The longest decay time, 3.3 msec, was about one-third the value expected for pure deuterium gas. This result is also found for a plasma produced by dissociation in the background gas.

The DCX group is continuing deuterium arc development for their own particular application.

4.3.3 Spectroscopic Investigation

A spectroscopic analysis[19] of the arc's radiation in the visible and near-ultraviolet region of the spectrum revealed mostly lines of

---

[18]See also this report, sec 1.2.

[19]The authors are grateful to M. R. Skidmore of the Spectroscopy Group for the loan of the spectrometer and for assistance in its operation.

atomic deuterium and ionized carbon and oxygen of the same order of intensity. There were also molecular deuterium lines an order of magnitude less intense. The line widths of a few of the lines were measured with a 0.5-m Ebert-type scanning spectrometer (Jaco 8200). If the observed line widths are interpreted as the effect of Doppler broadening, the mean energies are 30 ev for the carbon ions and 4 to 5 ev for the deuterium atoms.

The most probable source of the carbon and oxygen contamination has previously been shown to be the background gas evolved from the walls and the diffusion pumps.[17]

Because of the large difference in the carbon and deuterium energies, it seems likely that the source of the excited deuterium atoms is the background gas of deuterium, rather than electron capture by deuterons in the arc plasma. The following points tend to support this hypothesis:

1. The deuterium line intensities are proportional to the deuterium pressure.
2. The kinetic energy of the atoms is about that expected from the dissociation of molecular deuterium.
3. The calculations of the rate of radiative recombination of deuterons give a value that is much too low to explain the observed atomic line intensities.
4. Dissociative recombination of molecular ions cannot be ruled out; however, it seems unlikely that very many of those produced in the anode would survive to reach the point at which the spectrum is observed.

4.3.4 Anode Properties

Examination of the anode interior during arc operation verifies that the arc column extends to the base as expected. (The anode in current use was shown previously.[20]) The temperature at the hottest point, as measured by an optical pyrometer, was found to be 2850°C, which we regard as a lower limit. The upper limit was evidently below the melting point of tungsten, 3400°C.

The power carried off by the anode cooling water was measured. The anode was found to be dissipating about two-thirds of the total electrical

---

[20]R. A. Gibbons *et al.*, Thermonuclear Project Semiann. Rep. Jan. 31, 1960, ORNL-2926, Fig. 2.25.

power in the arc. Since about one-third of the arc current is carried by the ions (as indicated by gas accountability), this measurement suggests that the electrons suffer essentially no energy loss in traversing the arc column. This point has important consequences for the formation of a conceptual arc model.

4.4 ARC STUDIES PERTINENT TO DCX-EP-B

J. S. Luce W. L. Stirling C. W. Blue H. C. Hoy

Considerable work has been done by the EP Group with arcs of various kinds. It is beyond the scope of this report to cover all studies now underway, so only two closely related systems which are immediately applicable to EPB are considered. It is not planned to use a carbon arc in the presence of the trapped particles although carbon or similar arcs may be used as radiation sources and vacuum pumps.

4.4.1 Cooperative Neutralization of High Energy Ions and Energetic Electrons

A hollow tungsten cathode is used in these experiments with a large rotating water cooled anode (Fig. 4.9). It was reported at Geneva that careful reduction of the gas which is fed through the cathode can force the electrons to "blow up" radially into well formed hollow cones. These arcs appear to contain more electrons than ions and when a high-energy molecular ion beam is passed through this discharge, the dissociated trapped atomic ions tend to reduce or eliminate the negative space charge and consequently the arc blowup. If the gas to the cathode is reduced further the blowup again appears. To date no measurements have been made

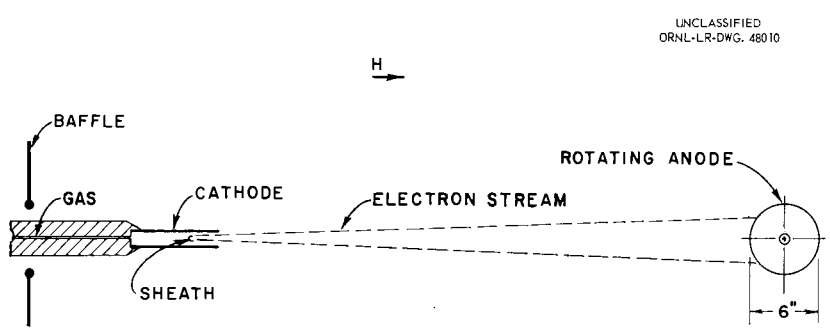

Fig. 4.9. Hollow Cathode Arc with Water Cooled Rotating Anode.

of the space potential or oscillatory electric fields in this plasma. While a great deal of work and better understanding are needed on this system, it does appear to have interesting possibilities. It is worth noting that the applied cathode voltage is quite high, approximately 1000 v which is the limit of our present supply. When the gas flow is reduced the mean free path of the electrons is increased because of the lower density in the discharge. It can thus be assumed that the mean electron energy is exceptionally high. Energy loss from the trapped ions to cold electrons normally encountered in the DCX system would be reduced with high-energy electrons. Any gas feed can be used, including hydrogen.

4.4.2 Electron Burnout[21]

The system described above has undergone several modifications so that the electrons can be reflected many times by the use of electron reflectors. Not only are the electrons reflected in the main body of the reflux arc, but a system has been developed where a portion of the electrons that blow up are reflected throughout the reacting volume. Figure 4.10 shows a typical assembly of this type. A symmetrical system is

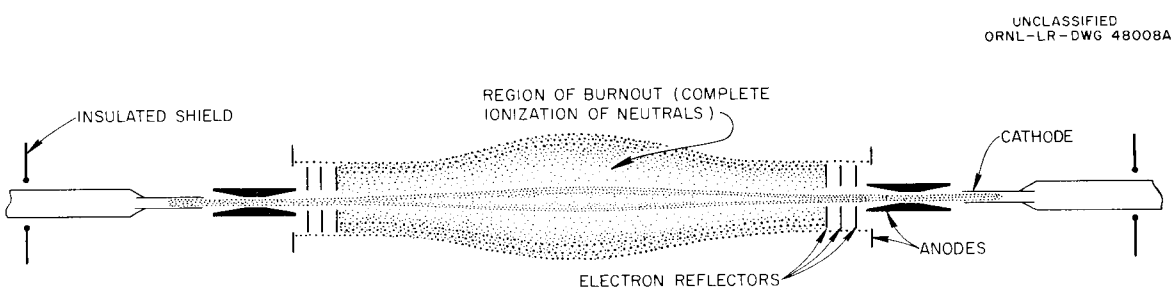

Fig. 4.10. Hollow Cathode Reflux Arc.

used, with cathodes, anodes, and electron reflectors on each end. Sputtered tungsten represents a serious impurity problem with these reflux arcs. The use of double cathodes reduces the power to each cathode by one-half for a given power input and greatly alleviates sputtering. The use of thoriated tungsten is also being investigated so that emission can be attained at a lower temperature. Since the sputtering rate is sensitive to the surface temperature any reduction in the cathode temperature will reduce sputtering.

[21]Complete ionization of background gas.

Further modifications will include large "ion reflectors" which will be placed a few inches from the anodes. The application of a high positive potential to the ion reflectors will cause the ions to be reflected back into the anode. Thus a stream of electrons at least partially free of ions can be obtained. This system is the same in principle as the electron gun used for the Neutralized Beam Injector. It is simply scaled up to a much higher electron output.

Experiments are now being conducted in EPA with reflux arcs of the types described above. If electron burnout can be achieved an important step toward attaining a thermonuclear plasma will be made. Another method is being considered that utilizes a plasma of modest energy to be produced in the machine by "entropy" trapping.[22] The plasma particles would then be used as targets to dissociate molecular ions injected into the machine by either or both of the injectors planned for EPB. The plasma temperature would be increased by the buildup of the trapped high energy ions. In addition to these burnout methods the use of r-f to accomplish complete ionization of the neutrals in the reacting volume is being studied by another group.

4.5 TITANIUM EVAPORATION IN AN ARC

J. S. Culver C. W. Wright R. J. Mackin, Jr.

The previous report[23] contained a description of preliminary efforts to develop an arc which operated on titanium vapor, produced by evaporation from a molten-titanium anode. The aim of the experiment was to evaporate titanium at a high rate in order to provide a high-capacity surface pump for deuterium gas. The major problem encountered was spinning of the titanium resulting from the motor action of the component of the anode current perpendicular to the magnetic field.

One solution to the problem appeared to lie in the use of a hollow tubular cathode from which ran a hollow cylindrical arc. It was found,

---

[22] J. L. Tuck, Proc. Intern. Conf. Ionization Phenomena Gases, 4th, Uppsala, 1959 2, 920 (1960).

[23] J. S. Culver, Thermonuclear Project Semiann. Rep. Jan. 31, 1960, ORNL-2926, p 51.

however, that a given cathode was effective only for a limited range of anode sizes, and then only at magnetic fields less than about a kilogauss.

Adaptation of an idea by Clausing[24] has resulted in a solution which may be valid under a more extended range of parameters. It is based on the observation that an alloy of titanium and niobium, over a broad range of composition and temperatures, exists as a semisolid sludge. The temperature range of this state is significantly above the melting point of pure titanium, and titanium evaporates from the surface at quite a substantial rate.

An anode was made by placing about 100 g of titanium metal and a 1-cm-thick disk of niobium (60 g), in a tantalum cylinder 3 cm in diameter.[25] An arc was struck, supported by argon until the anode contents had melted. It was then found that the arc, supported only by metal vapor, ran continously from an almost quiescent surface. On one occasion, a titanium evaporation rate of 8 g/hr was maintained for 30 min. A deposit of the evaporated titanium was analyzed and found to contain 0.5% tantalum and 0.05% niobium.

---

[24]This report, sec 11.3.

[25]The niobium metal was supplied by the Metal Forming Group of the ORNL Metallurgy Division.

5. ION SOURCE AND ACCELERATOR DEVELOPMENT

5.1 Development of the von Ardenne Source

O. B. Morgan N. H. Lazar
G. G. Kelley E. C. Moore

Using the modified von Ardenne ion source No. 2, Fig. 5.1, and the Einzel lens and analyzing arrangement, Figs. 5.2 and 5.3, hydrogen ion currents up to 340 ma have been obtained and the ones up to 100 ma have been analyzed. Numerous changes have been made in the ion source in an effort to obtain the maximum H_2^+ beam component. Ratios of 70–80% H_2^+ have been obtained in the current range of 20–50 ma and 60–70% H_2^+ with currents of 50–100 ma.

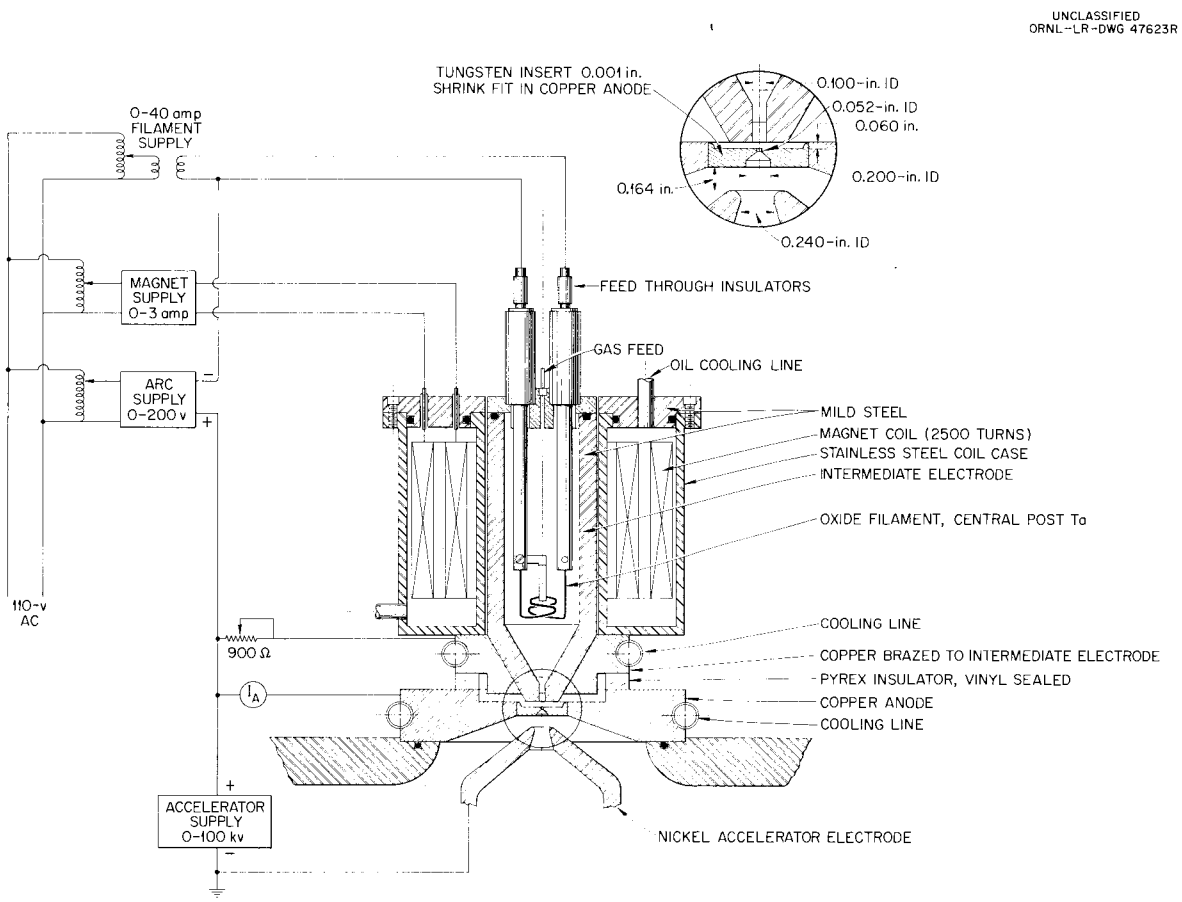

Fig. 5.1. Modified von Ardenne Ion Source No. 2.

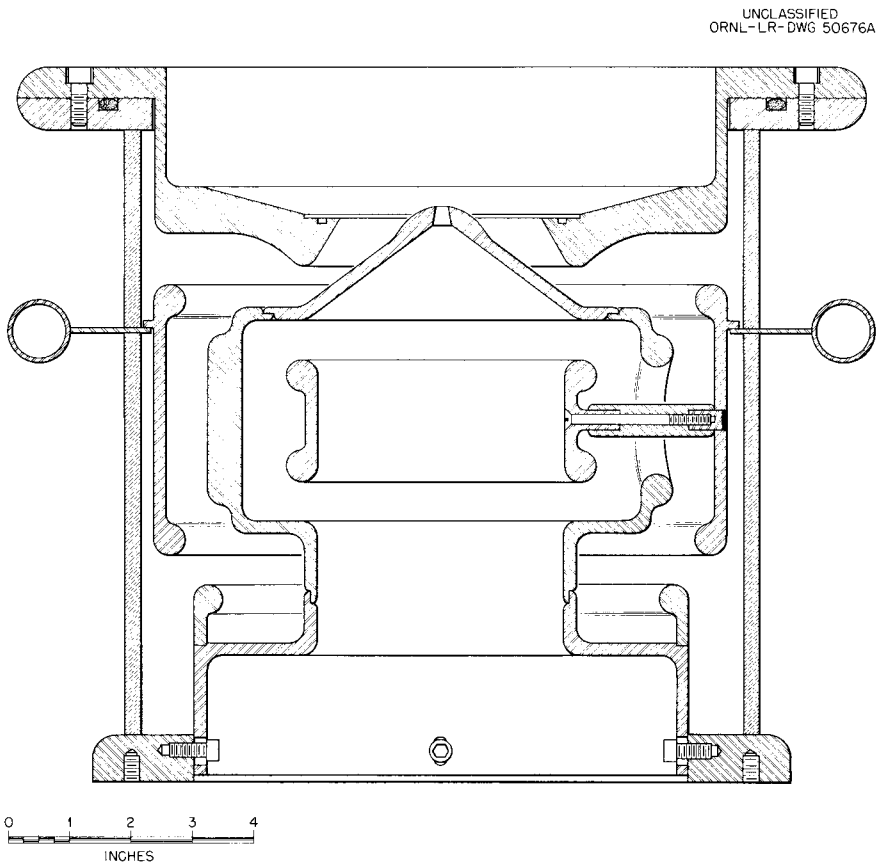

Fig. 5.2. Einzel Lens for High Current Beam Analysis.

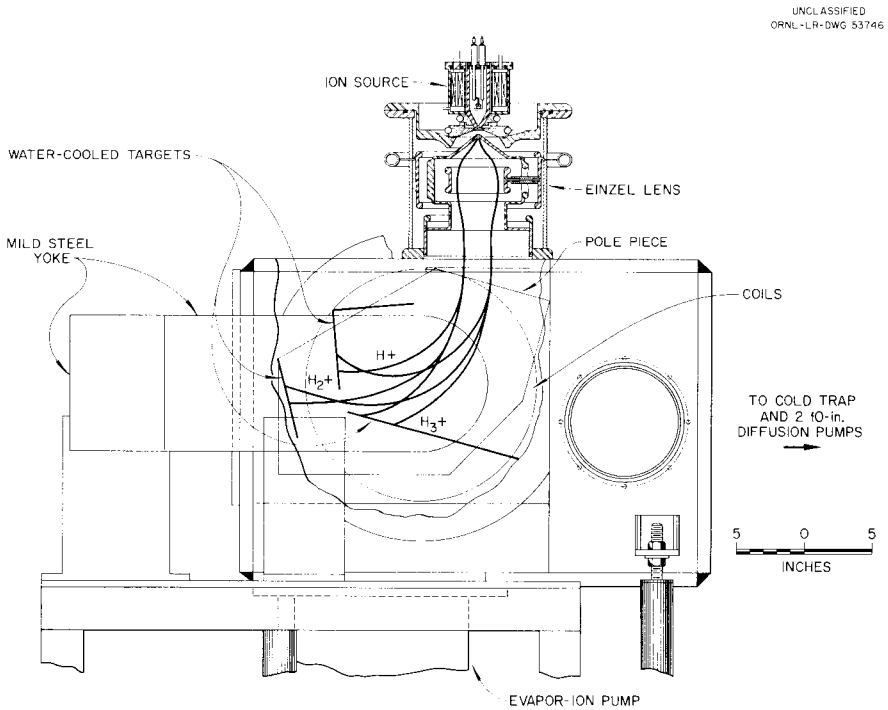

Fig. 5.3. Ion Source Analyzing System.

The ion source is the same as the one described earlier,[1] except that the external mild steel magnetic return path was found not to be necessary. The maximum current obtained from the source, 340 ma at 75 kv was in agreement with the Pierce limit.[1]

The Einzel lens limits the maximum current that can be analyzed to about 100 ma. A significant fraction of beam currents greater than this value is lost to various parts of the lens. The design of this lens is the result of an attempt to obtain the greatest possible current in a parallel beam of reasonably small cross section (~2–3 in. in diameter). Rough calculation of various configurations, taking space charge into account, indicated that, because of the necessarily low beam velocity in the decelerated region, the upper limit of current was about 100 ma.

After the lens was constructed several modifications were made in an unsuccessful attempt to increase the upper current limit. These included increasing the length of the center section by a factor of 1.5 and increasing the object distance by a factor of 2. Electromagnetic focusing by means of a solenoid lens was ruled out because the dependence of focal length on mass made it impossible to separate the beam component after analysis.

The analyzing apparatus, Fig. 5.3 is pumped by two 10-in. oil diffusion pumps with a liquid nitrogen trap and one "Evapor-Ion" pump. This combined system has a pumping speed of approximately 10^4 liters/sec for hydrogen and has reached a base pressure of 3×10^{-8} mm Hg. Ninety-degree deflection of the ion beam is obtained in the magnetic fields of 0–3.5 kilogauss. The entrance angle of the beam into the magnetic field is chosen so that double focusing is provided in the vicinity of the targets. The use of three targets makes it possible to read all beam fractions simultaneously. The target currents can be measured both electrically and calorimetrically. The two methods have agreed within 5% in numerous checks. No electrostatic secondary electron suppression is necessary on the targets because of the magnetic field.

The source geometry which has so far given the maximum H_2^+ beam fraction is shown in Fig. 5.1. The geometry just above the anode button is

[1] Thermonuclear Project Semiann. Rep. Jan. 31, 1960, ORNL-2926, p 62.

of particular importance for H_2^+ yield. For a constant amount of extracted current the H_2^+ beam component decreases as the intermediate electrode to anode spacing is increased(see Table 5.1). On the other hand, as this spacing is increased the extracted current per ampere of arc current increases. Currents greater than 100 ma have been extracted per ampere arc current at a spacing of 0.310 in. with the source shown in Fig. 5.1. When the diameter of the intermediate electrode is increased from 0.1 in. to 0.2 in. the ion current per ampere of arc current decreases, and for a constant extracted current the H_2^+ beam fraction also decreases in favor of H^+. The H_3^+ fraction remains essentially constant. For a constant output the H_2^+ beam fraction decreases as the source pressure increases (see Table 5.2).

The pressures listed by Table 5.2 are thermocouple readings, corrected to hydrogen, obtained with no discharge in the source. However, in view of the location of the gage in the vicinity of the filament, and the fact that the readings vary depending on operating conditions, there is some question as to their relation to the operating source pressure.

Table 5.1. Relative Ratios of the Mass Species of Hydrogen from Source for Various Intermediate Electrode to Anode Spacings with Extracted Ion Current Constant (70 ma)

Intermediate Electrode to Anode Spacing (in.)	H_1^+ (%)	H_2^+ (%)	H_3^+ (%)
0.060	24	71	5
0.110	36	50	15
0.210	41	41	16

Table 5.2. Relative Ratios of the Mass Species of Hydrogen from Source for Various Source Pressures with Extracted Ion Current Constant (70 ma)

Source Pressure	H^+ (%)	H_2^+ (%)	H_3^+ (%)
77	24	71	5
110	27	66	7
165	38	47	15
240	42	37	21

Some of the changes made which had no noticeable effect on the mass ratios were the following:

1. A large quantity of platinum gauze was placed inside the intermediate electrode in the hope of increasing the recombination rate of any H_1^0 atoms formed.
2. The tip of the intermediate electrode was replaced with cooled copper.
3. A noncooled stainless steel insert was placed in the tip of the intermediate electrode.
4. The gas leak was introduced both in the general region below the intermediate electrode and through a manifold directly into the arc column.
5. The source was differentially pumped through apertures in the anode plate.

5.2 High-Current Ion Beam Injection System

R. C. Davis
R. R. Hall
G. G. Kelley
N. H. Lazar
O. B. Morgan
R. F. Stratton

The high-current accelerator tube has been installed and the tube is now being tested. The vacuum system has been modified by the replacement of two of the anticipated four "Evapor-Ion" pumps by liquid nitrogen trapped MCF-1400 oil diffusion pumps. This change was brought about following the experience of poor reliability with the "Evapor-Ion" pumps and their extremely low pumping speed for most organic gases. The reliability has been improved by the addition of a control circuit which senses when the titanium feed wire has frozen to the heater post and prevents further wire feed. In addition, improvements have been made by the manufacturer in the rigidity of the interior framework of the pump and in improved power supplies for grid and post. To date, the pumps have shown satisfactory reliability. Figure 5.4 is a photograph of the bottom of the accelerator platform and the lower section of the beam tube and target cup.

The pumping speed for the system has been determined for hydrogen. Gas was bled into the target cup assembly to simulate a beam of H_2 ions. For an input of 1/5 atmospheric cc/sec, equivalent to a beam of 0.88 amp, the pressure in the manifold was 1.1×10^{-5} mm Hg, which is equivalent to a net pumping speed of 15,200 liters/sec.

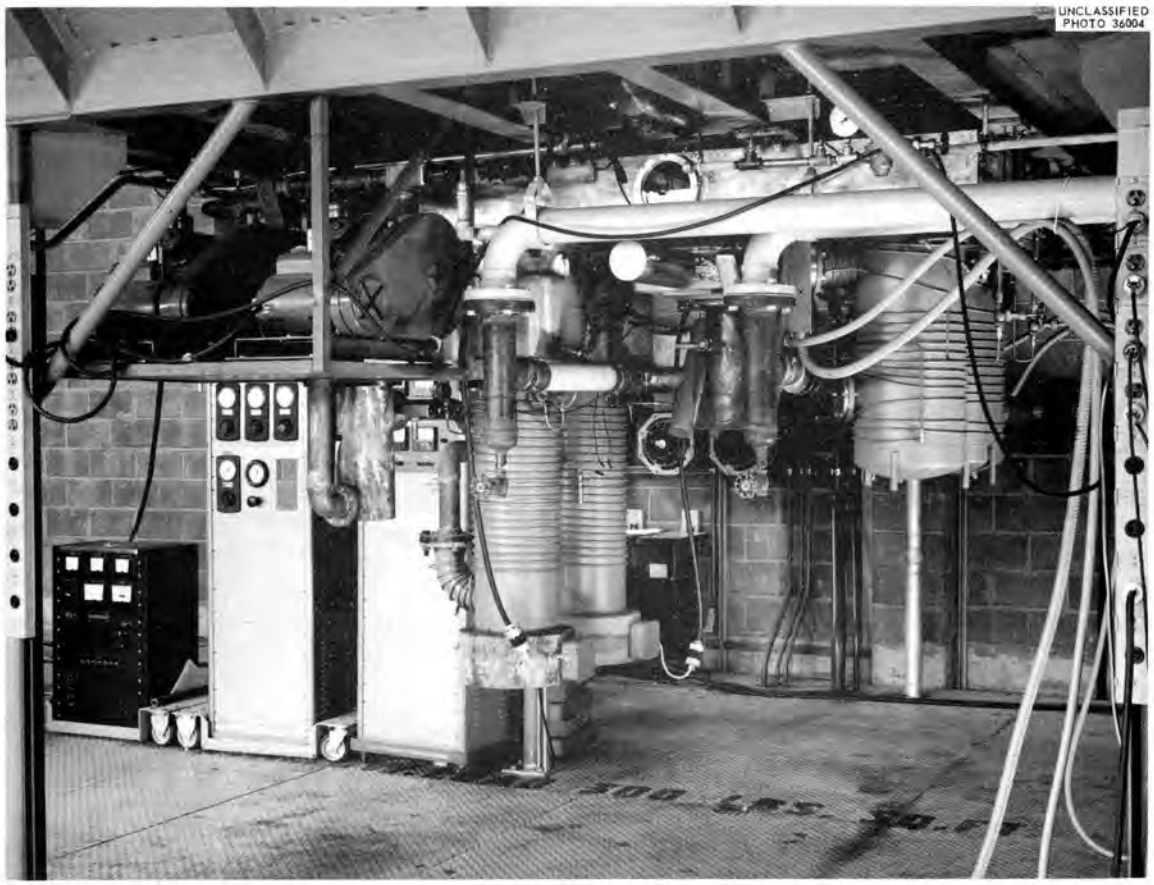

Fig. 5.4. Bottom of Accelerator Platform Showing Target Cup Assembly and Pumping Manifolds.

Preliminary high-voltage tests have been carried out on the insulator supports and the accelerator tube. The insulator supports (Fig. 5.5) have held 600 kv satisfactorily. The accelerator tube has held voltage up to 475 kv. Cleanup of the accelerator tube resulted in 20 to 50 discharges of sufficient magnitude to shut off the power supply. When the tube was examined following these tests, the source-mount assembly was found to have 15 severe pits about an inch above the bottom of the re-entrant source "bucket" corresponding to the 15 pump-out holes in the 450-kv electrode.[2] No other damage could be seen anywhere in the tube, and, particularly, no damage to the 450-kv electrode. The pits apparently were the result of hollow cathode discharges from these holes, either as a primary breakdown

[2]For accelerator design, see R. C. Davis et al., Thermonuclear Project Semiann. Rep. July 31, 1959, ORNL-2802, p 72.

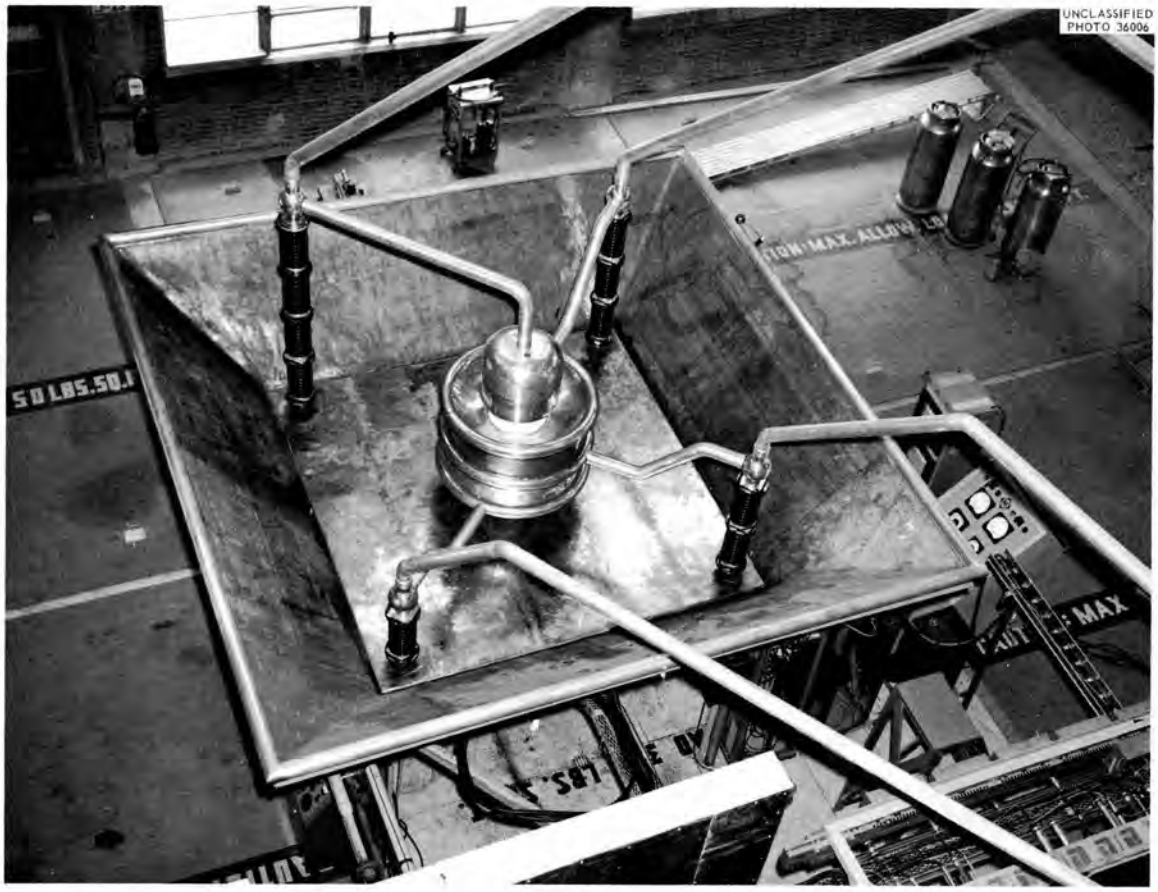

Fig. 5.5. Accelerator Tube and Lead Shielded Platform Taken from Above Showing Corona Rings and Insulator Supports.

or triggered by a discharge in another part of the tube. These holes have been filled and further tests are being carried out.

Concerning these primary tests, it is of interest to mention that the large amount of energy stored in the filter condenser ($1/2\ CV^2 = 2.25 \times 10^5$ joules) and the current surges resulting from charge stored in distributed capacity in the transformer windings did no major damage to the accelerator tube, despite the fact that the sole overload protection was based on an over-current relay which opens vacuum switches in the primary of the first cascade transformer. In fact, below 400 kv the current was limited by power supply impedance to below the automatic trip level. The supply was turned off manually, in those cases, with an average delay of perhaps 0.15 sec.

The source has been operated at 50 ma with 300 kv on the tube. The arrangement of the power supplies and metering (see Fig. 5.6) on the isolating transformer stack has proved highly satisfactory. The pneumatically driven controls have also operated satisfactorily.

To shorten the fault-sensing time, an instrument has been built which measures the electric field in the vicinity of the accelerator tube and provides a signal whenever there is a sudden change in this field. This signal is then used to open the vacuum switches.

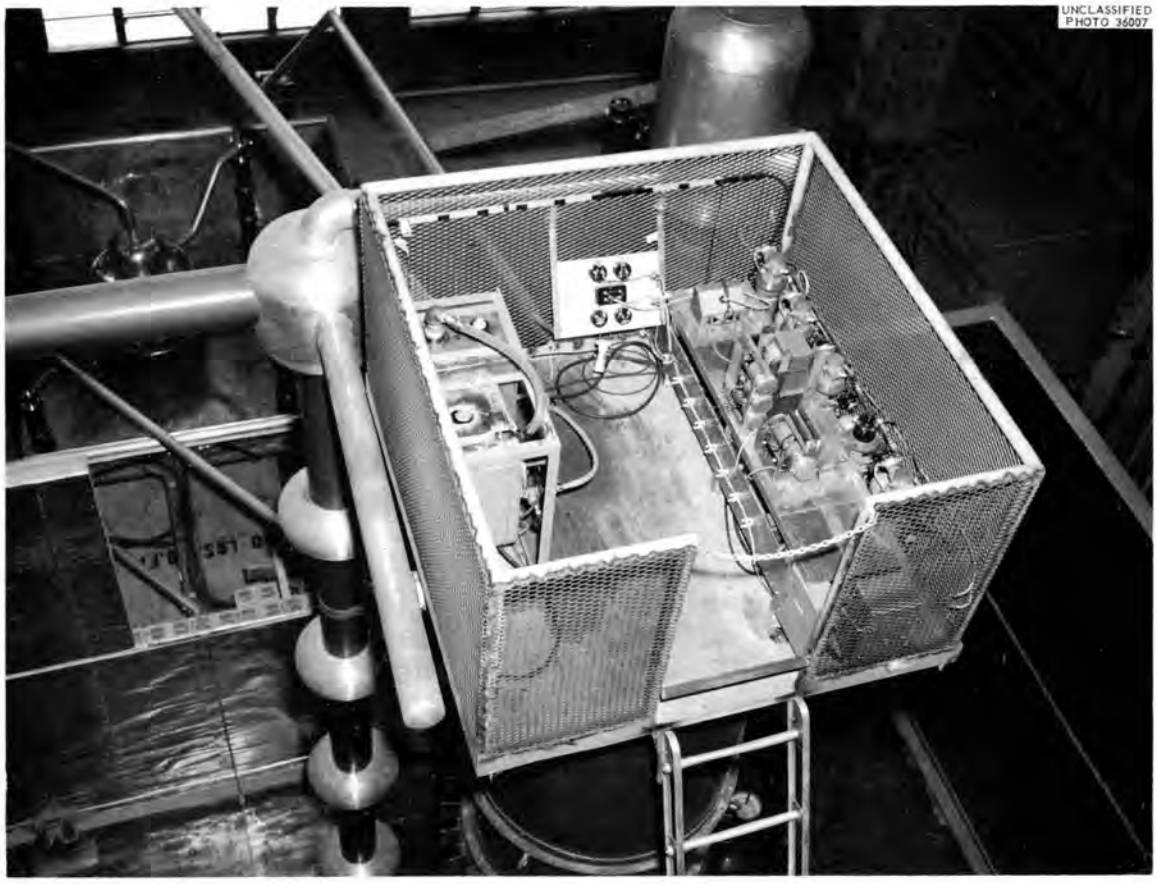

Fig. 5.6. Power Supplies and Metering Layout on Isolation Transformer. Photograph taken looking toward accelerator platform area.

6. THEORY AND COMPUTATION

6.1 FOKKER-PLANCK COEFFICIENTS FOR A PLASMA INCLUDING RADIATION

A. Simon E. G. Harris[1]

The Rostoker-Rosenbluth expansion of the Liouville equation has previously[2] been used to obtain a set of coupled integral equations for the particle-particle pair distribution function $g(1,2)$ and the particle-oscillator pair distribution function $g(1,\lambda)$. The asymptotic solution of these equations enables one to immediately obtain the proper coefficients which then go into the Fokker-Planck equations for both particles and radiation.

We have solved the pair correlation equations exactly for the zero-order case in which the plasma is static, uniformly distributed in space, and isotropic in direction. There are no zero-order external fields and the radiation field is taken to be absent in zero order. The exact solution was obtained by a generalization of the method of Lenard.[3] The resulting coefficients consist of two terms. One corresponds to direct particle interactions via the Coulomb field. The second is due to interactions via transverse electromagnetic waves.

The resulting coefficients require cutoff only at minimum impact parameters. The maximum parameter is automatically determined by self-shielding. The Coulomb term agrees with previous calculations obtained for the case of a Maxwell-Boltzmann distribution.[4] The transverse term represents an additional contribution which is numerically small except for relativistic electrons or under special resonant conditions.

There is no radiation from this particular zero-order plasma to this order. Cyclotron radiation is obtained if one now introduces a magnetic field. Calculations on this latter case are now in progress.

---

[1]Consultant, University of Tennessee.
[2]A. Simon and E. G. Harris, Phys. Fluids 3, 245 (1960).
[3]A. Lenard, MATT-25 (November 1959).
[4]N. Rostoker and M. Rosenbluth, Phys. Fluids 3, 1 (1960).

6.2 ION ENERGY DISTRIBUTIONS, ION ENERGY DEGRADATION, AND DCX-TYPE CRITICAL CALCULATIONS

D. J. Rose[5]

One difficulty in the way of calculating high-energy ion energy distributions in a plasma is the form of the time constant τ_{ie} for ion energy degradation by the sea of cooler electrons. If the speed of a test ion with energy U is much less than the mean speed of the Maxwellian electrons at temperature T_e, the time constant approaches

$$\tau_{ie} \rightarrow \tau_1 \propto (kT_e)^{3/2} \quad , \tag{1}$$

provided only that $kT_e \ll U$. On the other hand, if the ion is much faster than the electrons, we have

$$\tau_{ie} \rightarrow \tau_2 \propto U^{3/2} \quad . \tag{2}$$

The physical interpretation is simple: the slowing down time is determined by the Coulomb cross sections, and the relative motion is that of the faster particle. Between the limits (1) and (2), the dependence is a complicated function of the relative energies.[6,7]

It is found that the approximation

$$\tau_{ie} = \tau_1 + \tau_2 \tag{3}$$

under all circumstances (provided only that $kT_e \ll U$) is exact at both limits and in error by less than 10% everywhere in between. We shall be concerned here only with cases where $kT_e \ll U$, and the problem of mutual thermalization does not arise. One form of Eq. (3) is:

$$\tau_{ie} = \tau_2 \left[1 + \frac{3\sqrt{\pi}}{4} \left(\frac{m_i T_e}{m_e u} \right)^{3/2} \right] \quad , \tag{4}$$

where here and henceforth T_e and the ion energy u are measured in kev. The approximation permits calculation of simple ion energy distributions.

[5]Consultant, Massachusetts Institute of Technology.

[6]S. Chandrasekhar, Astrophys. J. 97, 255 (1943).

[7]L. Spitzer, Physics of Fully Ionized Gases, p 79, Interscience, New York, 1956.

For later reference, we write the form applicable to protons in an electron gas, in mks-kev units, with $\ln \Lambda = 20$:

$$\frac{1}{\tau_{ie}} = \frac{2.1 \times 10^{-13}\, n_e}{u^{3/2}\left[1 + (3\sqrt{\pi}/4)(m_i T_e/m_e u)^{3/2}\right]} . \tag{5}$$

The factor $(3\sqrt{\pi}/4)(m_i/m_e)^{3/2} = 1.04 \times 10^5$ for protons.

It is possible to solve in a straightforward way for the fast-ion energy distribution (including the fast-ion density n_i itself) under the following steady-state conditions:

1. A flux $\Phi(m^{-2}\ sec^{-1})$ of monoenergetic molecular ions passes through a plasma with fast-ion density n_i, breakup cross section σ_{Bi}, and other breakup centers n_j with appropriate breakup cross sections σ_{Bj}. The released fast atomic ions have initial energy u_0.
2. These ions lose energy only by dynamical friction to an electron cloud of density n_e and temperature T_e. (We do not solve for T_e, and n_e may not be equal to n_i, depending upon the presence of slow ions, arcs in the region, etc. The ion energy losses to neutral gas and to cold ions can safely be neglected.)
3. Fast ions at all energies of interest are lost by charge transfer to various species n_h with cross section $\sigma_{th}(u)$. Ions that cool to low energy by avoiding charge transfer are lost by "magic" (in actuality, Coulomb scattering) at an uninterestingly low energy.

The ion distribution function $f(u)$ is found by writing down the flows in energy space, performing a trivial integration, and applying the boundary condition that the flow at u_0 equals the input flow. The result, with numbers appropriate to a distribution of fast protons, is:

$$f(u) = \frac{4.75 \times 10^{12}\Phi}{n_e}\left(\sigma_{Bi} n_i + \sum_j \sigma_{Bj} n_j\right) \times$$
$$\times \left[1 + \frac{3\sqrt{\pi}}{4}\left(\frac{m_i T_e}{m_e u}\right)^{3/2}\right] \exp\left[-\int_u^{u_0} dx(u)\right] , \tag{6}$$

where

$$dx(u) = du\, \frac{2.1 \times 10^{18}}{n_e}\, u \sum_h n_h \sigma_{th}(u) \left[1 + \frac{3\sqrt{\pi}}{4}\left(\frac{m_i T_e}{m_e u}\right)^{3/2}\right] . \tag{7}$$

If $T_e = 0$ and all $\sigma_{th} = 0$, then $f(u) \propto u^{1/2}$ out to u_0 [the term $f(v)$ = constant out to v_0] and the average energy $\bar{u} = 3u_0/5$. Since charge transfer removes ions as they slow down, $\bar{u} > 3\,\bar{u}_0/5$; this conclusion is not altered for all $T_e \neq 0$ of interest.

The distribution $f(u)$ has a weak spurious pole at $u = 0$ because we have neglected to provide the "magic" removal process at low energy. This pole causes no difficulty in any real calculation, and may be removed by cutting off $f(u)$ at any uninterestingly low energy u_ℓ. The ion density itself is

$$n_i = \int_{u_\ell}^{u_0} du\, f(u) \quad . \tag{8}$$

Since $f(u)$ itself contains n_i, the ion density can diverge in a real sense if

$$\int_{u_\ell}^{u_0} \left[\frac{\Phi\sigma B_i}{\sum_h n_h \sigma_{th}(u) v} \right] dx(u)\, \exp\left[-\int_u^{u_0} dx(u) \right] \geqq 1 \quad , \tag{9}$$

where v is the corresponding ion speed. We recognize this expression as a modification of the simple auto-exponentiation criterion

$$\frac{\Phi_0 \sigma_{Bi}}{\sum_h n_h \sigma_{th}(u_0)\, v_0} \geqq 1 \quad , \tag{9a}$$

for balance of breakup on ions vs charge transfer calculated at u_0. Criterion (9) is more severe than (9a) because

1. $\sigma_{th}(u)$ increases with decreasing u.
2. Even with the first quantity in square brackets set equal to 1, the integral is less than 1 (i.e., some ions are not lost by charge transfer at all).
3. Criterion (9) contains n_h in the exponent; if any of the densities n_h increase with Φ, then as $\Phi \to \infty$, Eq. (9) $\to 0$, a behavior not hitherto recognized.

Provided the densities n_j and n_h are interpreted as the densities inside the plasma, criterion (9) is exact for the "upper critical current."

The ratio

$$D_U \frac{\Phi_0}{\Phi} = \int_{u_\ell}^{u_0} \left[\frac{\sum_h n_h \sigma_{th}(u_0)}{\sum_h n_h \sigma_{th}(u)} \right] \left(\frac{u_0}{u} \right)^{1/2} dx(u) \exp\left[-\int_u^{u_0} dx(u) \right] < 1 \quad , \qquad (10)$$

obtained from (9) and (9a) at their critical values, is a measure of how much the criterion (9a) is wrong in guessing the "upper critical current." For example, if criterion (9a) predicts 0.5 amp, and $D_U = 0.1$, we really require 5 amp, even if all the n_j's and n_h's are independent of the flux Φ. In general, n_h and n_j will increase with Φ, and the situation may be worse.

Figure 6.1 shows the distribution f(u) of fast protons, normalized to $u^{1/2}$ at u_0 for the following conditions:

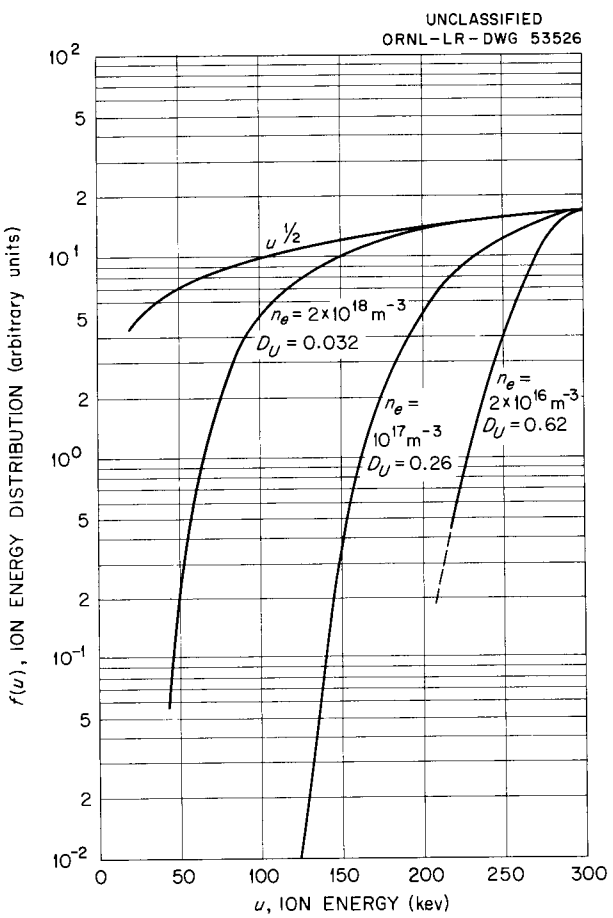

Fig. 6.1. Fast Proton Energy Distribution for Breakup of H_2^+ in the Presence of a Hydrogen Arc. $T_e = 100$ ev, $u_0 = 300$ kev, $n(H_2) = 3 \times 10^{16}\ m^{-3}$.

$u_0 = 300$ kev,

$T_e = 0.1$ kev,

$n(H_2) = 3 \times 10^{16}\ m^{-3} (\cong 9 \times 10^{-7}$ mm Hg),

$n_e = 2 \times 10^{18}, 1 \times 10^{17}, 2 \times 10^{16}\ m^{-3}$.

Note that D_U has the pessimistic value 0.032 for the highest electron density. The distribution f(u) is much degraded; the corresponding density n_i is itself reduced by a factor $\cong D_U$ from the value obtained by simple number balances at u_0. Indeed, this is the heart of the matter: if fast ions are unlikely to be lost by charge transfer near the injection energy u_0, they cool by dynamical friction instead, and disappear at lower energy where σ_t is suitably higher. We can oversimplify the case, and state that in the limit

of $\sigma_t = 0$ in the range $u_\ell < u < u_0$, $\sigma_t = \infty$ at $u \leq u_\ell$, an ion lasts only until it cools to u_ℓ.

The energy degradation has similar effects on the destruction of neutral gas (burnout) and other quantities of interest. These matters will be discussed further in a forthcoming ORNL report.

6.3 DCX PLASMA POTENTIAL BEFORE BURNOUT

T. K. Fowler

The DCX plasma potential before burnout has been estimated, using a model similar to that employed earlier for the post-burnout case,[8] and was found to be at most a few volts under present operating conditions. The interest in the calculation lay in the following mechanism degrading the energy of trapped ions.

Since the electric field develops so as to confine electrons, it accelerates out of the system slow positive ions resulting from ionization of neutrals. Each such ion carries away an energy ϕ, the potential difference between the plasma interior and machine walls, which must be supplied eventually by trapped ions with electrons serving as intermediary. Electrons, initially cold, are heated by collisions with hot ions just to energy $\sim\phi$, whereupon they are able to penetrate the potential barrier and escape. But, in being decelerated by the field, they give up all this energy which, through the field, is in turn passed on to the escaping slow ions. Since in DCX under present conditions ϕ is small, the energy drain is not great, even though each hot ion ionizes several hundred neutrals (300-kev protons) before being lost by charge exchange.

To determine ϕ, we consider the following equations describing the steady state before burnout, when ions are lost primarily by charge exchange:

$$\frac{I}{V} = n_+ n_0 \sigma_x \sqrt{\frac{2E_+}{M}} \quad , \tag{1}$$

---

[8]T. K. Fowler, Effect of Plasma Potential on DCX Steady State, ORNL-2914 (Mar. 7, 1960).

$$\frac{\sigma_i + \sigma_x}{\sigma_x} \frac{I}{V} \phi = n_+ \left(n_- \frac{80\pi e^4}{\sqrt{2ME_+}} \frac{M}{m} \right) , \tag{2}$$

$$n_- = n_+ + \frac{\sigma_i \sigma + \sigma_x}{\sigma_x} \frac{I}{V} \sqrt{\frac{2M_c L^2}{\phi}} . \tag{3}$$

Equation (1) balances the ion input rate, I, against their loss rate due to charge exchange with neutrals, density n_o, and cross section σ_x. The hot ion mean energy, E_+, is assumed to be approximately their input energy, a valid assumption if the results indicate little degradation; n_+ is the hot ion density, V is the plasma volume, and M and m are the ion and electron masses.

Equation (2) equates the rate of energy loss to slow ions, on the left, with the rate of energy transfer from hot ions to cold electrons, assumed isotropic in velocity, on the right.[9] Each hot ion makes $(\sigma_i + \sigma_x)/\sigma_x$ slow ions, with σ_i being the ionization cross section; n_- is the electron density.

Equation (3) establishes electrical neutrality. The second term on the right is the density of slow ions, mass M_c, the square root factor being their residence time taken to be the time for the electric field, assumed uniform, to accelerate them out of the machine, a distance L.

Combining equations, we find that the slow ion density is negligible, $n_- \sim n_+$, and, for 300-kev protons, we get

$$\phi \sim \left(\frac{n_+}{n_0} \right) (150) \text{ ev} .$$

Since at present $n_+/n_0 < 1$ in DCX, ϕ is at most a few volts. For larger ion densities, ϕ may become appreciable, but the various assumptions entering the calculation are invalid if $\phi > (m/M)E_+ \sim 160$ ev.

[9] L. Spitzer, Physics of Fully Ionized Gases, chap. 5, Interscience, New York, 1956.

6.4 ELECTRON CAPTURE CROSS SECTION IN H_2^+

R. G. Alsmiller

The cross section for the capture of an electron from the hydrogen molecular ion by a proton has been calculated in the Brinkman-Kramers approximation; that is, in the Born approximation with the interaction between the incident proton and the molecular proton omitted from the matrix element. In the calculation LCAO wave functions and the Franck-Condon principle were used, and only capture into the ground state was included. The cross section, σ, varies from $\sigma = 8.6 \times 10^{-16}$ cm^2 at 30 kev to $\sigma = 2.12 \times 10^{-18}$ cm^2 at 225 kev. Since the Brinkman-Kramers approximation usually gives a result which is too large, the above values must be considered as upper limits rather than true values. This is borne out by the fact that our values are somewhat larger than a previous estimate of the cross section given by Gerjouy.[10]

6.5 CONTAINMENT ZONES

M. Rankin

Figures 6.2 and 6.3 give the revised containment zones[11] for the 5.3-in. DCX-1 geometry. These are based on $r_0 = 5.3$ in., which with

$$\frac{B_z(r = 5.3,\ z = 0)}{B(r = 0,\ z = 0)} = 0.87776$$

implies that $B(0,0) = 9457$ gauss for D^+ or 6687 gauss for H^+.

Figure 6.4 gives the containment zones for the 3.26-in. DCX-1 geometry. These are based on $r_0 = 3.26$ in., which with

$$\frac{B_z(r = 3.26,\ z = 0)}{B(r = 0,\ z = 0)} = 0.95345$$

implies $B(0,0) = 14{,}154$ gauss for D^+ or 10,008 gauss for H^+.

---

[10] E. Gerjouy, Dissociation and Ionization of H_2^+ by Fast Protons, Westinghouse Research Laboratories, Research Report 60-94439-1-R2 (Sept. 22, 1951).

[11] T. K. Fowler and M. Rankin, Thermonuclear Project Semiann. Rep. July 31, 1959, ORNL-2802, p 87.

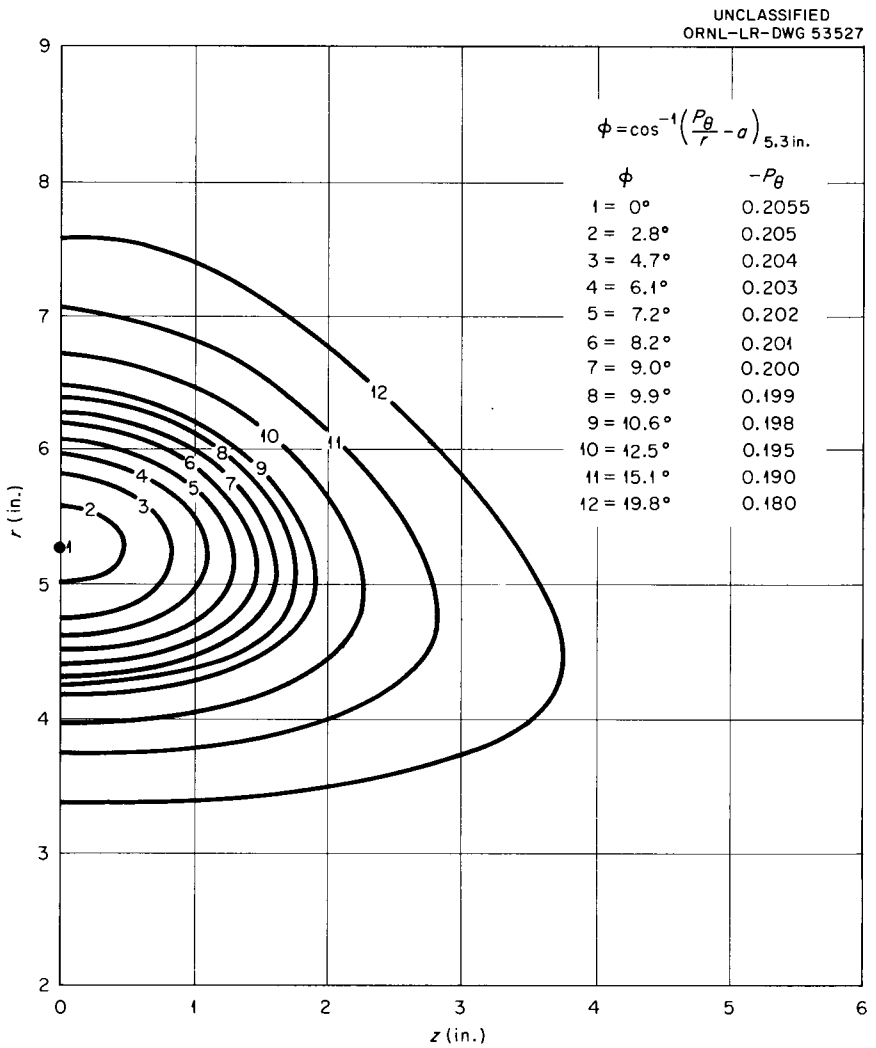

Fig. 6.2. Containment Zones for 5.3-in. DCX-1 Geometry.

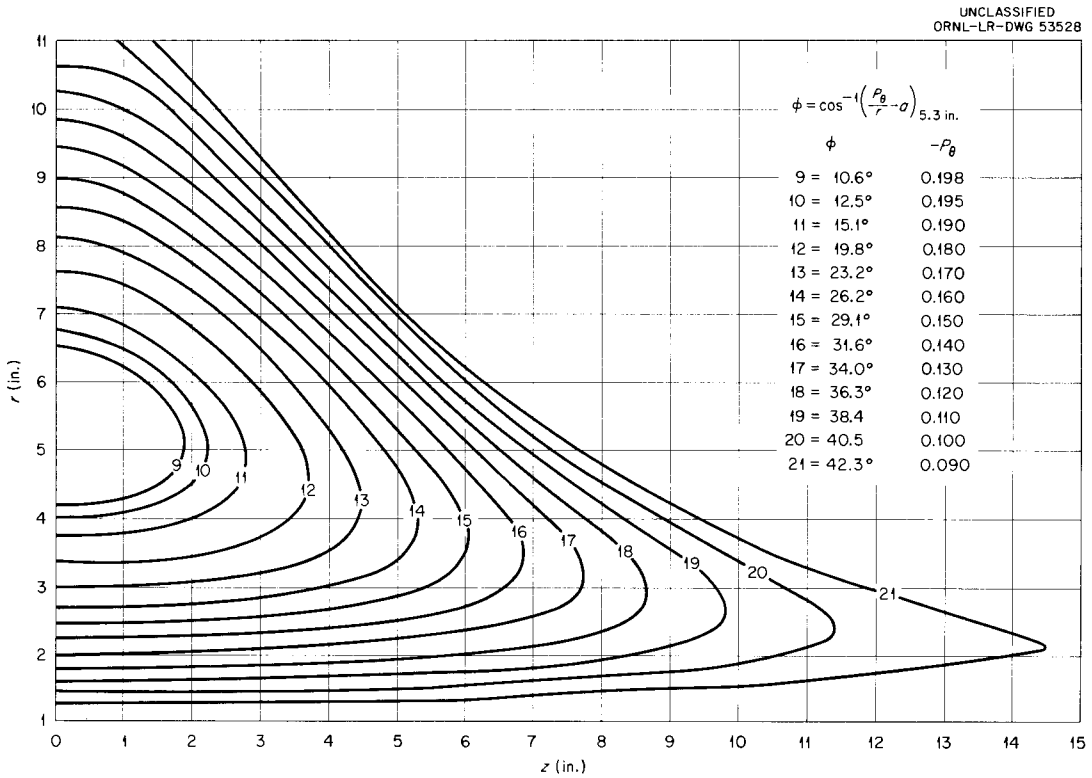

Fig. 6.3. Containment Zones for 5.3-in. DCX-1 Geometry.

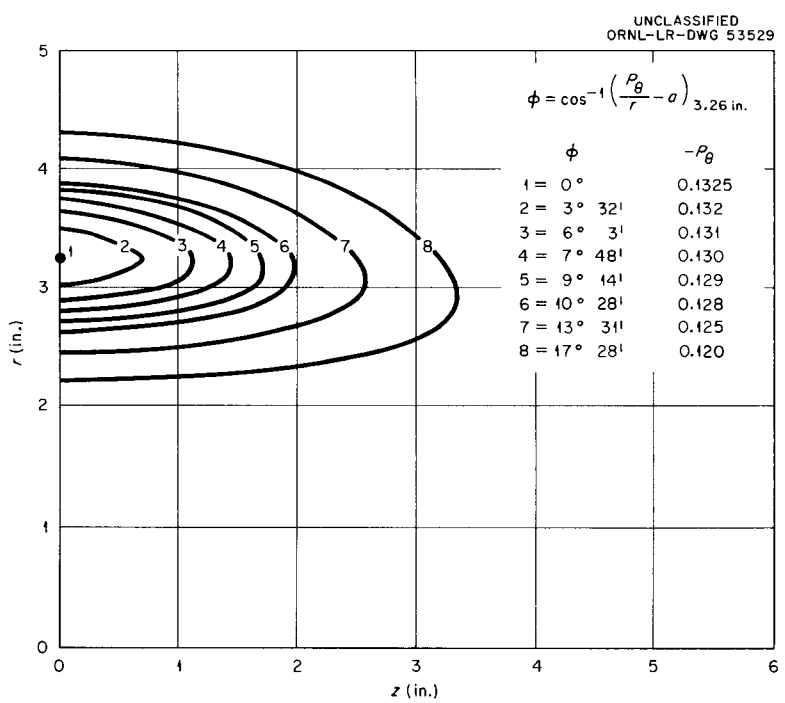

Fig. 6.4. Containment Zones for 3.26-in. DCX-1 Geometry.

6.6 PARTICLE DISTRIBUTION IN THE DCX ION RING

M. Rankin

An average particle distribution, using eight cases of initial conditions, was found for the $P_\theta = -0.15$ containment zone in DCX-1 (ref 12). The following cases were run with the Oracle code CENSUS. In all cases $P_\theta = -0.15$ (corresponding to a scattering angle of 29°); $(r_0, Z_0) = (5.3$ in., 0); $\lambda = (P_z/P_r)_0$. The value $\eta = \tan^{-1}(P_z/P_r)$ is also recorded as another indication of the sampling used.

Case		η
1	$\lambda = +2$	+63°
2	$\lambda = -2$	−63°
3	$\lambda = +1$	+45°
4	$\lambda = -1$	−45°
5	$\lambda = -0.588$	−30°
6	$\lambda = +0.216$	+13°
7	$\lambda = -0.216$	−13°
8	$\lambda = \infty$	+90°

Figure 6.5 shows the percentage distribution for each of these cases (cases 1, 4, 5, 6, and 8 are based on 100 ft orbits; cases 2 and 3 on 80 ft; and case 7 on 60 ft). Figure 6.6 shows the average distribution for the eight cases. Figure 6.7 shows a comparison for the $\lambda = +2$ case for distributions recorded at S = 100 ft and S = 200 ft.

These observations were also made on this series of runs: (1) There is a great similarity in the runs for + and − values of λ, indicating that the initial direction assigned to the r-momentum has little effect on the later distribution. (2) Only three types of patterns were found from the Oracle r-z plots. Cases 1 through 5 gave the typical pattern shown in Fig. 6.8. Cases 6 and 7 gave the pattern shown in Fig. 6.9 and case 8 gave the type of pattern shown in Fig. 6.10. The results of cases 1 through 5 are quite similar to that found previously in quasi-periodic orbit studies.[13] (3) Figure 6.7 indicates that a steady state distribution for this quasi-periodic orbit has possibly been obtained.

---

[12] G. R. North and M. Rankin, Thermonuclear Project Semiann. Rep. Jan. 31, 1960, ORNL-2926, p 64.

[13] M. Rankin, T. K. Fowler, and G. R. North, Thermonuclear Project Semiann. Rep. July 31, 1959, ORNL-2802, p 88–91.

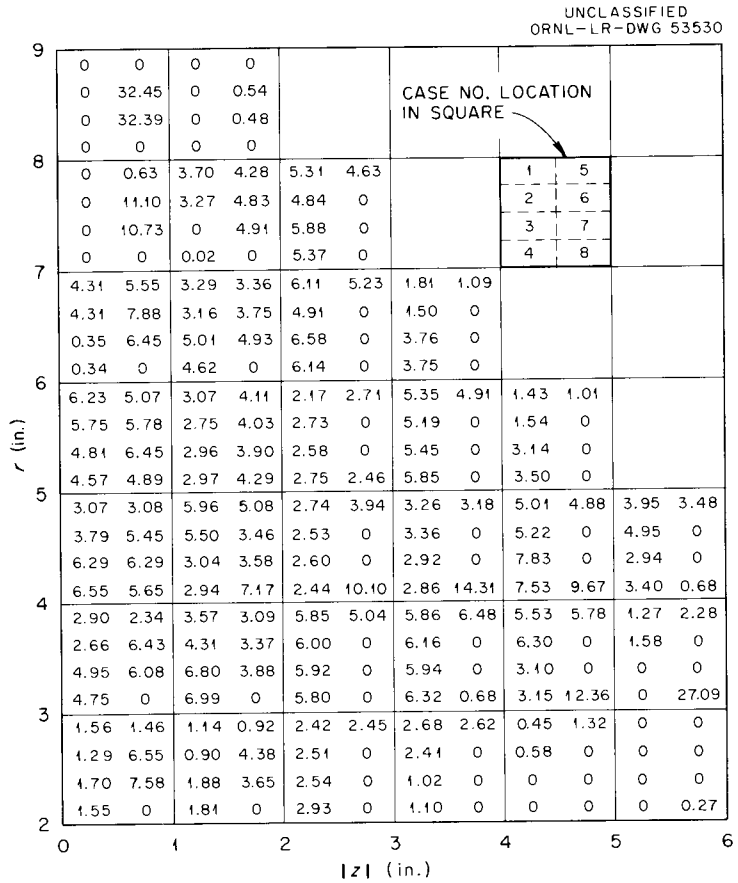

Fig. 6.5. DCX Particle Distributions for Eight Cases. Numbers in squares are percentages.

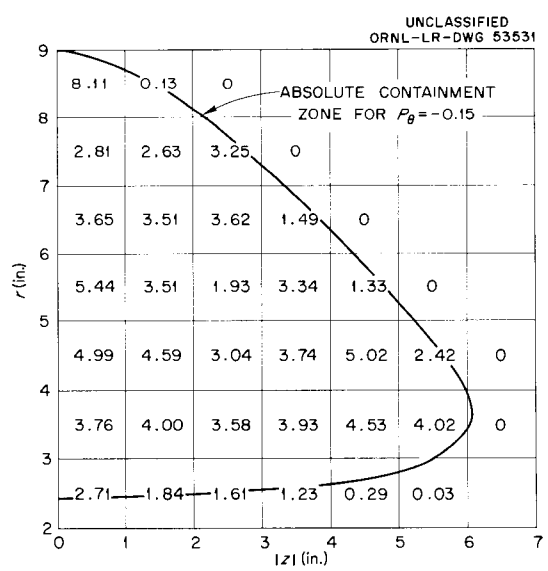

Fig. 6.6. Average DCX Particle Distribution. Percentages shown are based on 1 in.^{2}. Consideration of this should be made for those squares only partially in the containment zone.

UNCLASSIFIED
ORNL-LR-DWG 53532

r (in.)	0–1	1–2	2–3	3–4	4–5	5–6
8–9	0 0	0				
7–8	0 0	3.70 3.63	5.31 5.36			
6–7	4.31 4.26	3.29 3.31	6.11 5.96	1.81 1.77		
5–6	6.23 6.10	3.07 3.04	2.17 2.32	5.35 5.38	1.43 1.48	
4–5	3.07 3.23	5.96 5.80	2.74 2.70	3.26 3.25	5.01 4.97	3.95 4.02
3–4	2.90 2.99	3.57 3.69	5.85 5.88	5.86 5.82	5.53 5.52	1.27 1.27
2–3	1.56 1.54	1.14 1.15	2.42 2.42	2.68 2.70	0.45 0.45	0 0

|z| (in.)

Fig. 6.7. DCX Particle Distribution for $\lambda = +2$ Case. In each square the upper percentage is based on S = 100 ft and the lower percentage on S = 200 ft.

UNCLASSIFIED
ORNL-LR-DWG 54056

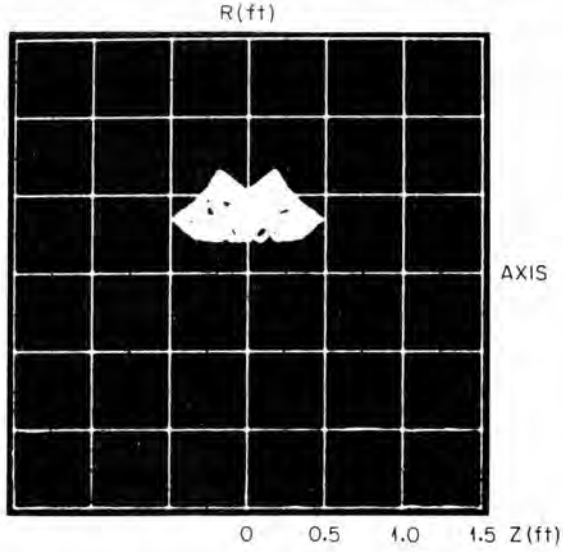

Fig. 6.8. DCX Particle Orbit for Cases 1–5.

UNCLASSIFIED
ORNL-LR-DWG 54057

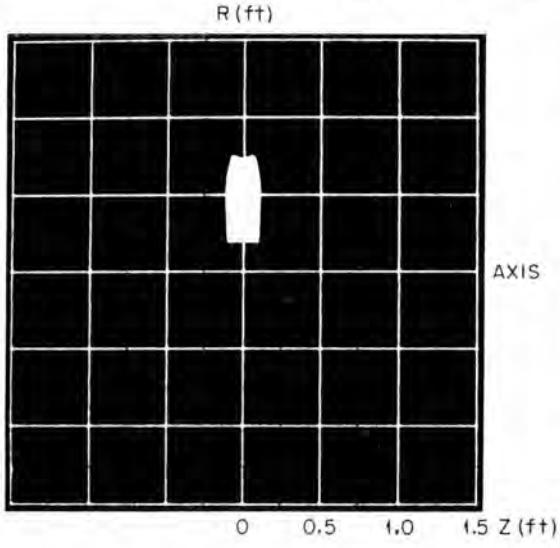

Fig. 6.9. DCX Particle Orbit for Cases 6 and 7.

UNCLASSIFIED
ORNL-LR-DWG 54058

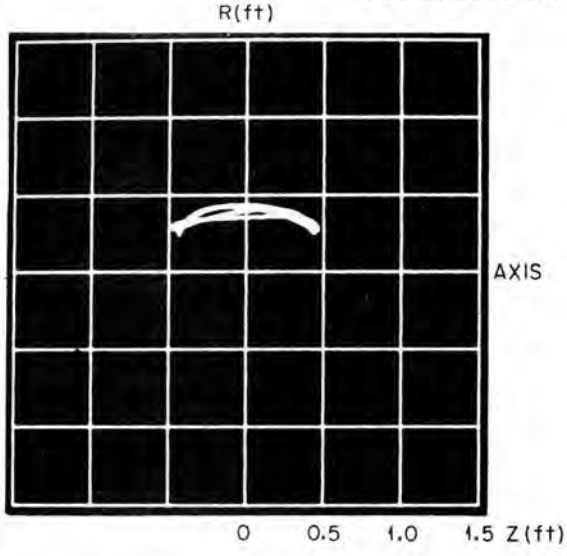

Fig. 6.10. DCX Particle Orbit for Case 8.

7. INSTRUMENTATION

7.1 ENERGY MEASUREMENTS WITH SOLID STATE DETECTORS

H. Postma J. A. Ray

Silicon surface-barrier detectors made at ORNL[1] have been calibrated in DCX. Neutral particles resulting from charge-exchange collisions of H^+ and H_2^+ in DCX give particles of a known energy and provide a means of calibrating these detectors.

The detector was mounted on a movable probe and the energetic neutral particles were collimated by a 0.005-in. hole that reduced the number of particles striking the detector's sensitive area. Pulses resulting from these particles were analyzed for their height. The energy of the injected beam into DCX was changed and the pulses from the detector were again analyzed. The result of this energy calibration may be seen in Figs. 7.1 and 7.2.

Figure 7.1 shows the pulse height distribution for 400-kev H_2^+ injection. The peak at channel 73 is due to H_2^0 resulting from the H_2^+ charge-exchanged particles and the peak at channel 33 is coming from the trapped H^+ charge-exchanging or from background gas in DCX. At these energies, the energy resolution is about 15% for H^0.

Figure 7.2 shows the response of this detector to the energy by plotting the peak position vs the energy. The result is linear down to the cutoff energy of 35 kev.

These detectors are insensitive to the magnetic fields in DCX and thus may be used in any orientation. They operate well at room temperature, are compact, are 100% efficient, and may be repeatedly let up to air or pumped down without affecting resolution or energy response.

Plans are underway to use this device to detect the energy and directions of motion of the particles emerging from the trapped ring in DCX. By this means one may find the particle distribution as well as energy loss for gas breakup and arc breakup.

---

[1]J. L. Blankenship, Instrumentation and Controls Division, ORNL.

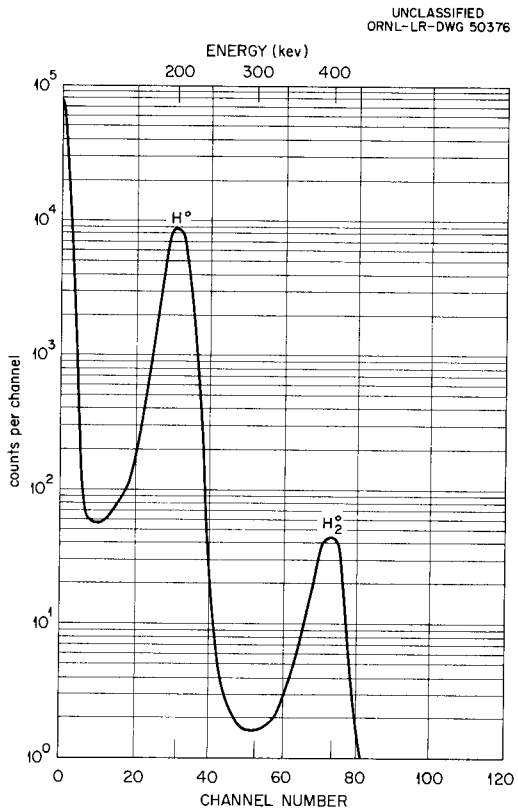

Fig. 7.1. Pulse Height Distribution for 400-kev Injection.

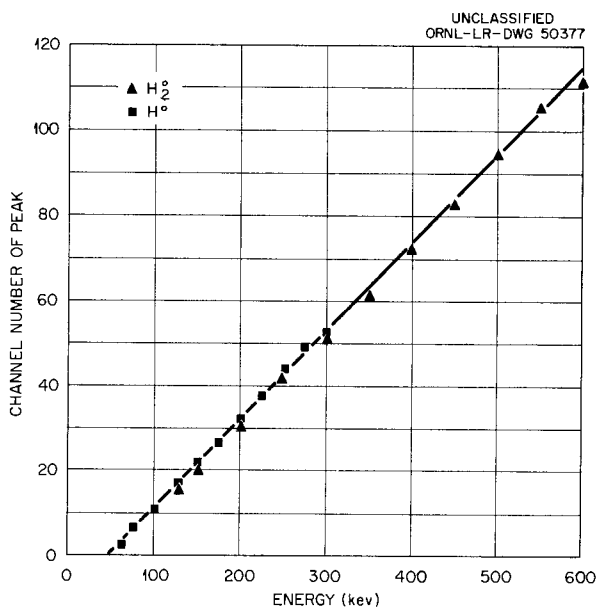

Fig. 7.2. Energy Response of Silicon Barrier Detector.

8. MAGNETIC FIELD CALCULATION, ION TRAJECTORIES, AND MAGNETIC COIL DESIGN

8.1 DESIGN OF MAGNETIC MIRROR FIELDS WITH EXTREMELY HOMOGENEOUS CENTRAL ZONES

D. L. Coffey W. F. Gauster J. E. Simpkins

In experimental devices like DCX-EPB or DCX-2 the injected molecular ions are assumed to move in helical orbits with a small pitch angle in order to achieve a large number of passes through the "breakup" arc. An ideal magnetic field configuration would consist of two magnetic mirrors and a central zone which is perfectly homogeneous, with the exception of a "field dip" which serves to change the injection angle (as determined by the injection snout) into the pitch angle of the helix.[1] Because of the necessary accessibility (port holes for plasma diagnostics, space for injection snout), lumped magnet coils must be provided and it is therefore impossible to make the central zone perfectly homogeneous. G. R. North's calculations for an infinite array of lumped solenoids[2] predict for similar coil dimensions a ripple amplitude in the order of several parts in 10^5. One cannot expect to produce the same extremely good homogeneity in the central magnetic field zone of a DCX device, since only a limited number of coils can be provided, and since the magnetic field strength has to increase over a short distance to the full value under the mirror coils, that is, to 350%.

Figure 8.1 shows a proposed coil arrangement for DCX-2; because of symmetry it is sufficient to draw only one quadrant. The dimensions are indicated in inches; the current densities i are referred to the total coil cross sections and are expressed in amperes per square inch. The power dissipated in one mirror coil is assumed to be 6 Mw (assuming operation with deuterium) producing a magnetic flux density of 59 kilogauss, and each outside booster coil is energized with 0.875 Mw.

In Fig. 8.1 three plots in different scales represent the axial magnetic flux density component B_z, normalized to the value at the center of

---

[1]P. R. Bell *et al.*, this report, sec 2.3.

[2]G. R. North, Some Properties of Infinite, Lumped Solenoids, ORNL-2975 (Aug. 10, 1960); see also sec 8.3, this report.

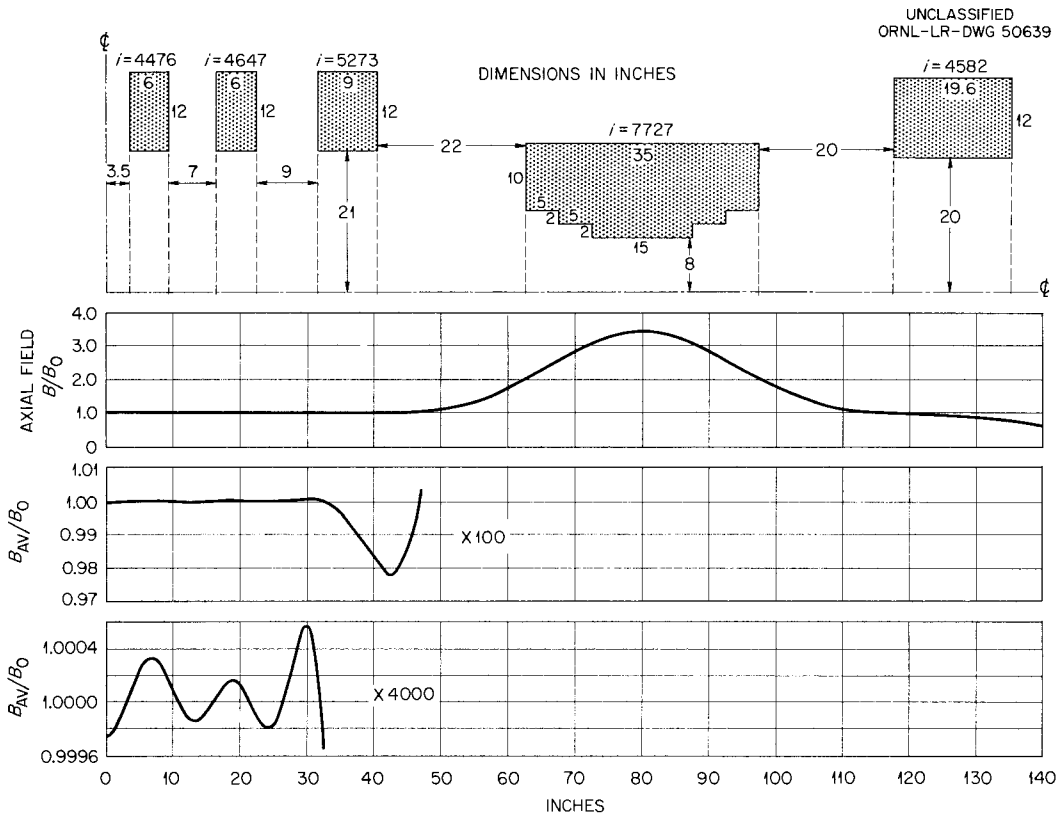

Fig. 8.1. An Alternative of the Magnetic Field Design of DCX-2.

the coil system. For calculating the appropriate "field dip," the average flux density

$$B_{av}(z) = \frac{5}{8} B_z(z,0) + \frac{3}{8} B_z(z,r = 10 \text{ in.}) \qquad (1)$$

is used instead of the component B_z on the axis.[3]

The first plot shows the homogeneous central zone extending on both sides of the center for a distance of more than 30 in. The mirror ratio is approximately 3.5. On the second plot, drawn 100 times enlarged, the field dip is easily recognizable. By a favorable coincidence, the field dip resulted as a "by-product" of the optimization performed in order to achieve the best homogeneity of the central zone. The scale of the third plot is 4000 times enlarged. B_{av} ripples of several parts in 10^4 can be seen; the ripples of $B_z(z,0)$ are still appreciably smaller. From this

[3]R. J. Mackin, Jr., "Field Dip Problems I — Particle Orbits," DCX-2 Technical Memorandum No. 21.

fact, it follows that the ripples of the DCX-2 coil arrangement are only a few times larger than those of a corresponding infinite coil array. This result seems to be very satisfactory when the relatively large mirror ratio 3.5 is considered.

For the field design shown in Fig. 8.1 the following procedure was used, which is similar to the method of "Fitting Magnetic Fields Over Specified Volumes."[4] As mentioned previously, the mirror coils and the outside booster coils have been matched to the power of existing d-c generators of 6 and 0.875 Mw respectively. All geometrical coil dimensions, including distances between the coils, have been assumed for a first trial calculation. Free variables are the current densities i_1, i_2, and i_3 in the three inside booster coil pairs, and the average flux density B_0 in the central zone. The field deviation along the axis is

$$\Delta B = B_z(z) - B_0 \quad . \tag{2}$$

The optimization is performed by making

$$\int_0^L (\Delta B)^2 dz \rightarrow \text{minimum} \tag{3}$$

or

$$\begin{aligned} &\frac{\partial}{\partial i_k} \int_0^L (\Delta B)^2 dz = 0 \quad , \quad k = 1,2,3 \quad , \\ &\frac{\partial}{\partial B_0} \int_0^L (\Delta B)^2 \, dz = 0 \quad . \end{aligned} \tag{4}$$

The half-length of the central zone is represented by L. From Eq. (4) the current densities i_k and B_0 can be obtained by solving four linear equations ("optimization with floating mirror ratio"). In order to achieve finally the desired B_0 value, the procedure has to be repeated with other distances between the mirror coils. Computer codes have been programmed[5] which permit performing this optimization procedure for any similar coil arrangement in a very convenient way.

---

[4]W. F. Gauster, Thermonuclear Project Semiann. Rep. Jan. 31, 1960, ORNL-2926, p 84; E. W. Laing, A Note on Magnetic Field Shaping, UKAEA AWRE (Harwell), report M522 (1959).

[5]G. R. North and M. Rankin, this report, sec 8.2.

8.2 MAGNETIC FIELD CODES

G. R. North M. Rankin

For DCX-2 design studies several new magnetic field codes have been written:

(1) A modification of the "standard" magnetic field code No. 668, to store the quantities B_z, A, rA, and B_r at a specified location on magnetic tape.

(2) A code, SUPERPO, which selects field quantities from magnetic tape, multiplies them by prescribed current densities, and adds together these quantities for an arbitrary number of coils. This code exists in several versions: one gives values of B_z normalized to B(0,0), one gives unnormalized values of B_z in kilogauss, and one gives unnormalized values of rA in kilogauss-in.^{2}.

(3) A code to calculate

$$\Delta H = \sum_{K=1}^{n} i_K f_K - H_0$$

for axial fields. For a coil pair,

$$f_K = \frac{2\pi}{2.54} [F(z - c_{11}) - F(z - c_{12}) + F(z + c_{12}) - F(z + c_{11})] \quad , \quad (1)$$

where

$$F(z) \equiv Z \ln \frac{a_2 + \sqrt{a_2^2 + z^2}}{a_1 + \sqrt{a_1^2 + z^2}} \quad ; \quad (2)$$

here

a_1 = inside radius of coil,

a_2 = outside radius of coil,

c_{11} = distance from midplane to near side of coil,

c_{12} = distance from midplane to far side of coil.

This code prints out the contribution of each coil pair, the total field, and the deviation of the field from a given value of H_0.

(4) A code, EFFIE, which evaluates the integrals which are coefficients in the system of linear equations used in solving for optimum current densities for a given coil arrangement.[6] This code permits evaluation of an arbitrary number of integrals of the forms

$$\int_0^a f_K dz \quad \text{and} \quad \int_0^a f_K f_{K'} dz \quad ,$$

where f_K is a function of the type given in Eqs. (1) and (2).

(5) A code, TIM, which is a combination of codes EFFIE, (8-32) equation solver, and SUPERPO. TIM applies only for the coil arrangement proposed for DCX-2 (four rectangular coils plus a three section mirror coil).[6] This single code calculates coefficients, solves a set of linear equations for optimum current densities, and uses these values to calculate and print out the field due to the coil system. This code exists in two versions. In one the value of H_0 is fixed and the optimization is with respect to the current densities of the three inside boosters. In the other, the optimization is with respect to H_0 and also the current densities of the three inside boosters.

8.3 PROPERTIES OF INFINITE, LUMPED SOLENOIDS

G. R. North

In producing magnetic fields for thermonuclear devices, the question of field uniformity often arises. Since many machines are of a solenoidal type, an interesting problem arises in calculating the field due to an infinite sequence of coaxial current loops, equally spaced and of equal radii and current. The homogeneity of such a field is closely related to the homogeneity of the field due to a finite number of loops.

Since the field is periodic, B_z on the axis is expanded in a Fourier series. The coefficients in the series are obtained in a closed form. When the radius, R, of the loops is large compared to the separation, λ, the field reduces to the simple form

$$B_z(z) \cong B_{SOL}\left(1 + 2\pi\sqrt{\frac{R}{\lambda}}\, e^{-2\pi R/\lambda} \cos\frac{2\pi}{\lambda} z\right) \quad ,$$

[6] D. L. Coffey, W. F. Gauster, and J. E. Simpkins, this report, sec 8.1.

where B_{SOL} is the field due to an infinite, solenoidal current sheet surrounding the axis. The second term represents a small harmonic perturbation to this uniform field. Knowing that the Laplacian of the vector potential vanishes in a current-free region, we are able to calculate all the field quantities, both on and off the axis. The approximate equation above is integrated over a coil cross section to approximate the form of an infinite system of rectangular coils. These results and procedures are discussed more thoroughly elsewhere.[7]

8.4 SIMULATION OF AXIALLY SYMMETRIC MAGNETIC FIELDS

W. F. Gauster H. Mott[8] C. E. Parker

The external fields of experimental devices such as DCX-EPB and DCX-2 are of special interest for the following reasons:

1. Large stray fields will affect measuring instruments in the vicinity of these machines.

2. Ferromagnetic materials magnetized by the external field could significantly affect the internal field of such a device.

In order to avoid cumbersome and questionable calculations, experiments using a coil system ("model") which simulates the original external field are desirable. The simplest model would consist of one pair of coils only, but since the DCX device is of appreciable axial extension, the outside field would be sufficiently simulated at great distances only. Therefore a model made at least of two pairs of coils should be used.

The numerical data of the original coil system (DCX-2) (see Fig. 8.2) are as shown in Table 8.1.

Four coils (a_1 = 6 in., a_2 = 14.525 in., 2b = 4 in.) constructed for the 10-ft Long Solenoid[9] are available for building the model (see Fig. 8.3).

---

[7]G. R. North, Some Properties of Infinite, Lumped Solenoids, ORNL-2975 (Aug. 10, 1960).

[8]Summer employee, University of Alabama.

[9]W. F. Gauster and J. N. Luton, Jr., Thermonuclear Project Semiann. Rep. July 31, 1959, ORNL-2802, p 111.

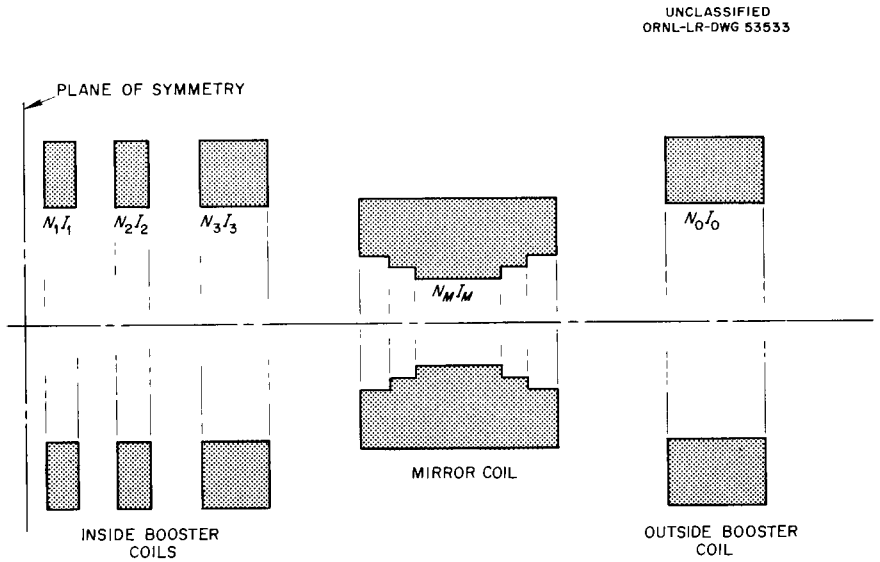

Fig. 8.2. DCX-2 Coils.

Table 8.1. Original Coil System (DCX-2) Data

Coil	Inner Radius (in.)	Outer Radius (in.)	Axial Thickness (in.)	Distance from Origin to Coil Midplane (in.)	NI (ampere turns)
					$\times 10^6$
First booster	21	33	6	6.5	0.6
Second booster	21	33	6	19.5	0.6
Third booster	21	33	12	37.5	0.6
Mirror (top rectangle)	12	22	35	77.5	5
Mirror (middle)	10	12	25	77.5	
Mirror (bottom)	8	10	15	77.5	
Outside booster	21	33	17.6	123.8	1.5

The starting point of the calculation is a development of the original field in Legendre polynomials[10]

$$B_{IZ} = \sum_{k=1}^{\infty} C_{2k} P_{2k}(\cos\theta)\, \rho^{-(2k+1)} \quad , \tag{1}$$

[10]M. Rankin and W. F. Gauster, Thermonuclear Project Semiann. Rep. July 31, 1959, ORNL-2802, p 105; M. W. Garrett, J. Appl. Phys. 22, 1091 (1951).

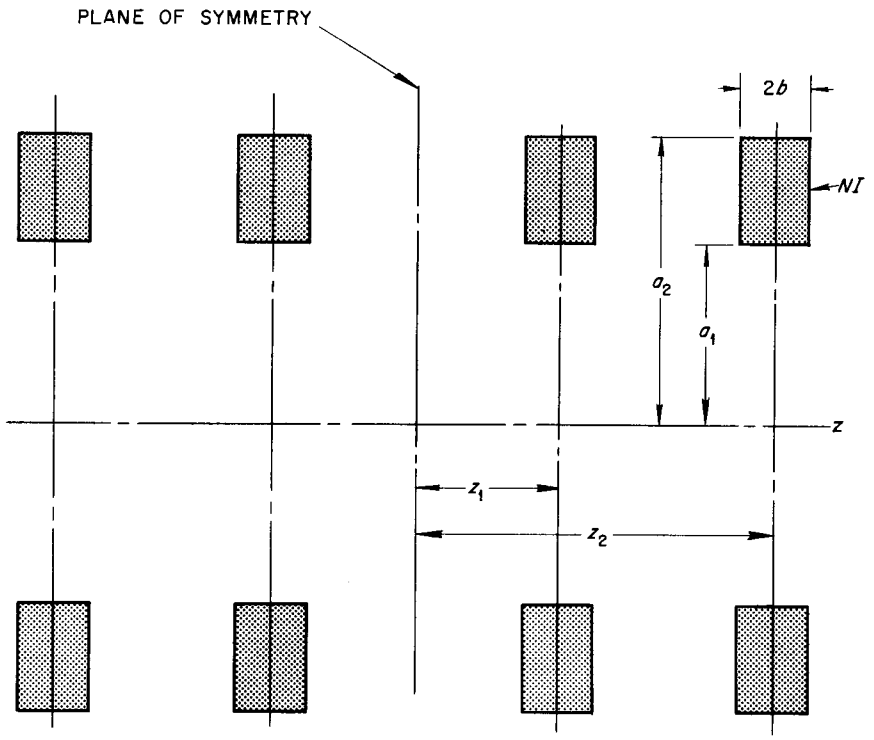

Fig. 8.3. Model Coils.

where ρ and θ are the spherical coordinates of a field point in the rotationally symmetric magnetic field. The first three coefficients have the following numerical values:

$$\left.\begin{aligned} C_2 &= 4.718220 \times 10^{9} \quad , \\ C_4 &= 1.907013 \times 10^{14} \quad , \\ C_6 &= 5.501861 \times 10^{18} \quad . \end{aligned}\right\} \tag{1a}$$

The model (Fig. 8.3) is determined if the three quantities Z_1, Z_2, and NI are known. The ampere turns of all coils are supposed to be equal, which simplifies the performance of the experiment. The external magnetic field of the model, developed in Legendre polynomials, is

$$B_{IIZ} = \sum_{k=1}^{\infty} K_{2k} P_{2k}(\cos\theta)\ \rho^{-(2k+1)} \tag{2}$$

Since Z_1, Z_2, and NI are free parameters it is possible to satisfy three equations:[11]

$$\left.\begin{aligned} K_2 &= C_2 \quad , \\ K_4 &= C_4 \quad , \\ K_6 &= C_6 \quad . \end{aligned}\right\} \tag{3}$$

The coefficients K_{2k} are linear functions of NI, but depend in a very complicated way on Z_1 and Z_2. It would be possible to find Z_1 and Z_2 by means of a computer code based on Garrett's development of fields produced by coils with solid cross sections in Legendre polynomials. For our purposes, however, it is sufficient to simplify the problem by using Lyle's theorem.[12] This theorem states that the magnetic field produced by a solenoid with rectangular cross section and constant current density can be approximated by the field of two loops. In case (a) of Fig. 8.4

$$\begin{aligned} r_1 &= \frac{a_1 + a_2}{2}\left[1 + \frac{2}{3}\left(\frac{b}{a_1 + a_2}\right)^2\right] - \frac{1}{\sqrt{3}}\sqrt{\left(\frac{a_2 - a_1}{2}\right)^2 - b^2} \quad , \\ r_2 &= \frac{a_1 + a_2}{2}\left[1 + \frac{2}{3}\left(\frac{b}{a_1 + a_2}\right)^2\right] + \frac{1}{\sqrt{3}}\sqrt{\left(\frac{a_2 - a_1}{2}\right)^2 - b^2} \quad . \end{aligned} \tag{4}$$

In case (b)

$$\begin{aligned} r &= \frac{a_1 + a_2}{2}\left[1 + \frac{1}{6}\left(\frac{a_2 - a_1}{a_1 + a_2}\right)^2\right] \quad , \\ \ell &= \frac{1}{\sqrt{3}}\sqrt{b^2 - \left(\frac{a_2 - a_1}{2}\right)^2} \quad . \end{aligned} \tag{5}$$

In both cases the number of ampere turns of each loop is half of the original number of ampere turns. This approximation is not based on the identity of a certain number of Legendre coefficients of the solid

[11]The general conditions will not be discussed here; cf. a similar problem, A. and F. Sauter, Z. Physik 122, 120 (1940).

[12]T. R. Lyle, Phil. Mag. [6]3, 310 (1902).

UNCLASSIFIED
ORNL-LR-DWG 53535

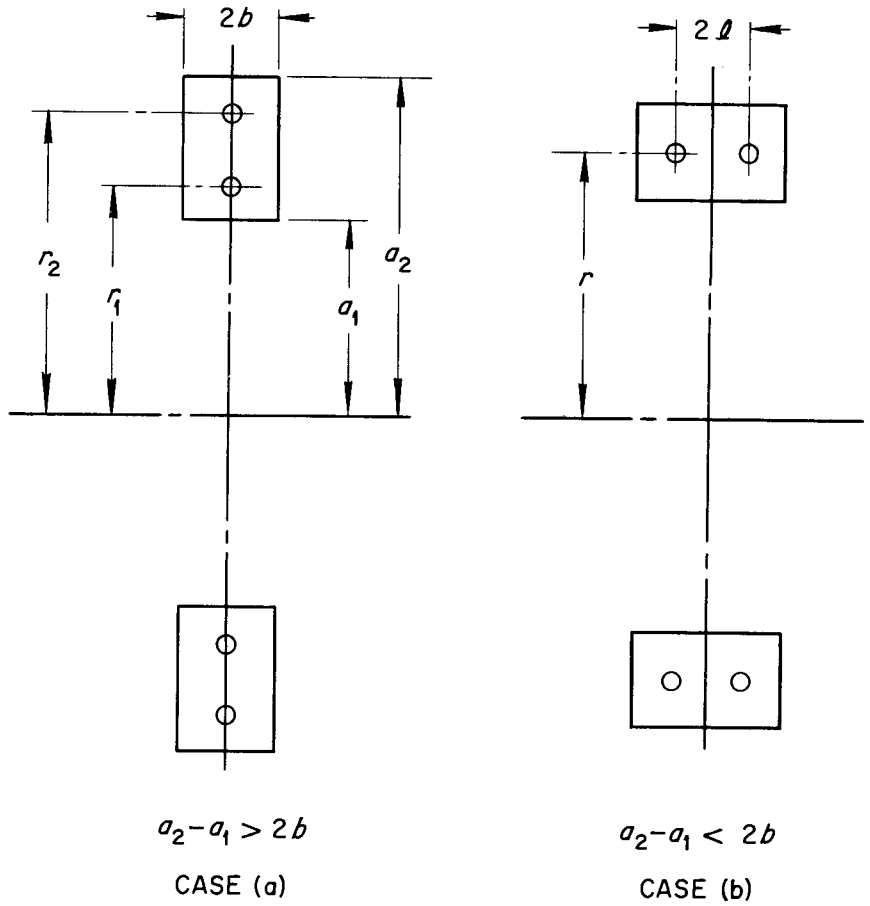

Fig. 8.4. Lyle's Theorem.

coil and the equivalent loops respectively. Rather, all corresponding coefficients differ slightly from each other; however, for cross sections not too large compared with the mean radius, the approximation is very good.

The external magnetic field produced by one loop pair[13] (see Fig. 8.5) is

$$B_Z = \frac{2\pi}{5} \frac{I \sin^2\alpha}{R} \sum_{k=1}^{\infty} P'_{2k-1}(\cos\alpha) P_{2k}(\cos\theta) \left(\frac{R}{\rho}\right)^{2k+1} . \qquad (6)$$

[13]Compare the forms for the internal magnetic field; see W. F. Gauster, Thermonuclear Project Semiann. Rep. Jan. 31, 1960, ORNL-2926, p 84, Eq. (5).

UNCLASSIFIED
ORNL-LR-DWG 53536

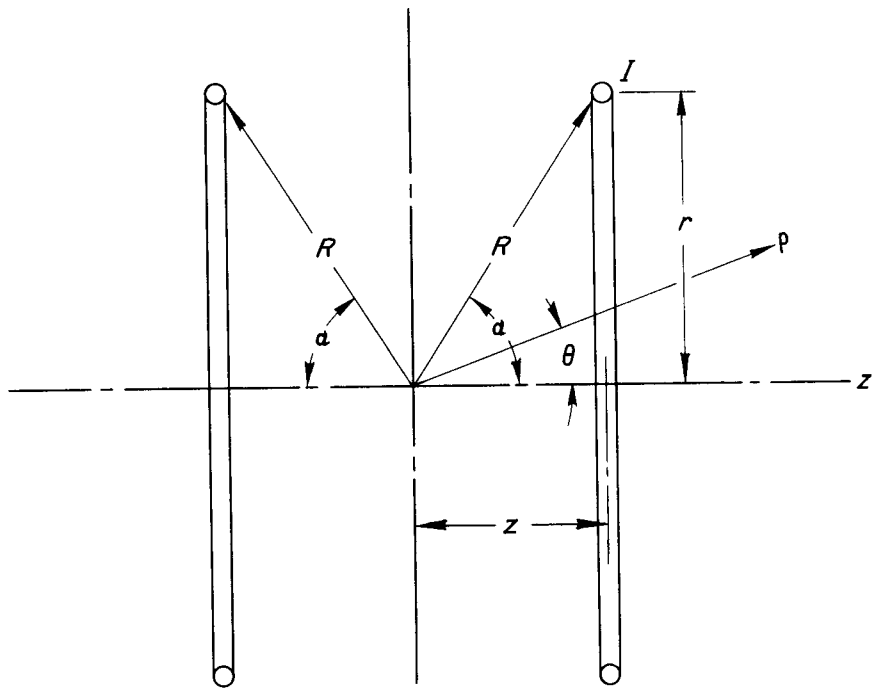

Fig. 8.5. Loop Pair.

Cylindrical coordinates are introduced ($r = R \sin \alpha$, $Z = R \cos \alpha$). Then the first three coefficients of a Legendre polynomial development which represents the field produced by the four loop pairs equivalent to the two coil pairs of the model (see Fig. 8.3) are

$$K_2 = \frac{2\pi}{5} NI(r_1^2 + r_2^2) \quad ,$$

$$K_4 = \frac{3\pi}{5} NI[2(r_1^2 + r_2^2)(Z_1^2 + Z_2^2) - (r_1^4 + r_2^4)] \quad , \tag{7}$$

$$K_6 = \frac{3\pi}{4} NI[4(r_1^2 + r_2^2)(Z_1^4 + Z_2^4) - 6(r_1^4 + r_2^4)(Z_1^2 + Z_2^2) + (r_1^6 + r_2^6)] \quad .$$

In these equations r_1 and r_2 follow from Eqs. (4); NI, Z_1, and Z_2 are unknowns. By using the identities of Eqs. (3) and the numerical values of Eqs. (1a), all unknowns are easily calculated, since Eqs. (7)

are linear in NI and quadratic in Z_1^2 and Z_2^2. The numerical values are

$$\left.\begin{aligned} NI &= 16.8 \times 10^6 \text{ ampere turns} \;, \\ Z_1 &= 31.7 \text{ in.} \;, \\ Z_2 &= 112.0 \text{ in.} \end{aligned}\right\} \qquad (8)$$

Of course the model coils will not be operated with a current corresponding to the calculated very high number of ampere turns, rather with a convenient current. Figure 8.6 shows B_Z measured along the axis

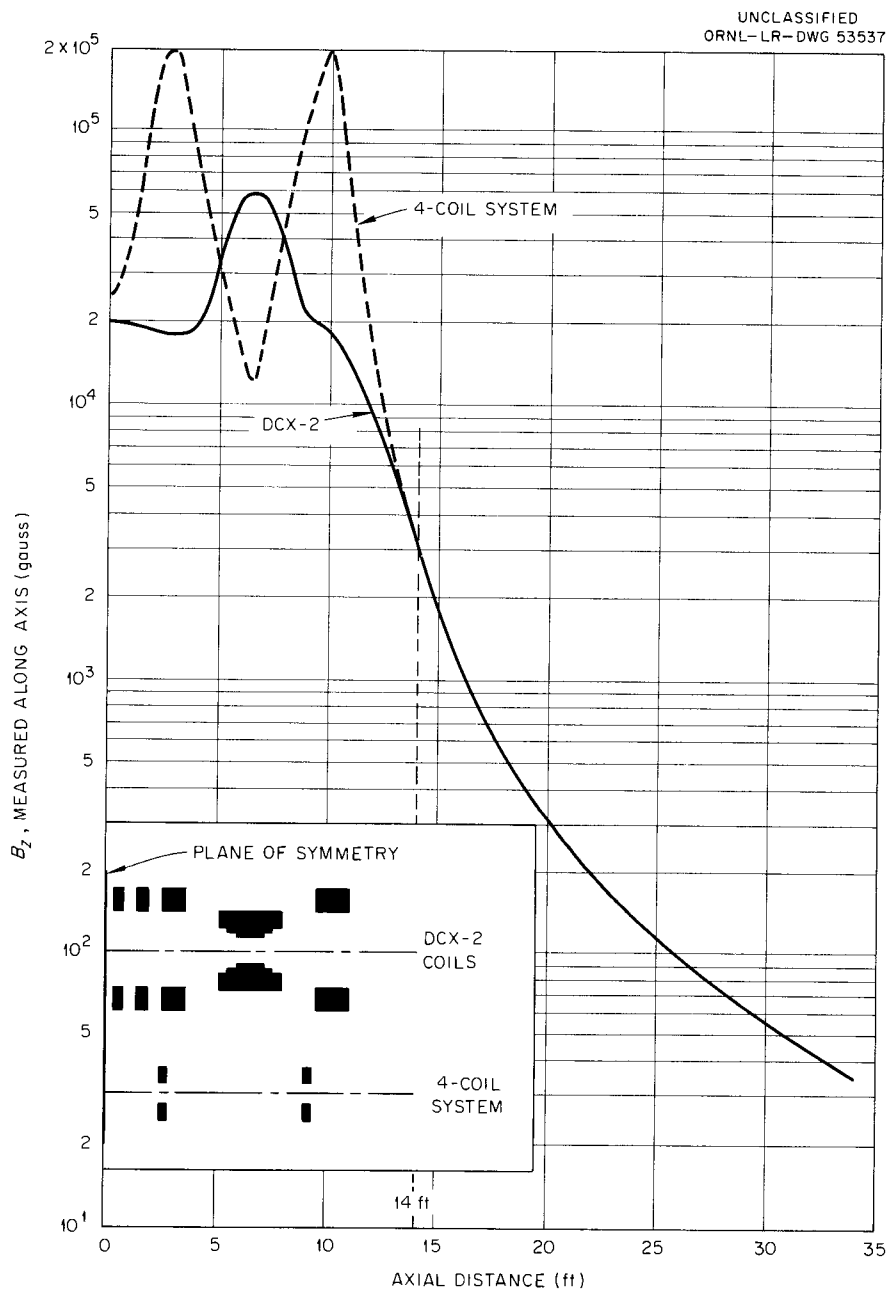

Fig. 8.6. Axial Fields of DCX-2 and Equivalent 4-Coil System.

for the original DCX-2 coil arrangement (solid line) and for the model (dashed line). Finally Fig. 8.7 represents B_Z measured in the plane of symmetry. The approximation is very good beyond Z = 14 ft in Fig. 8.6, and beyond r = 7 ft in Fig. 8.7.

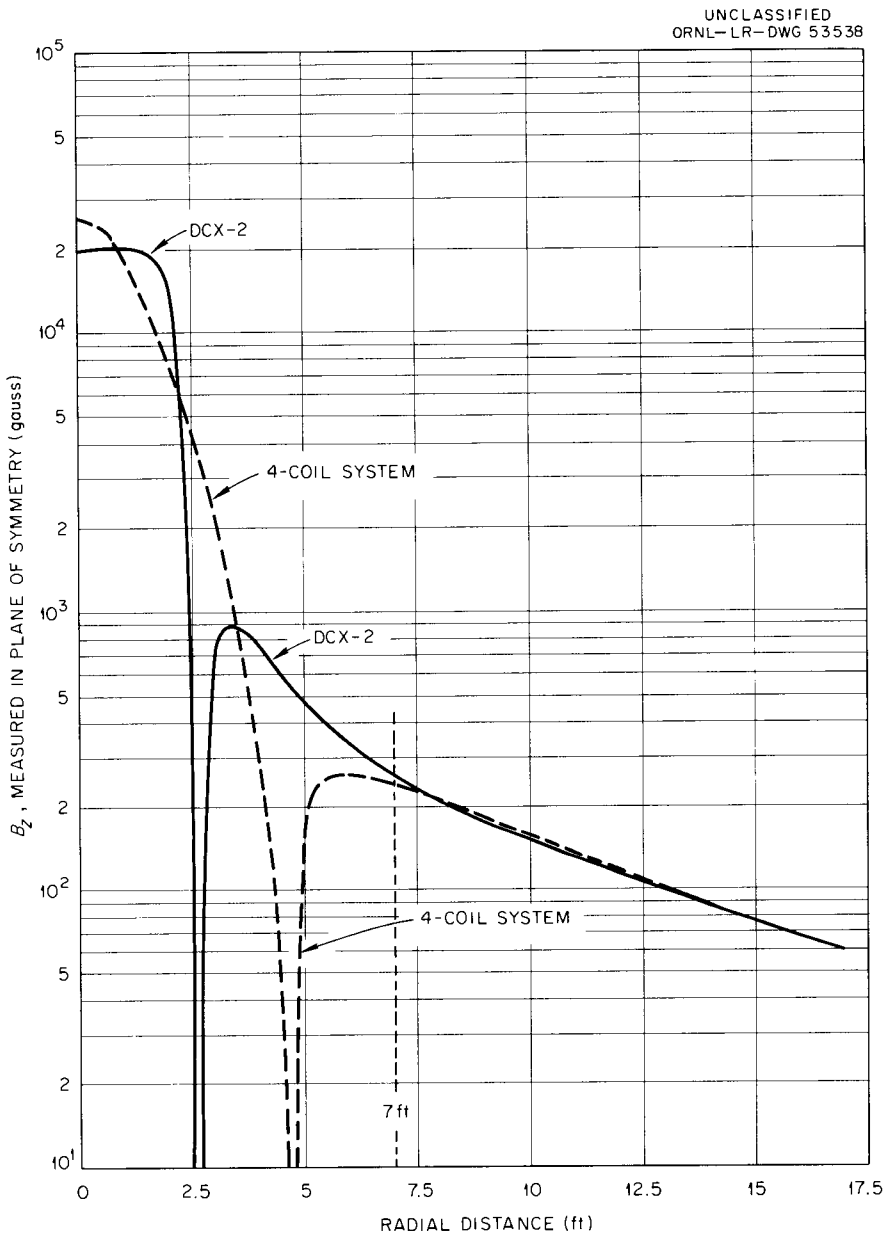

Fig. 8.7. Fields of DCX-2 and Equivalent 4-Coil System in the z = 0 Plane.

8.5 DESIGN OF AN ION INJECTION SNOUT

R. L. Brown W. F. Gauster

DCX-2 and EPB require ion injection snouts which are field free on the inside, do not disturb the external field, and occupy as little space as possible. It was decided to shield the injection tube with ferromagnetic material and compensate the external effects of this material by means of a special cosine coil around it.[14] The design of a model coil is shown schematically in Fig. 8.8. Due to the space requirements at

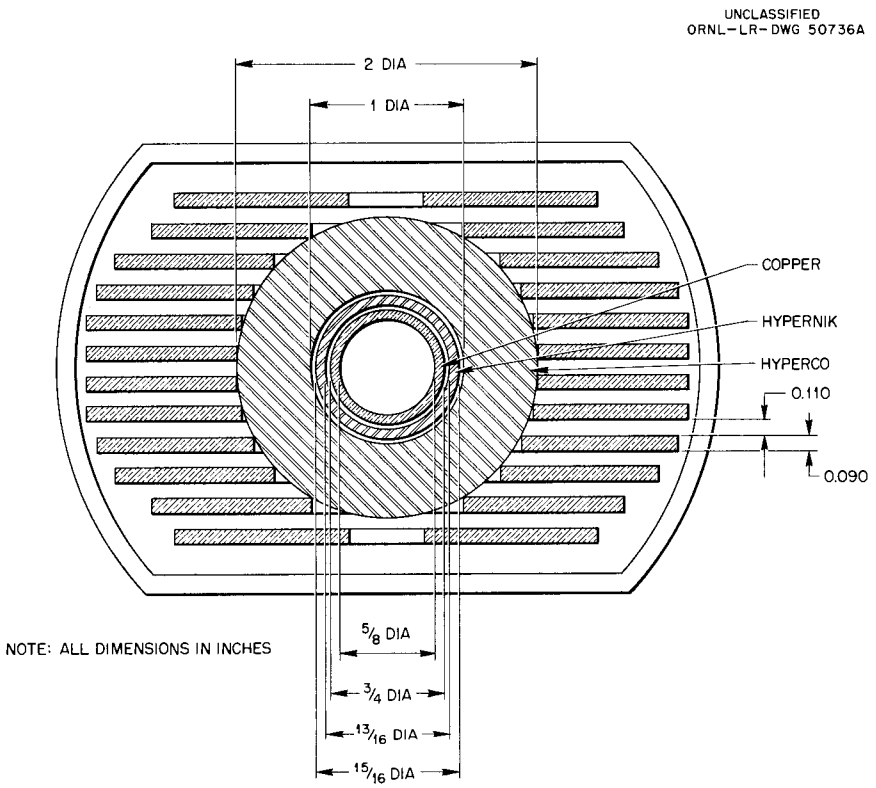

Fig. 8.8. Ion Injection Snout (Schematic Cross Section).

the ends where the conductors must go around the injection hole, it is necessary to make the coil conductors from copper sheets. Current densities of the order of 100,000 amp/in.^{2} or more must be used requiring short water paths, thin conductors, and large cooling surfaces. It is

---

[14]F. C. Gilbert, A Beam Inflector, UCRL-56[illegible] (1960); see also sec 2.4.2, this report.

expected that the bulk heating of the water will be small, the temperature drop in the copper moderate, and the film drop large.

A model of the ion injection snout has been constructed and partially tested. Measurements have been started of the magnetic field which results when the injection snout (with energized windings) is brought into a homogeneous magnetic field. These data will allow designing the midray trajectory of the injected molecular ion beam,[15] and studying the influence of the injector fringe field on the focusing of the ion beam. This problem is a very difficult one. It can be shown easily, however, that the fringe field does not influence considerably the midray trajectory of the injected ion beam.

If the magnetic field strength would change suddenly at the snout end point A (Fig. 8.9) from zero to the full value B_o of the homogeneous

[15]R. L. Brown and D. L. Coffey, Thermonuclear Project Semiann. Rep. July 31, 1959, ORNL-2802, p 107; R. L. Brown, Thermonuclear Project Semiann. Rep. Jan. 31, 1960, ORNL-2926, p 81.

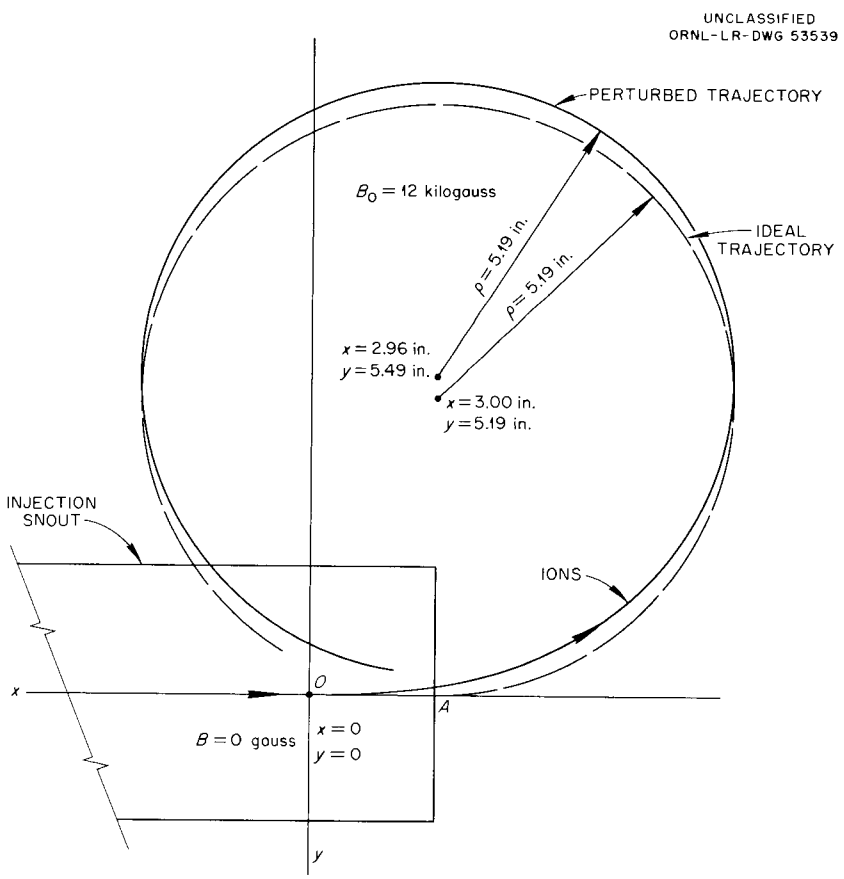

Fig. 8.9. DCX-2 H_2^+ Beam Entry, E = 600 kev.

field zone, a circular trajectory ("ideal trajectory") would result. In order to estimate the actual trajectory, the following consideration can be made. Suppose the z component of the magnetic field strength would increase along the trajectory at a constant rate starting from zero at a point O (see Fig. 8.10) up to the full value B_o at a point P. The length $\overline{OP}$ is assumed to be $\ell = nc$ (n = 3 shown in Fig. 8.10), c being the length of a trajectory segment. The values of B_z at the midpoints

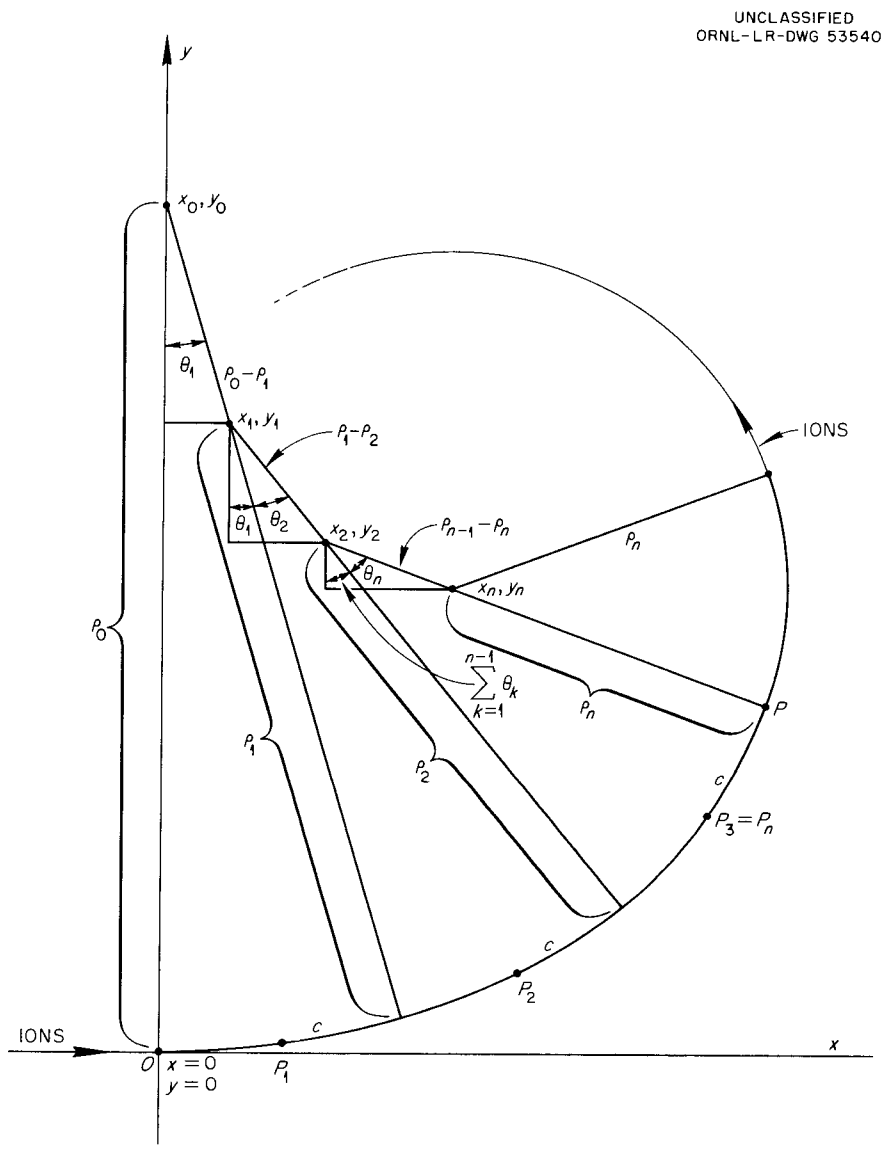

Fig. 8.10. Perturbation of the Injected Ion Beam in the Fringe Field of an Injector Snout.

of the trajectory segments are

$$B_1 = \frac{B_o}{2n} \quad , \quad B_2 = \frac{3B_o}{2n} \quad , \quad \cdots \quad , \qquad (1)$$

$$B_n = \frac{(2n-1)B_o}{2n} \quad , \quad B_k = \frac{(2k-1)B_o}{2n} \quad .$$

The average radii of curvature are

$$\rho_k = \frac{p}{qB_{k+1}} \quad , \qquad (2)$$

where

p = ion momentum,

q = ion charge.

The angles θ_k (see Fig. 8.10) are

$$\theta_k = \frac{c}{\rho_{k-1}} \quad . \qquad (3)$$

The coordinates of the centers of the circles of curvature can be found step by step as follows:

$$x_0 = 0 \quad , \quad x_1 = (\rho_0 - \rho_1)\sin\theta_1 \quad ,$$
$$y_0 = \rho_0 \quad , \quad y_1 = \rho_0 - (\rho_0 - \rho_1)\cos\theta_1 \quad ,$$

$$x_2 = x_1 + (\rho_2 - \rho_1)\sin(\theta_1 + \theta_2) \quad ,$$
$$y_2 = y_1 - (\rho_2 - \rho_1)\cos(\theta_1 + \theta_2) \quad ,$$

and finally,

$$x_n = x_{n-1} + (\rho_n - \rho_{n-1})\sin\left(\sum_{k=1}^{n}\theta_k\right) \quad ,$$
$$y_n = y_{n-1} - (\rho_n - \rho_{n-1})\cos\left(\sum_{k=1}^{n}\theta_k\right) \quad . \qquad (4)$$

The coordinates of the center of curvature of the circular trajectory in the undisturbed homogeneous center zone are x_n and y_n.

As mentioned before, this calculation is based on the very arbitrary assumption that the magnitude of the path length $\ell = nc$ in the fringe

field is known and that the gradient of the magnetic field strength along this part of the ion trajectory is constant. By assuming a large value of ℓ, however, it is possible to estimate a safe limit for the magnitude of perturbation of the trajectory by the fringe field of the snout. In Fig. 8.9 numerical values are shown, assuming $\ell = 6$ in. As can be seen, the difference between the perturbed and the ideal trajectory is not considerable.

8.6 CONNECTION OF WATER COOLED CONDUCTORS

R. L. Brown J. N. Luton, Jr.

DCX-2 and EPB magnet coils are designed to consist of "pancakes," wound of hollow copper tubes. Copper current densities of approximately 20,000 amp/in.^{2} will be used, requiring water path lengths of 50 to 90 ft. The joining of the large number of water paths (900 for DCX-2) requires reliable, low resistance electrical joints between tubes. The joints should also fit in a small space, operate at a reasonably low temperature, and produce no magnetic disturbances. In some cases they must be capable of being disconnected and reconnected in a different manner, in order to change the over-all electrical resistance of the coil.

It appeared that standard joints might not fulfill all of the above requirements. For that reason a facility was set up to test newly designed electrical joints for rectangular water cooled copper tubes. Two 7000-amp rectifiers in parallel were used to feed the test section, which consisted of two pieces of copper tubing (cross section 0.565 in. square with 0.30-in.-dia hole), each 4 ft long, with their ends connected by the test joint. Water flow was held near 8.5 gpm for all tests. The current most commonly used was 11,000 amp (46,500 amp/in.^{2}), more than twice the anticipated normal current.

Temperatures were measured by thermocouples on the conductor near the water inlet, and at several locations on the test joint. Voltages were measured between one fixed point 6 in. from the center of the joint and a series of 12 points spaced at 1 in. intervals along the conductor. The resistances between the fixed and the 12 reference points were calculated and plotted as a function of the distances; such a curve is shown in Fig. 8.11. The observed points scatter only slightly (which

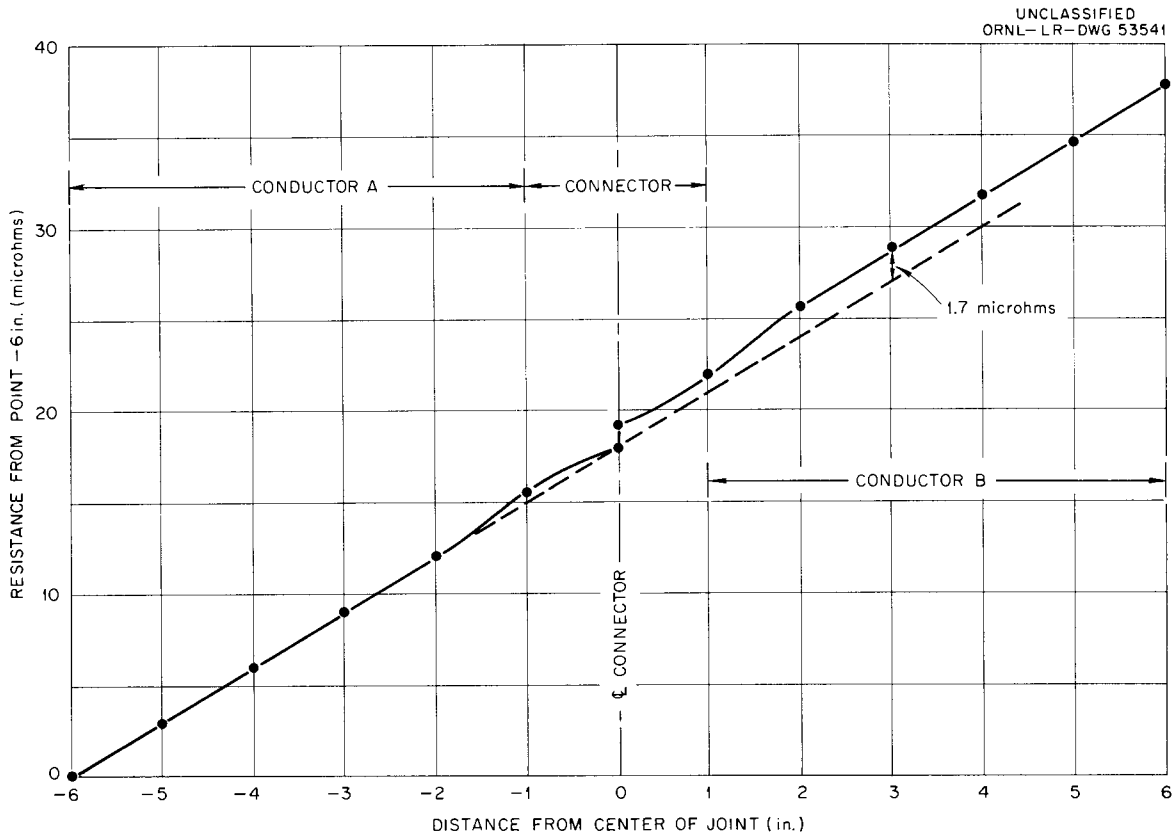

Fig. 8.11. Resistance Distribution Along Two Conductors Joined by Bolted Connector.

indicates the consistency of the measurements) about two parallel straight lines. This shows that the effect of water temperature rise on resistance was small, and confirms that the conductor was uniform (for 1 ft) in cross section and resistivity. The vertical distance between the lines represents the increased resistance due to the joint, which in most cases was less than 1.7 microhms, an acceptably low value. Some of the joints, such as the 4-in. soldered joint, had a much greater cross section than the conductor itself, and therefore a lower resistance than an equal length of conductor. In this case, the joint gives a "negative additional resistance" to the circuit, and line B of Fig. 8.11 falls below the extension of line A. Figure 8.12 shows several types of the tested joints. The tabulated resistances are, in each case, the total resistance values of the joint and of 6 in. of conductor on both sides.

The temperature rise of the hottest portion of the various joints depended much less upon the joint resistance than upon the effectiveness

UNCLASSIFIED
ORNL-LR-DWG 50679A

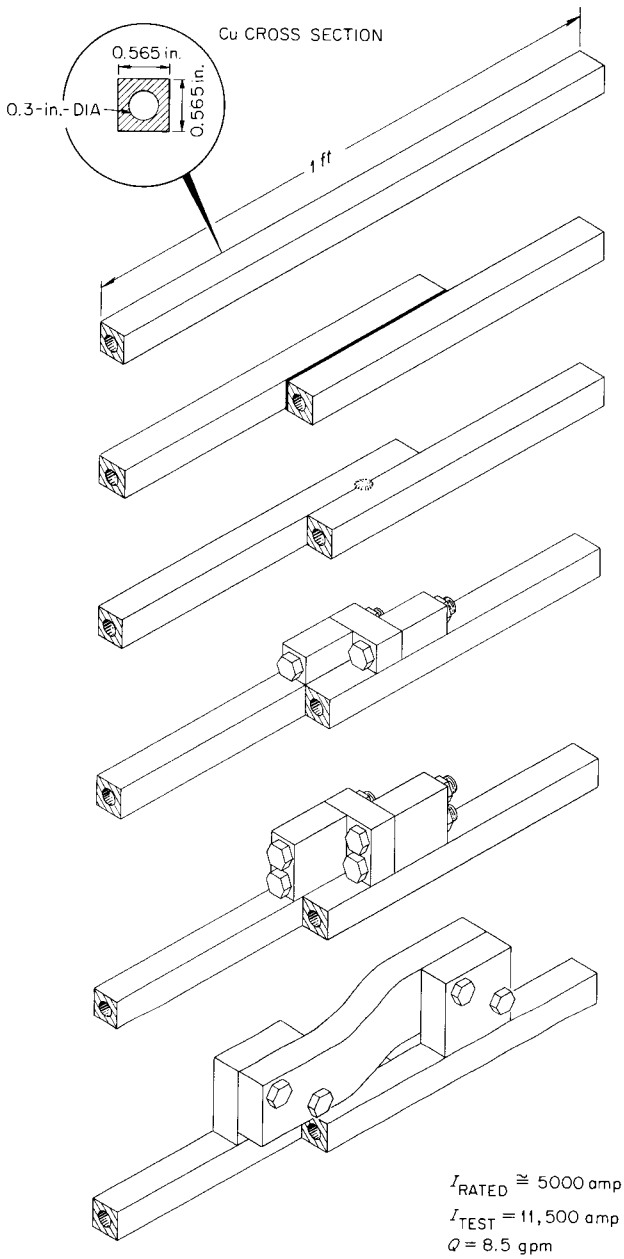

CONNECTION	RESISTANCE (microhms/ft)	TEMPERATURE RISE (°C)
NONE	35.7	0
3-in. SOFT SOLDER	31.6	−3.5
3/8-in. Cu SPOT WELD	39.3	112.3
SINGLE BOLTED BAR	37.7	108.5
DOUBLE BOLTED BAR	34.6	34.5
EXTENDED BAR	31.5	>150

Fig. 8.12. Connection of Water Cooled Conductors.

of the cooling. None of the joints were of large enough cross section to be sufficiently cooled by natural air convection at the currents used. Their cooling depended almost entirely on the water flow through the conductor. The heat liberated at the top center of the joint flows as follows: (1) through the metal of the joint, (2) across the interface between the conductor and the joint material, (3) across the conductor cross section, and (4) through the stagnant water surface film, before it is finally removed by the cooling water. Paths (3) and (4) are the same for all joints. The electrical and thermal resistance of the interface (item 2) is negligible in the case of a well-made soldered, brazed, or welded joint. These resistances can also be made extremely small for a bolted, clamped, or wedged removable joint, if only the two metal surfaces are clean and brought into intimate contact at several points.[16] Thus the effect of item 2 in a removable joint can be made negligible if the surfaces are carefully cleaned and if the pressure is sufficient to inelastically deform one of the joint metals. A uniform conductor with uniform current density, cooled at one end only, has a temperature difference between hot and cold ends proportional to the square of the length. This temperature rise is equal to 70°C for a 2-in.-long copper conductor at 20,000 amp/in.^{2} Item 1 above, then, is not negligible, but stands as the determining factor of the joint hot spot temperature, a fact borne out by the test results. Joints with current carrying parts far from the cooling water always ran hot, even though their cross section was large and their electrical resistance was low (see extended bar connector in Fig. 8.12). Temperatures beyond the 150°C range of the recorder were encountered.

A few of the removable joints were run at the overload current for several days, and were subjected to 10 min cycling of the rated current for a day. No change in resistance, either permanent or temporary, was noted.

For permanent connections the soft-solder joint, as shown in Fig. 8.12, seems ideal. It can be made without heat damage to the adjacent insulation when used with inorganic insulating material, and can even

[16]R. Holm, Electric Contacts Handbook, Springer, Berlin (1958).

be used with insulators such as Mylar if cooling air is passed through the conductor hole while the joint is being soldered. The completed joint is small, has an extremely low resistance, and changes only very little the magnetic field of the coil. However, a conductor so joined cannot easily be removed and reconnected to a different lead.

No decision has yet been made concerning the definite design of the removable joint to be used on DCX-2. The joints which are mechanically rugged and easy to connect tend toward high temperatures and bulkiness, whereas the smaller joints have yet to be proved sufficiently strong to stand up under the inadvertent forces encountered when disconnecting and reconnecting the joints several times. The tests are being continued.

9. SPECTROSCOPIC INSTRUMENTATION

9.1 THE TRANSMISSION GRATING AS A DIAGNOSTIC TOOL

G. K. Werner

Transmission gratings are found to be useful in arc diagnostics when used as "slitless spectroscopes." By well-known laws of diffraction an arc image upon passage through the grating is separated into an array of monochromatic arc images. The advantages of this type of spectroscopy are:

1. It is easier to operate than a slit spectroscope since there are no mechanical adjustments. Alignment is easier because one does not lose orientation with respect to the light source.
2. Spatial analysis of the spectrum is possible. For example, one can observe that certain wavelengths are emitted only from the core of the arc, while others seem to come from the whole tank interior, from the fringe of the arc, or from the hot region near the anode. This type of spectroscopy is virtually impossible with slit spectroscopes.
3. Using the transmission grating with standard photographic equipment it is possible to use high apertures and short exposure times. Apertures of f/1, or possibly higher, can be used. Standard spectrographs have apertures of f/10 to f/40.

The disadvantages are:

1. Resolution is low, usually being limited by the angular size of the light source.
2. If the spectrum is not intense one must shield the grating from stray room light.

For visual work an inexpensive grating film with 13,400 lines/in. has been used. The film was cut into 5/8-in. disks and mounted in cardboard tubes about 6 in. long to reduce stray light.

For more exacting photographic work, where uniform ruling over a larger aperture is required, a 15,000 lines/in. plane glass transmission grating made by Bausch and Lomb was used. It has very high efficiency with 50 to 70% of the light in the first order and only 5 to 10% in the undiffracted beam. Figure 9.1 shows the spectrum in the anode region of a lithium arc, photographed with a Polaroid camera. Motion picture color photography has also been used.

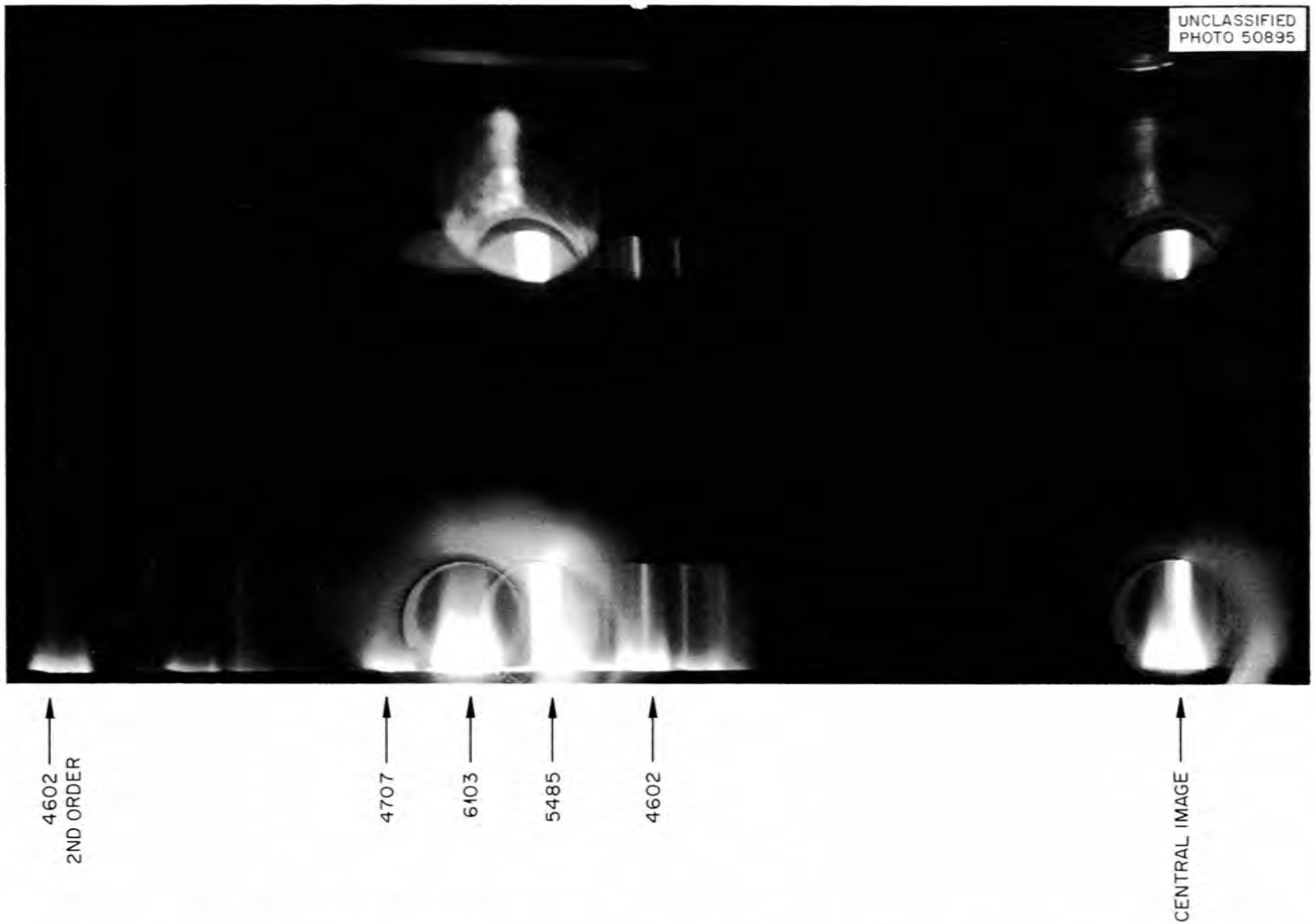

Fig. 9.1. Anode End of Lithium Arc Photographed Through a Diffraction Grating. The 5485 A emission is from Li^+. All other images are from neutral lithium.

9.2 GRATING CALIBRATION SPECTROMETER

W. F. Peed

During this period, engineering design, both mechanical and instrument, on the grating calibration spectrometer has been completed and submitted to shops for fabrication. The unit is scheduled for completion during December 1960. With the exception of the angle (wavelength) measuring equipment and the gratings, all items for fabrication are on hand. Gratings are scheduled for delivery in September 1960.

10. H_2^+ CROSS-SECTION MEASUREMENTS

10.1 DEVELOPMENT OF CROSSED-BEAM APPARATUS

D. P. Hamblen
H. Postma
L. A. Massengill
F. E. Dunnam[1]

Apparatus is being developed for the purpose of measuring the dissociation products of H_2^+ ions in collision with electrons.[2,3] A 90° analyzing magnet and focusing system have been installed to increase the intensity and focus of the 20-kev H_2^+ beam. This has reduced considerably the problem of small-angle scattering from the beam tube walls and slit dissociation on the beam defining slits. An intensity of 120 ma/cm^2 in the collision region has been achieved with a subsequent increase in signal by a factor of 5 over previous attempts.

The electron source now produces 3 ma/cm^2 of 13.4-v electrons by means of parallel plate electrode construction and an indirectly heated cathode. The beam spreads, due to space-charge influence, to a diameter three times greater than the diameter of the cathode. There is still a slight nonuniformity in the spatial homogeneity of the electron beam that is not explained.

The vacuum chambers have been modified, and pressures of 3×10^{-7} mm Hg are easily attained in the detection region with the beam on. The electronic circuits have been developed and testing is under way. The a-c component of the signal — that part of the signal arising from the modulated electron source — is amplified by a narrow-band amplifier. When the output of this amplifier is selected by a phase sensitive detector, the intensities of electron-dissociated beams are found. This method will increase the signal to noise ratio to 100 to 1.

Silicon barrier detectors were tried as another means of detection, but their inherent noise was equivalent to 20-kev ions and thus rendered them useless for detection of the lower energy ions of this experiment.

---

[1]Summer participant from University of Florida.

[2]C. F. Barnett *et al.*, *Thermonuclear Project Semiann. Rep. July 31, 1959*, ORNL-2802, p 115.

[3]D. P. Hamblen *et al.*, *Thermonuclear Project Semiann. Rep. Jan. 31, 1960*, ORNL-2926, p 94.

10.2 DISSOCIATION OF H_2^+ BY HYDROGEN

D. P. Hamblen L. A. Massengill
H. Postma

10.2.1 Introduction

The cross section for dissociation of H_2^+ by gases has been measured over a wide energy range by several investigators. The target gas hydrogen has received the most attention; nonetheless, the measured cross sections offer a wide variety of choices. The absolute cross sections have been in disagreement by as much as a factor of 3 in the region of present thermonuclear interest (100 to 600 kev).

10.2.2 Apparatus

Figure 10.1 displays a schematic of the experimental apparatus. An ion beam from the high-voltage accelerator is magnetically analyzed to

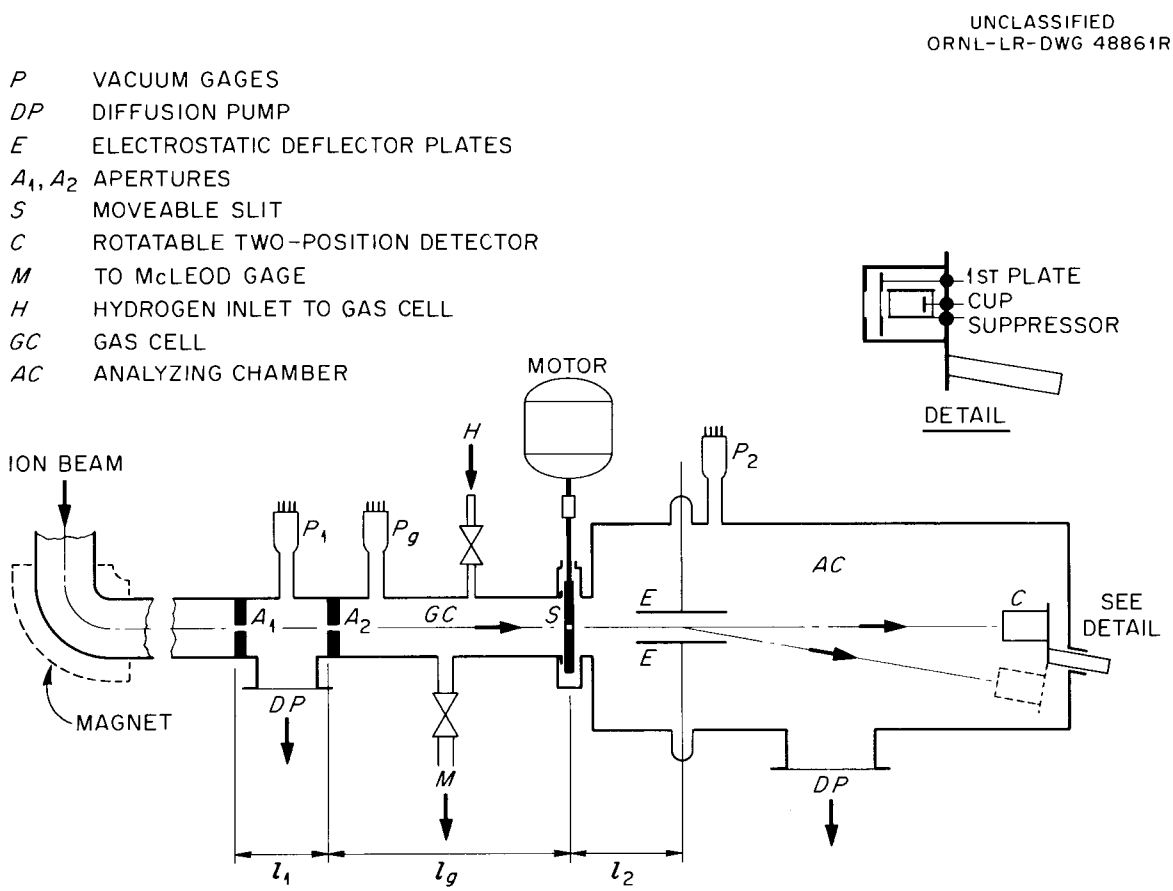

Fig. 10.1. Schematic of Experimental Apparatus.

give H_2^+ of a known energy. The ions are first collimated and then enter a differentially pumped target gas chamber. The H_2^+ interacts with the hydrogen gas in this chamber, and then H_2^+ together with its dissociated particles H^0 and H^+ exit through a motor-driven slit whose travel extends 1 in. in a direction perpendicular to the beam. The pressure in the gas cell is maintained at a constant value by the balance between gas flow inward through the needle valve and flow outward through aperture A_2 and slit S. This pressure is measured by a liquid-nitrogen-trapped mercury McLeod gage. The emerging particles are energy analyzed by a set of electrostatic deflection plates and are detected by a Faraday cup and a secondary-electron emission collector. The resulting currents were measured by an electrometer, displayed on a recorder, and integrated over the path of travel of the slit. Both n, the density of hydrogen gas, and ℓ the effective length of the gas cell over which n is constant comprise the areal density ($n\ell$) of the target. The effective length of the cell was the geometrical length ℓ_g of the cell plus a calculated ℓ_s due to gas streaming from the cell in the direction of the beam plus a length ℓ_b due to background pressures in the immediate vicinity of the cell. This effective length ranged from 45.1 to 45.4 cm, depending upon the operating pressures of the cell.

The details of the Faraday cup and the secondary-electron collector are shown in the insert of Fig. 10.1. The aperture of the detector was 1 in. square. The first plate suppressed the departure of electrons from the Faraday cup assembly and was biased at −115 v. The Faraday cup assembly was a square plate "cup" surrounded by a "square box suppressor." When a positive beam was detected (either H^+ or H_2^+) this suppressor was biased at −22.5 v to prevent secondary electrons (emitted when the beam hit the cup) from leaving the cup. An electrometer between the cup and ground measured the current of the impinging beam. This same assembly was also used to detect a neutral beam (either H^0 or H_2^0); in this case, the secondary electrons emitted when the neutral beam struck the cup were collected on the "square box suppressor" by biasing the "cup" at −22.5 v. An electrometer between the suppressor and ground measured the secondary-electron emission current. This method of collecting electrons also was used to detect the electrons resulting from H^+ and H_2^+ striking the cup.

The bias voltages used were experimentally chosen so that the number of particles detected was independent of the voltage applied. In summary: the voltage on the electrostatic plates and the position of the detector determined whether a neutral beam, H^+ beam, or H_2^+ beam entered the detector. Then when the cup was connected to the electrometer and the suppressor biased at −22.5 v, only the charged beams were measured. However, when the suppressor was connected to the electrometer and the cup biased at −22.5 v, then secondary-electron emission current was measured.

10.2.3 Experimental Procedure

For a known amount of target gas in the collision chamber, the exit slit of the gas chamber was scanned across the emerging particles and the resulting beam current collected by the detector was integrated. The following results were measured: H_2^+ in Faraday cup (FC), H^+ in FC, $H_2^+ + H^+$ in FC, H^0 in secondary-electron collector (SEC), H^+ in SEC, H_2^+ in SEC, and $(H_2^+ + H^+ + H^0)$ in SEC. From the integration and graphical display of these currents, it was possible to calculate the dissociation cross section and angular spread of the beam. The pressure in the cell was then changed and a set of currents corresponding to this new pressure was measured at the same energy. From the functional change of current ratios with $n\ell$, the cross sections could be found.

The loss of H_2^+ occurs in these various modes in the energy range of our interest:

Mode	Cross Section
$H_2^+ \rightarrow H^0 + H^+$	σ_1
$H_2^+ \rightarrow 2H^+$	σ_2
$H_2^+ \rightarrow 2H^0$	σ_3
$H_2^+ \rightarrow H_2^0$	σ_4

If one assumes that only reactions σ_1 and σ_2 are important, then the cross sections are related to measured currents in the following manner:

$$\sigma_T n\ell + A = -\log_e [I(H_2^+)/I_0] \quad , \qquad (1)$$

$$\sigma_1 n\ell + B = \frac{I(H^0)}{I_0}\left\{\frac{-\log_e\,[I(H_2{}^+)/I_0]}{1 - [I(H_2{}^+)/I_0]}\right\}, \tag{2}$$

$$\sigma_2 n\ell + C = \frac{I(H^+) - I(H^0)}{2I_0}\left\{\frac{-\log_e\,[I(H_2{}^+)/I_0]}{1 - [I(H_2{}^+)/I_0]}\right\}, \tag{3}$$

where $I_0 = I(H_2{}^+) + [I(H^0) + I(H^+)]/2$ and $\sigma_T = \sigma_1 + \sigma_2$ = total loss cross section. Another combination of these cross sections convenient to use is the proton production cross section $\sigma_p = \sigma_1 + 2\sigma_2$.

In the above expressions, $n\ell$ is the areal density, the letters A, B, and C are the lumped effects which arise from background dissociation by slits and residual gas in the system. The effect of these backgrounds is eliminated by plotting these expressions vs $n\ell$. The slopes of the resulting lines give σ_T, σ_1, and σ_2, and the intercepts give A, B, and C. (See Fig. 10.2.)

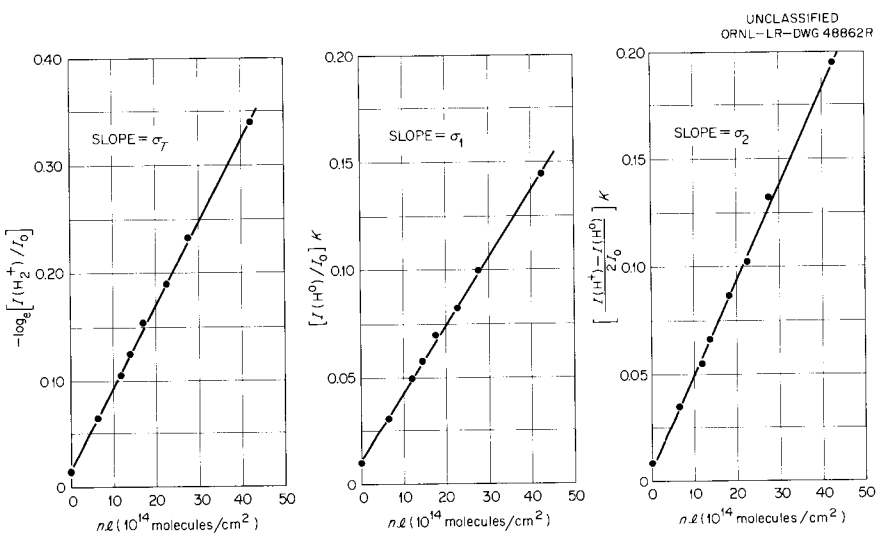

Fig. 10.2. Variation of Beam Current Ratios with Pressure Changes for 600-kev $H_2{}^+$.

The values A, B, and C also result from the measurement of the current when n = 0. This was confirmed experimentally by shutting off the gas supply and measuring the currents, giving A, B, and C directly. Independent runs that were made to check reproducibility of the results agreed to 3% with the previous runs at the same energy.

10.2.4 Results

Cross Sections

The results of these experiments (displayed together with published data in Figs. 10.3 and 10.4) show good agreement with Sweetman to 500 kv but agree more closely with Barnett at higher energies. The investigators

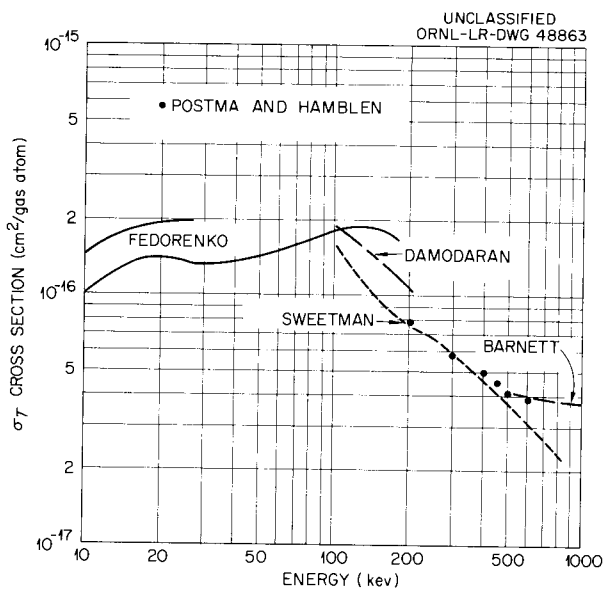

Fig. 10.3. Total Cross Section for H_2^+ Loss in H_2.

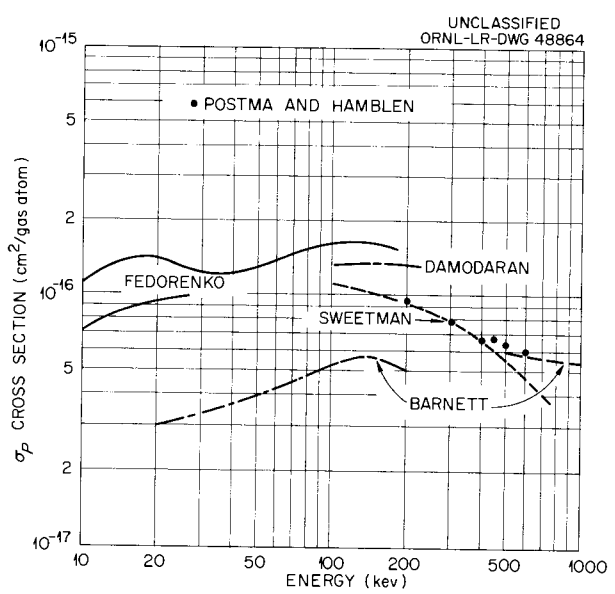

Fig. 10.4. Proton Production Cross Section for H_2^+ in H_2.

have been: Sweetman[4] (100 to 800 kev); Barnett[5] (20 to 200 kev and 500 to 2250 kev); Fedorenko[6] (5 to 180 kev); Damodaran[7] (100 to 220 kev); and Postma and Hamblen (200 to 600 kev). Although the agreement between Sweetman and this experiment may be fortuitous, the different methods of measurement of the reactions, the checks incorporated into the measurements, and the methods of calculation, all support the contention that the grouping of these separate measurements is probably a more genuine agreement.

The errors in the absolute cross section for this experiment are of the order ±15%. The trend of the present data shows agreement with Barnett's high-energy results, but it is also apparent from present work that Barnett's low-energy results do not fall in the region of the other data.

Angular Distributions

An energetic H_2^+ in collision with a target molecule may be excited into a repulsive state by making an electronic transition which obeys the Franck-Condon principle. Classically, the individual particles resulting from such a dissociative transition share the energy equally and are isotropically distributed in space in the center-of-mass system. The dissociated H^0 and H^+ from a beam of H_2^+ thus acquire a slight angular deviation from the original direction of the H_2^+ beam.

Since all the beams were scanned by the exit slit, it was possible to observe experimentally the widths of these beams at the exit aperture. Figure 10.5 shows typical widths of H_2^+ and H^+ beams for incident 200-kev H_2^+. By convolution of the two curves, the effect of the spread of the incident H_2^+ beam may be subtracted to leave only the spread of the H^+ (or H^0) resulting from the dissociation process.

---

[4]D. R. Sweetman, Phys. Rev. Letters 3, 425 (1959).

[5]C. F. Barnett, Proc. U.N. Intern. Conf. Peaceful Uses Atomic Energy, 2nd, Geneva, 1958 32, 398 (1958).

[6]N. V. Fedorenko et al., Zhur. Tekh. Fiz. 24, 769 (1954); Zhur. Eksptl. i Teoret. Fiz. 36(9), 267 (1959).

[7]K. K. Damodaran, Proc. Roy. Soc. (London) A239, 382 (1957).

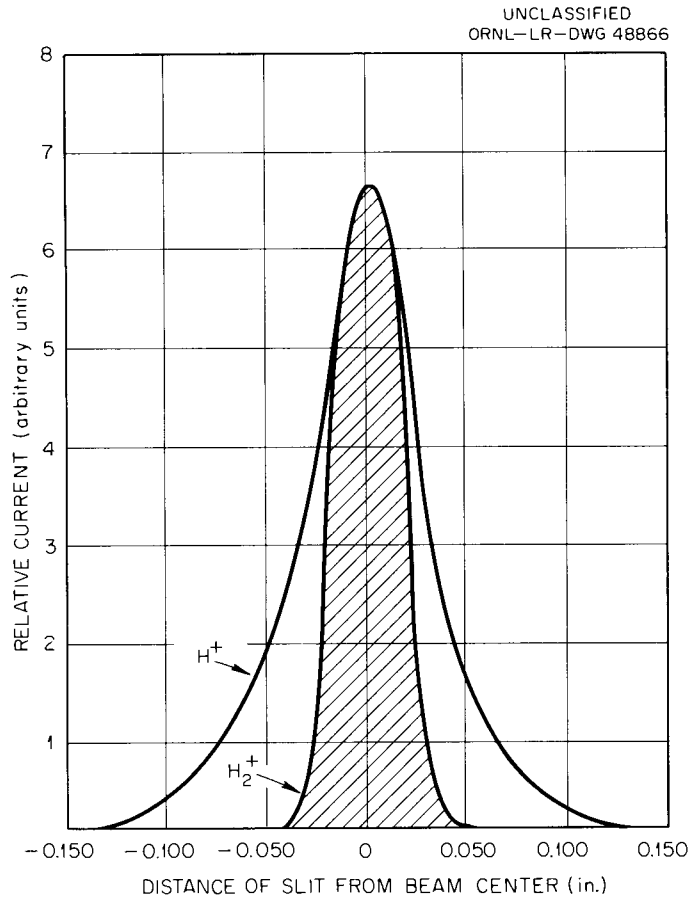

Fig. 10.5. Beam Widths at 200 kev.

This points out strongly that one must be very careful to have large enough exit apertures to ensure collection of all the broken up beams. The data show that if the entrance and exit aperture were of the same diameter, then σ_p would be too low by more than a factor of 2 at 200 kev. Experimentally this reduction in cross section was measured at 300, 400, and 500 kev, with an entrance aperture of 1/16 in. in diameter, and an exit aperture of 3/32 in. in diameter. The reduction for σ_p was 1.75 at 300 kev, 1.50 at 400 kev, and 1.27 at 500 kev. The linear spread depends strongly on the gas cell length. This is perhaps a reason for Barnett's cross sections being lower at the low energies than the other reported measurements.

Theoretical attempts to calculate the dissociation cross section using the Born approximation have been made by Salpeter[8] and by Gerjuoy.[9] The extension of their predictions into the lower energy region where our work was done is not adequate in accounting for the dissociation cross section.

---

[8]E. E. Salpeter, Proc. Roy. Soc. (London) A63, 1295 (1950).

[9]E. Gerjuoy, Research Report 60-94439-1-R2, Westinghouse Research Laboratories, Pittsburgh, 1955.

11. VACUUM SYSTEMS AND TECHNIQUES

C. E. Normand
F. A. Knox
R. V. Neidigh
R. E. Clausing[1]
R. A. Strehlow
J. D. Redman[2]
R. E. Wells

11.1 INTRODUCTION

Vacuum systems research carried out in the past six months has continued to be concerned primarily with pumping methods. An increasing amount of attention has been given to vapor deposited metal film pumping in addition to the continuing studies of diffusion and ionization-getter pumping. The evaluating of other vacuum system components and instrumentation has dealt with the development and operation of a vacuum gage test facility, the preliminary study of zeolite trapping, and the application of a mass spectroscope to low-pressure gas analysis. Outgassing and permeability studies were restricted to the measurement of the helium permeability of three ceramics.

11.2 DIFFUSION PUMPS

11.2.1 Tests of National Research Corporation 32-in. Diffusion Pump

Performance tests of four 32-in. diffusion pumps with matching angle valve were completed early in this period, and the results have been reported.[3] Operated at their rated power (10 kw), and with Convoil-20 as the pumping fluid, the four pumps showed essentially identical performance characteristics.

The results reported are summarized as follows:

1. Pumping speed for air: 18,000 liters/sec at pump inlet; 13,600 liters/sec at valve inlet.
2. Pumping speed for hydrogen: 25,000 liters/sec at pump inlet; 21,370 liters/sec at valve inlet.

---

[1]Metallurgy Division.

[2]Reactor Chemistry Division.

[3]F. A. Knox, Test Results NRC H-32-P Diffusion Pump, and Type 1259-32 Angle Valve, ORNL CF-60-5-94 (May 20, 1960).

3. Base pressure: 2×10^{-7} mm Hg.
4. Limiting static fore pressure: 200 to 250 μ.
5. Rate of oil backstreaming to valve inlet: 0.5 cc/day with cooled cap; 20 cc/day without cap.

Except in the matter of pumping speed, the observed performance equaled or excelled the manufacturer's claims for these pumps. Our measurements of pumping speed, however, were about 30% lower than the manufacturer's rating.

It appears now that the speed discrepancy arises from errors in calibration of the ionization gages used in both sets of measurements, and that the true pumping speed lies somewhere between the two values quoted.

11.2.2 Exposed Diffusion Pump Jets

The feasibility of enhancing the performance of an oil diffusion pump by raising the top diffusion stage to a point well above the top of the pump barrel, thereby fully exposing the uppermost vapor stream in the region being evacuated, has been under investigation. For these studies, a Westinghouse 20-in. diffusion pump with improved Distillation Products Industries jets and an 8-in. booster was modified by cutting a 20-in. section from the midpart of the pump barrel and rewelding the shortened bottom section onto the original upper flared section. The original jet assembly, when installed in this shortened barrel, projected a full 9 in. above the pump barrel into the test dome, which was a 36-in.-dia by 36-in.-high cylinder equipped with ion gages, a leak line, and oil collecting burets.

Observations were made of pumping speed, rate of oil streaming to the test dome, base pressure, and limiting fore pressure. Following initial tests of the original jet assembly unmodified, various modifications were made of the top jet assembly with a view to increasing pumping speed, reducing oil-streaming to the test dome, or both. The modifications involved changes in position, diameter, slope, and contour of the top jet cap, and changes in spacing and shape of the annular nozzle defining the vapor stream.

With these various modifications, pumping speeds have been observed ranging from a low 2000 liters/sec for very poor designs to a high of 13,000 liters/sec. High pumping speeds were usually accompanied by high

rates of oil collection in the test dome. This, together with the appearance of high temperature zones near the bottom of the test dome, implies a wide divergence of the primary vapor stream from the top jet, and an effective first stage pumping aperture of 36 in. in diameter. In most cases, the speeds observed were in the 7000- to 10,000-liters/sec range, which is probably not much greater than the unbaffled speed of the original 20-in. pump.

The rate of oil collection in the test dome also varied widely (from 0.2 to 22 cc/min) for different arrangements of the top jet. The lower collection rate is comparable to the backstreaming rate sometimes observed in pumps of this size, and may be due to simple backstreaming from the pump. The higher rates, however, are undoubtedly associated with a vapor jet diverging into the test dome. Some progress has been made in shaping the top jet nozzle to reduce this divergence; however, an optimum design has not been established. In spite of the high rate of oil-streaming into the test dome, base pressures with most of the jet assemblies were surprisingly low — usually about 2×10^{-7} mm Hg.

As expected, the limiting fore pressure for the 20-in.—8-in. pump combination was found to be just the 150 μ characteristic of the 8-in. booster, and was independent of changes made in the 20-in. pump.

11.2.3 Liquid Metal Diffusion Pumps

New liquid metals are being sought for use as diffusion pump fluids. Among the advantages of these elemental fluids are their low vapor pressure at room temperature and freedom from decomposition products in the atmosphere of the system.

Lithium and sodium have been tested in a small 4-in.-ID diffusion pump using a set of jets manufactured for use with mercury. The chemical activity of these metals as contrasted to mercury has presented problems in addition to those usually associated with diffusion pump operation. At temperatures approaching those needed for the production of metallic vapor sufficient for diffusion pump operation, hydrogen is liberated from some compound, probably the hydride, present with the metals sodium and lithium.

With both metals there is some evidence of gettering activity. With sodium this is greatest around 400°C and with lithium at 450°C. The low

pressure attained with sodium is a few microns, while that with lithium is about 0.1 μ. With sodium between 450 and 500°C the pressure of hydrogen increases to about 500 μ. The hydrogen was detected by mass spectrographic analysis. With lithium, the pressure increases to 1 μ at 725°C. While no analysis of this gas was obtained, it is presumed to be hydrogen.

The experiment is being continued with potassium as the liquid metal. It is hoped that the higher vapor pressure of potassium will enable diffusion pumping to occur at lower temperatures and that the compounds producing hydrogen will be decomposed and removed completely at the temperature of operation.

11.3 EVAPORATIVE PUMPING

11.3.1 Introduction

Examination of the vacuum requirements of existing and proposed thermonuclear experiments involving the injection of molecular ions into a steady state device leads to the conclusion that it would be advantageous to supplement the diffusion pumping systems with vapor deposited metal film pumps (commonly called "getter pumps"). The combination of such "getter" pumps and properly trapped diffusion pumps offers advantages over the use of either system alone. This may be more clearly seen after a consideration of some of the characteristics of diffusion and getter pumps. Diffusion pumps can remove all gases irrespective of their chemical nature, have a proved dependability and an extremely wide range of operating pressures, and require little or no maintenance over extended periods. The space requirements of manifolds and other components which are necessary to provide adequate diffusion pumping in these devices present difficult design problems. Vapor deposited metal film pumps have the advantages of permitting the use of virtually any water cooled surface as an active pump area, offering high speeds at low pressures, and requiring no manifolding, valving, or trapping.

By combining diffusion pumping and getter pumping the advantages of each are largely retained. Several experiments which have been undertaken to explore the possibilities of such combination pumping systems for application to experimental thermonuclear devices at ORNL are described herein.

11.3.2 Large-Scale Pump Test

Because of the potential usefulness of getter pumping techniques and the adaptability of these techniques to existing systems a large-scale getter test was constructed. This facility was built to simulate the conditions which might be readily attained in DCX-1 or other similar existing machines and to determine the operating characteristics of a large-scale pump of this type under a wide variety of conditions. This system is not bakable and is trapped by only a Freon cooled diffusion pump baffle. The design and important dimensions are shown in Fig. 11.1. The tank is constructed of aluminum and has numerous O-ring vacuum seals. The liner is

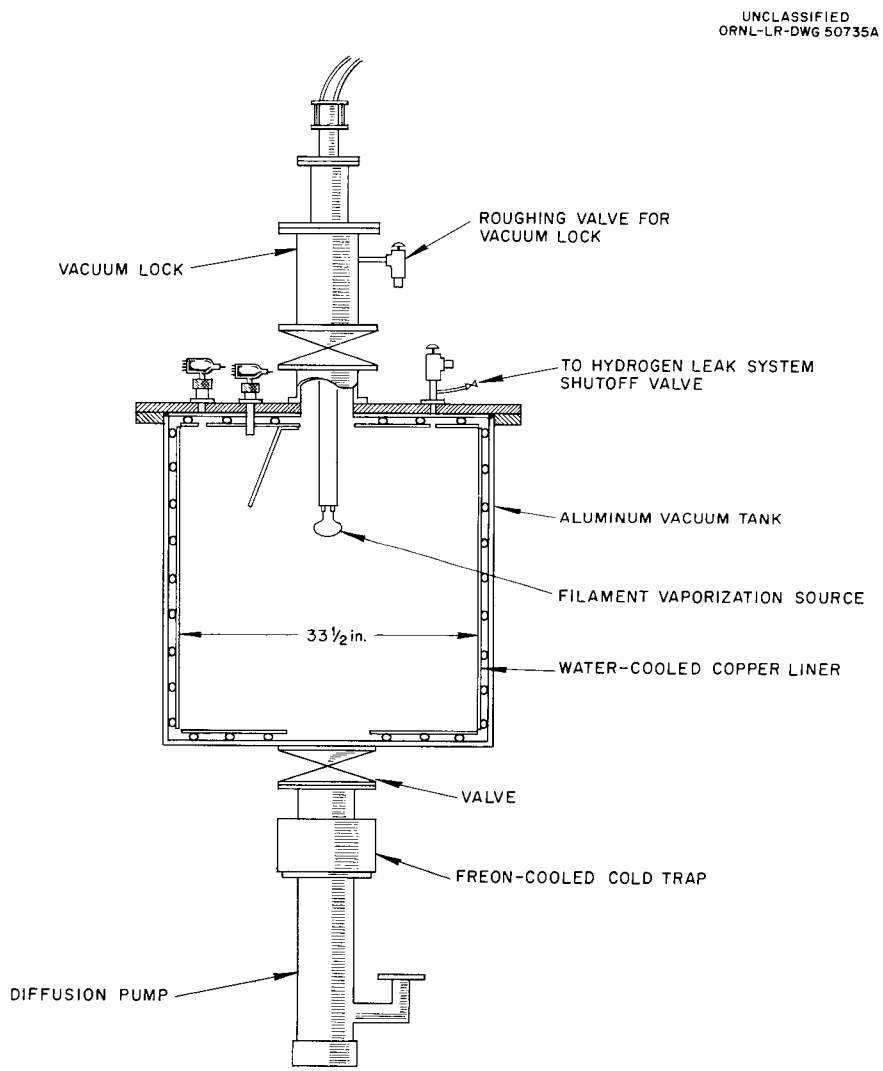

Fig. 11.1. Large-Scale Pump Test.

constructed of copper and is effectively water cooled. A vacuum lock in the upper flange permits evaporation sources to be changed while maintaining high vacuum conditions in the tank. Although a number of evaporation sources have been used, a filament source of the type used most frequently is shown.

A typical operation cycle consisted of (1) roughing and diffusion pump evacuation to below 1×10^{-5} mm Hg; (2) "formation" of a filament either in the vacuum lock or in the tank; (3) insertion of the filament into the tank if not done before (2); (4) evaporation and measurements. Step (1) may be omitted if the tank is already under vacuum and step (2) may be accomplished in a separate facility leaving only the insertion of the source through the vacuum lock to prepare for evaporation and measurements. The filament source and its "forming" are described below in the section on source development.

The speeds (gas feed rate per unit pressure) reported below are obtained by admitting a known quantity of gas to the system through a leak valve and measuring the increase in pressure (above the base pressure) due to this leak. In most cases the diffusion pump speed is small and can be neglected. Sensitivity corrections to ion gage readings are made whenever they are reasonably justified. The first column of Table 11.1 lists the more important system and operation parameters and the second column summarizes the results obtained. Figure 11.2 is a graph of some data showing the throughput of hydrogen obtained as a function of pressure. It should be noted that the ratio of titanium atoms evaporated to molecular hydrogen throughput is approximately one at pressures above 2×10^{-6} mm Hg. Figure 11.3 is a graph of speed vs pressure for the same data. Note that for an evaporation rate of 1.3 g/hr the speed drops approximately linearly with increasing pressure above 2×10^{-6} mm Hg indicating saturation of the evaporated film. Note also that below 1×10^{-6} mm Hg the calculated speed depends to a large extent upon the assumed base pressure.

The system has been operated on both continuous and batch evaporation cycles. Little difference has been observed. Batch evaporations of approximately 4.3 g each absorbed between 0.25 and 0.7 liter-atm of hydrogen at pressures of about 10^{-5} mm Hg before the speed fell appreciably. This corresponds to 5–10 atoms of titanium per molecule of hydrogen. Pumping

Table 11.1 Results of Evaporative Pumping Tests

Liner temperature: ~15°C
Source used: titanium wire wound on tantalum filament
Length of runs: 2–8 hr

Parameter	Large-Scale Test	Bakable Test
Liner surface area, cm^2	30,000	4000
Base pressure, mm Hg		
Diffusion pump	1×10^{-6} to 2×10^{-6}	8×10^{-7} to 3×10^{-6}
Diffusion pump plus titanium	3×10^{-8} to 1×10^{-7}	$< 6 \times 10^{-10}$
Pumping speed (hydrogen), liters/sec		
Diffusion pump and trap	~(300–500)	5 (estimated)
Diffusion pump plus titanium	30,000–60,000	8000–16,000
Specific pumping speed (hydrogen) of diffusion pump plus titanium, liters sec^{-1} cm^{-2}	1–2	2–4.3
Titanium evaporation rate		
g/hr	1–3	1
g/batch	3–8	2
Ratio [(atoms titanium evaporated)/(molecules hydrogen throughput)]		
Limiting	1	
Operating	2–200	100 to ~ 10,000
Range of hydrogen pressure over which speed measurements were made, mm Hg	5×10^{-5} to 2×10^{-7}	1×10^{-7} to 3×10^{-9}
Hydrogen leak rate, atmospheric cc/sec	0.005–1	0.0001–0.005
Cold trap coolant	Freon at −40°F	Liquid nitrogen
Previous history	Other speed measurement runs; previous coating still on walls; may or may not have been down to air or hydrogen; no baking	Coating from previous run not removed; baked before each evaporation

continued at progressively slower speeds until a ratio of approximately one hydrogen molecule was absorbed for each titanium atom evaporated.

11.3.3 Bakable Pump Test

Summarized in the third column of Table 11.1 are the principal results of an experiment designed to determine the ultra-high vacuum characteristics of a pumping system utilizing vapor deposited titanium. The differences between the results of this test and the large-scale test cannot be attributed with certainty to differences between specific details of the experiments.

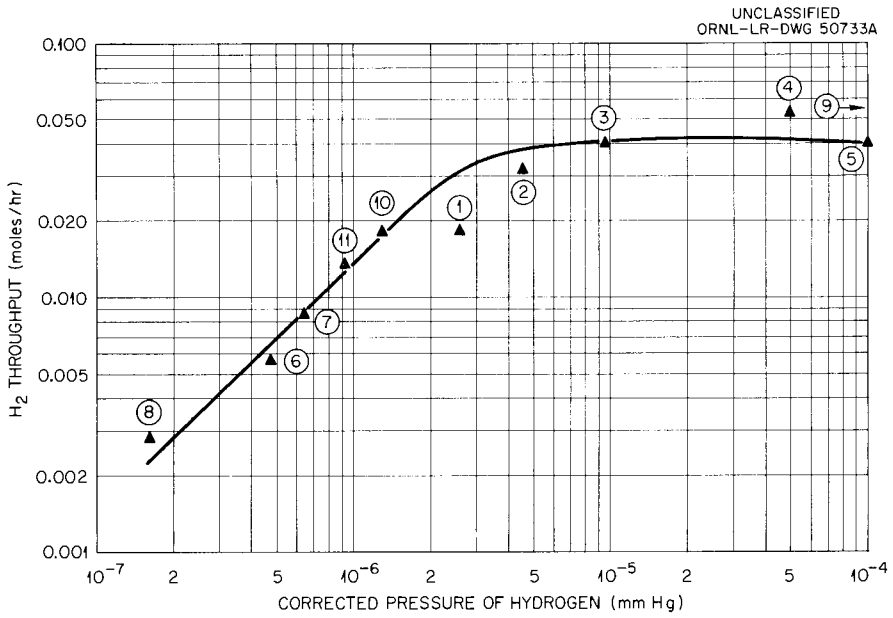

Fig. 11.2. Throughput of Hydrogen vs Pressure. Titanium evaporation rate 0.027 mole/hr.

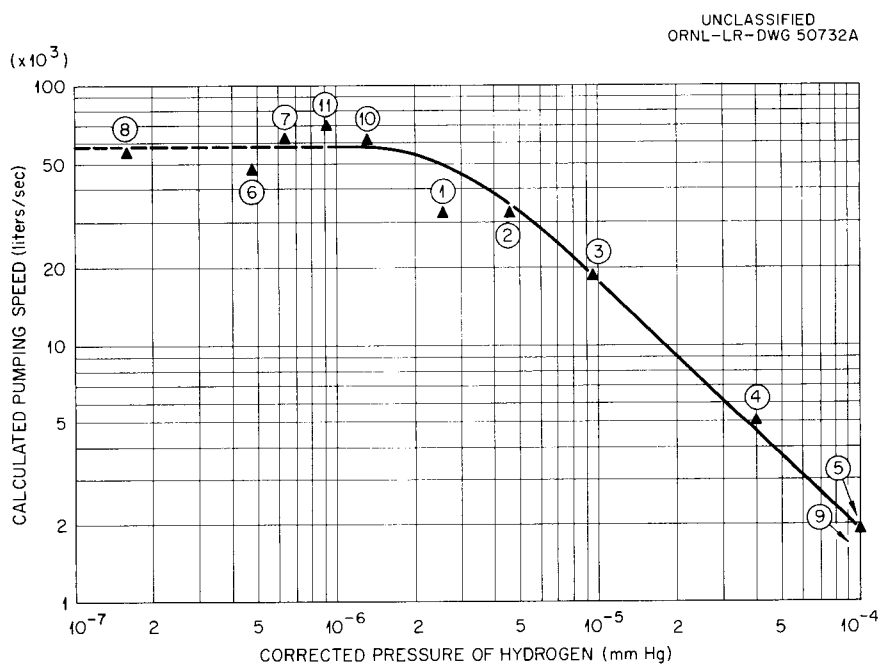

Fig. 11.3. Pumping Speed for Hydrogen vs Pressure. Titanium evaporation rate 1.7 g per 1.3 hr.

11.3.4 Techniques for the Evaporation of Titanium

The source development work described previously[4] is being continued with the objective of studying the operational characteristics of several source designs. Three evaporation methods include: evaporation from a resistance heated filament, evaporation by electron bombardment heating of a post or material in a water-cooled holder, and evaporation from a crucible used as the anode of a vacuum arc.[5]

The vapor pressure of titanium at its melting point is high enough to permit the design of evaporators suitable for some applications. It is desirable to achieve higher evaporation rates to increase the useful operating pressure range, permit the use of fewer sources, and shorten the evaporation periods in batch operation cycles. The design of molten titanium sources which operate at temperatures sufficient to yield high evaporation rates is indeed formidable.

A promising method of obtaining higher evaporation rates involves the use of titanium alloys instead of pure titanium. Figure 11.4 is a phase diagram of the titanium-tantalum alloy system. An alloy of 50 at. % tantalum at 2200°C has an estimated vapor pressure of titanium in equilibrium with the alloy of 3 mm Hg. Pure titanium at its melting point of 1680°C has a vapor pressure of 9×10^{-2} mm. The estimated evaporation rates for the alloy on this basis are 25 times greater than for pure titanium at its melting point. However, the diffusion rate of titanium through the solid alloy may reduce this evaporation rate somewhat. Tantalum has an insignificant vapor pressure compared to the titanium. This fact is utilized in the filament source described below.

Figure 11.5 shows a simple filament source which has proved very reliable. The filament is a 170-mil-OD tantalum rod on which is tightly wrapped one or two layers of 0.020–0.040-in.-dia titanium wire. In use the ends of the filament are clamped in water cooled holders and 200–400 amp of direct current provides the necessary evaporator power. The filament

---

[4]R. E. Clausing and J. W. Tackett, Thermonuclear Project Semiann. Rep. Jan. 31, 1960, ORNL-2926, p 100.

[5]See sec 4.5 of this report.

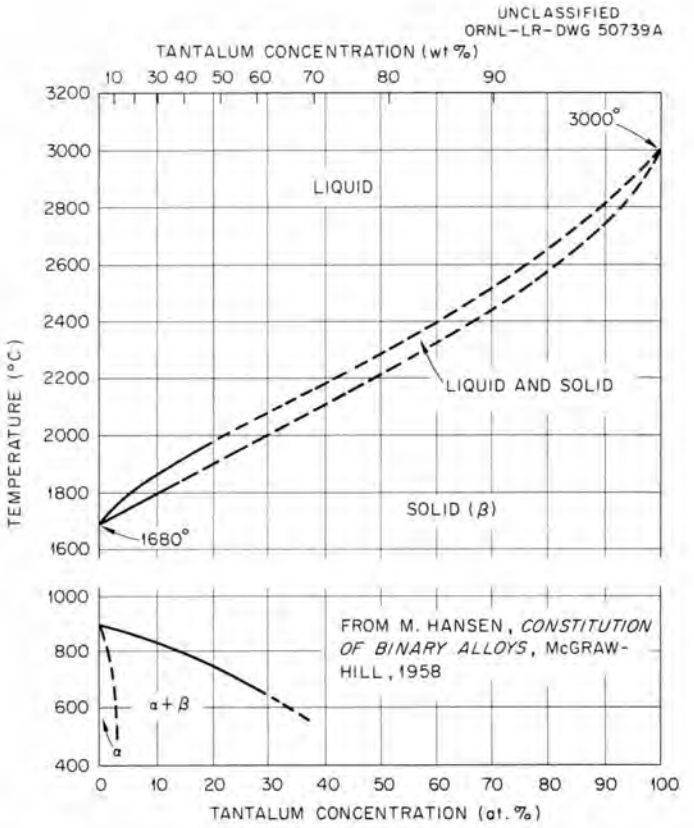

Fig. 11.4. Titanium-Tantalum Phase Diagram.

Fig. 11.5. Filament Source for Titanium Evaporation. Shown before use.

is generally "formed" by heating to the melting point of the titanium and holding constant or slowly increasing the temperature for periods of 10 min to 2 hr. This "forming" period allows outgassing of the filament and allows the titanium to alloy with the tantalum permitting subsequent operation at higher temperatures with resulting higher vaporization rates. Evaporation rates from these filaments have been as high as 1/2 g/hr per square inch of active filament surface. Figure 11.6 shows a filament made as a feasibility test from a 15 at. % tantalum alloy which was operated to determine the evaporation characteristics of a resistance heated wire filament. The filament shown evaporated somewhat more than 1 g of titanium from 3.6 in.^{2} of surface area in 50 min. Half of the available titanium was evaporated. This was a feasibility test only and no attempt was made to optimize alloy composition, filament geometry, or operating procedures.

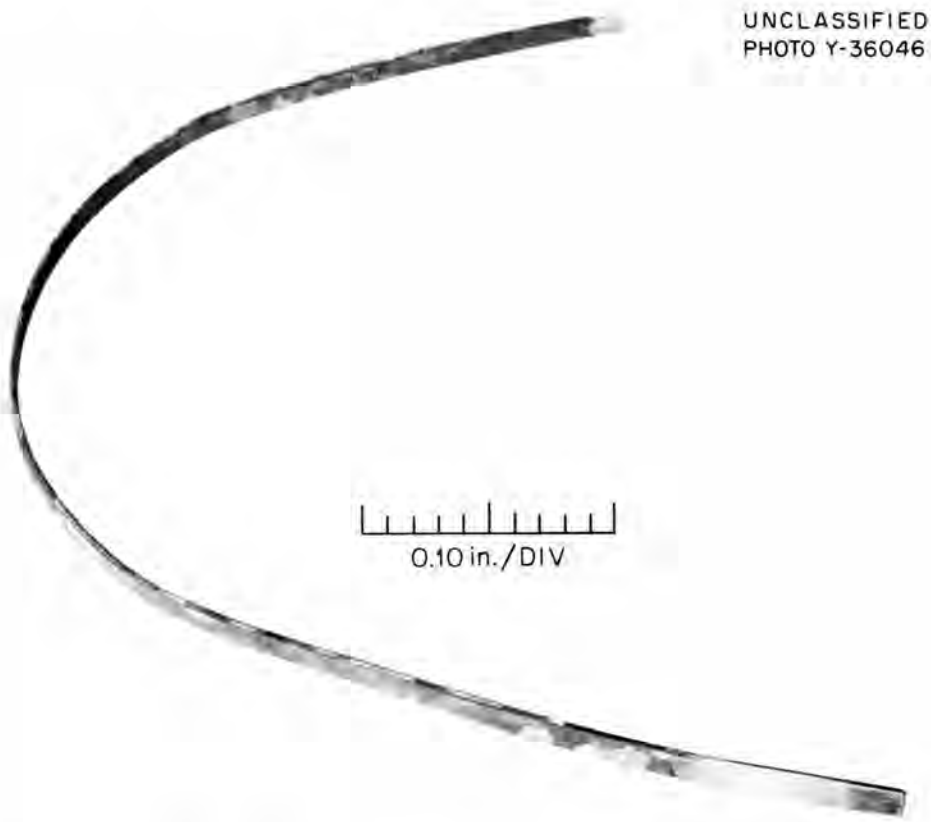

Fig. 11.6. Experimental Titanium Alloy Filament Source Used for Titanium Evaporation. Shown after evaporation.

Another titanium alloy system which offers interesting possible applications is that with niobium. The phase diagram is shown in Fig. 11.7. The system exhibits an unusually wide two-phase region. This feature allows these alloys to be used where it is desirable to have a liquid which should not flow freely. Certain of these alloys will behave as slushes

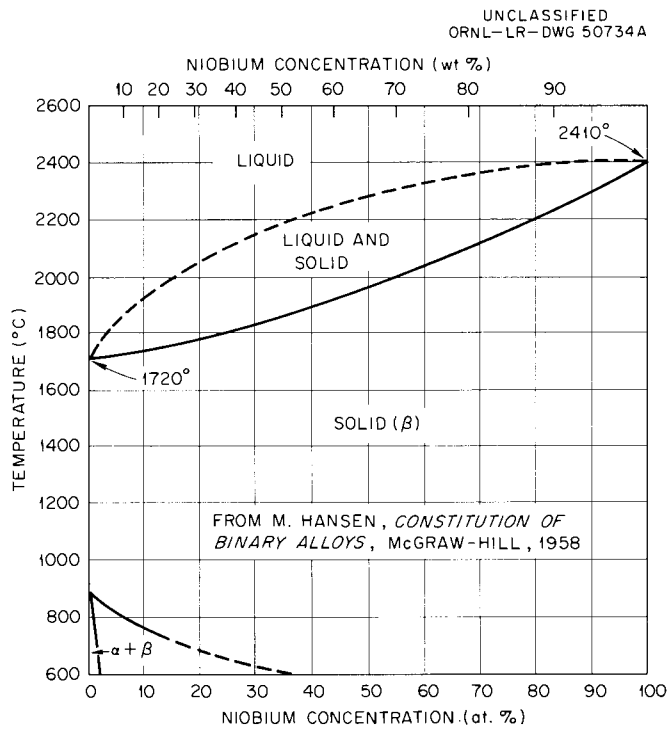

Fig. 11.7. Niobium-Titanium Phase Diagram.

over the temperature range in the two-phase region. These alloys have been used in the titanium arc experiment described in Sec 4.5 and in sources heated by electron bombardment.

A variation of the wire wound filament may be made by co-winding niobium or tantalum with the titanium. Evaporation rates of over 1 g hr^{-1} $in.^{-2}$ have been obtained with such modification.

11.3.5 A Test of Titanium Pumping

Preliminary studies have been made on the attainment of high ultimate vacua with high pumping speeds using baked and unbaked systems with evaporated titanium as the pumping medium. A schematic diagram is shown in Fig. 11.8.

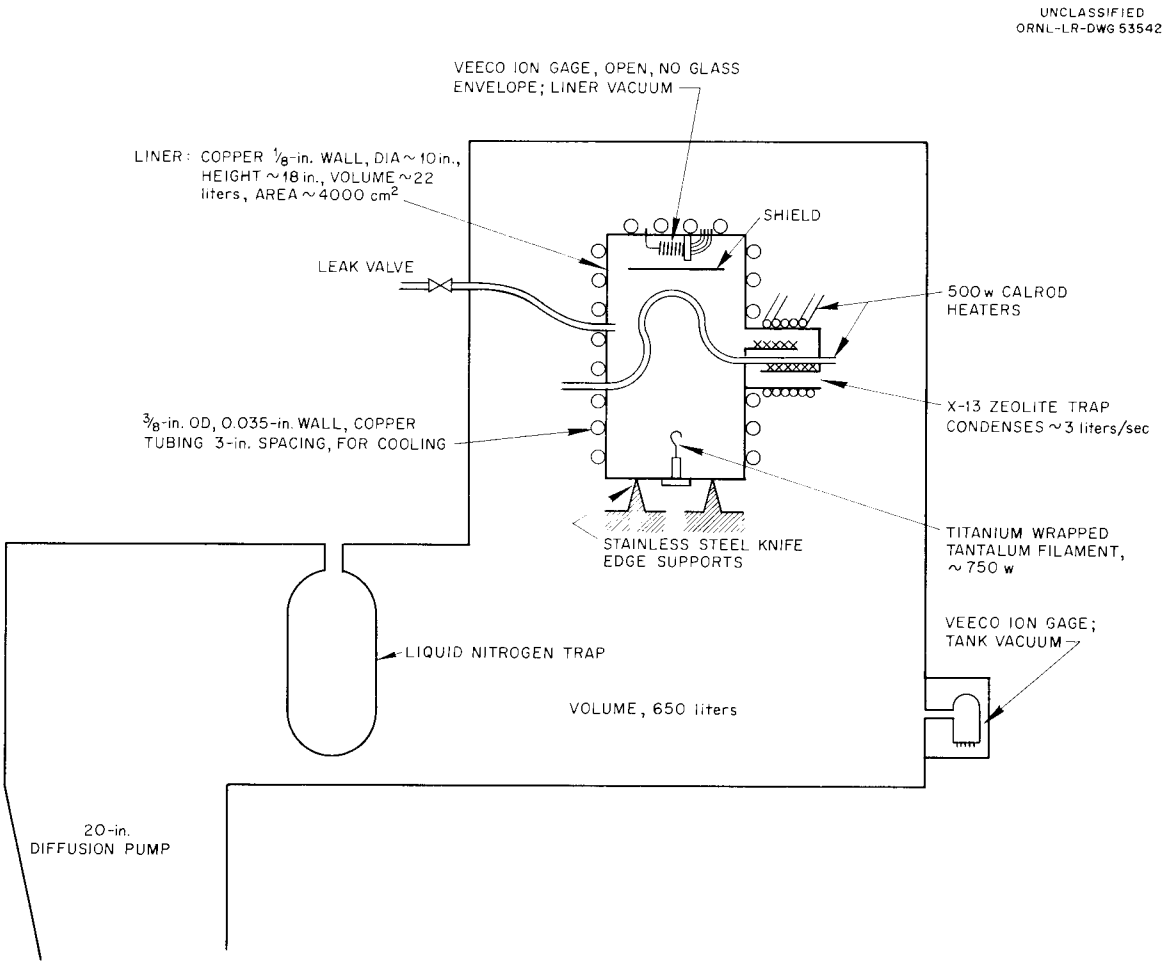

Fig. 11.8. Building 9735 Arc Research Facility Tank and Liner.

Base pressures in the inner system of 6×10^{-10} mm Hg, with a corresponding pressure in the outer system of 8×10^{-7} mm Hg, have been obtained by the following bakeout procedure:

(1) Bakeout (24 hr).

(a) No air or water in cooling lines.

(b) 500 w to Calrod in liner.

(c) 500 w to Ti-Ta filament (this heats the filament to a dull red; outgasses but does not vaporize titanium).

(d) 500 w to Calrod around X-13 zeolite trap.

(e) No liquid nitrogen in tank trap.

(f) Approximate maximum temperature of liner, 500°C.

(g) Liner pressure at end of bakeout, $\sim 5 \times 10^{-5}$ mm Hg.

(2) Air cool down and evaporation (40 min).

(a) Fill liquid nitrogen trap and keep full.

(b) All Calrods off.

(c) Ti-Ta filament raised slowly (10 min) to maximum power; Ti melts at about 750 w.

(d) Temperature at end of air cool down, ~100°C.

(e) Pressure at end of air cool down, $\sim 1 \times 10^{-8}$ mm Hg.

(3) Water cool down and continued evaporation.

(a) Calrods off; Ti-Ta filament at 750 w.

(b) Temperature at end of water cool down, > water temperature.

(c) Pressure at end of water cool down, $\sim 3 \times 10^{-9}$ mm Hg.

(4) Final cool down (30 min).

(a) All Calrods off; Ti-Ta filament off.

(b) Temperature at end of final cool down, water temperature.

(c) Pressure at end of final cool down, 8×10^{-10} mm Hg.

The titanium vaporized by the end of this period is about 2 g. It is not evenly distributed over the 4000 cm^2 of the inside surface. All the top surface of the ion gage shield, and all in the shadow of the shield (~400 cm^2), has received very little, if any, titanium. After the first pumping speed measurements for hydrogen gas (1–3 atm-cm^3 bled into the system), the base pressure is usually down to 6×10^{-10} mm Hg, gage reading. A minimum base pressure of 4×10^{-10} mm Hg has been achieved with liquid nitrogen instead of water in the cooling lines.

Pumping speeds and related data for several runs of particular significance are recorded in Table 11.2. Hydrogen for the pumping speed measurements was straight tank hydrogen, bubbled through an oil manometer to maintain atmospheric pressure. An oil filled U-tube was used to measure the leak rate. The specific pumping speed, expressed in liters sec^{-1} cm^{-2}, may be used to estimate the effective pumping speeds of any surface area under the conditions outlined. Repeated experiments have shown that for the conditions and techniques described:

1. Bakeout of the liner results in significantly lower base pressure than can be achieved without bakeout.
2. Cooling the liner to liquid nitrogen temperatures lowered the base pressure but did not give a corresponding increase in pumping speed.

Table 11.2. Pumping Speeds for Several Runs

Treatment	Base Pressure (mm Hg)	Gage Pressure (mm Hg)	Specific Pumping Speed (liters sec^{-1} cm^{-2})
No liner bakeout	1.3×10^{-8}	1×10^{-7}	1.4
Liner bakeout, 24 hr	6×10^{-10}	3×10^{-9}	3.4
No additional	6×10^{-10}	6.5×10^{-9}	4.3
No additional	6×10^{-10}	1×10^{-7}	2.3

3. A specific pumping speed of 4.3 liters sec^{-1} cm^{-2} has been realized at a corrected hydrogen pressure of 1.1×10^{-8} mm Hg.

11.4 TEST OF LARGE VACION PUMP

The large VacIon pump by Varian Associates has been tested under conditions simulating its proposed use as a "sink" for the unused portion of the high energy H_2^+ beam in DCX.

11.4.1 Startup Procedure

The pump was blanked off and roughed down to 5 μ with a model 1396 Welch pump pumping through a liquid nitrogen cooled trap. Roughing down required 3 hr, and an additional 3/4 to 1 hr of intermittent VacIon pumping was required to gas out the pump to a point at which roughing could be discontinued.

11.4.2 Ultimate Pressure

After an initial 96 hr of pumping, the pressure in the isolated pump was 5×10^{-8} mm Hg. With continued operation and testing over a period of some two weeks the base pressure gradually decreased to 1×10^{-8} mm Hg.

11.4.3 Pumping Characteristics for H_2

As with other pumps of this type, pumping speed depends on a number of factors, and may vary widely from one measurement to another. High

pumping speeds (up to 11,000 liters/sec) have been observed briefly at the beginning of a test, particularly if the pump had been operating at its base pressure for a long time previous to the test. After pumping for 1 to 2 hr at any moderate leak rate (less than 80 liter-μ/sec) the speed is usually about 6000 liters/sec. (Values as low as 4000 and as high as 8000 liters/sec have been observed.)

In its proposed use, it seems reasonable to expect the pump to have a pumping speed of 6000 liters/sec or higher, and at 12 liter-μ/sec input (equivalent to 62 ma H_2^+) the pressure should not exceed 2×10^{-6} mm Hg. At higher input (76 liter-μ/sec = 390 ma H_2^+) the pump retains its speed, and the equilibrium pressure is 1.3×10^{-5} mm Hg. At an input of 96 liter-μ/sec (494 ma H_2^+), however, the speed falls off, becoming less than 1500 liters/sec after 25 min, and the pressure rises indefinitely.

Since the maximum H_2^+ beam expected in DCX is less than 50 ma (equivalent to 10 liter-μ/sec) the capacity of the VacIon pump far exceeds the demand. Also, the equilibrium pressure at this input rate is low enough (2×10^{-6} mm) to ensure little back-diffusion into the DCX chamber. Thus the pump can be a highly efficient "sink" for ions directed into it.

11.4.4 Reliability Experience

Once the VacIon pump has been brought into operation, and assuming that it is kept under vacuum, continuous or intermittent operation is remarkably reliable and trouble-free.

One type of trouble did develop during the course of our test; this was failure of overloaded capacitors in the power supplies. These capacitors have now been replaced by heavy duty units which should meet the demands placed on them.

11.5 GAGE TEST FACILITY

A facility for checking the calibration of vacuum gages operating in the 10^{-6} to 10^{-3} mm pressure range is now in operation. Basically the system consists of a test chamber, carrying up to four gages for testing, pumped continuously, through an aperture of accurately known area, by a high speed (about 1200 liters/sec) pumping system. Pressure in the test

chamber can be varied from the base pressure ($< 10^{-6}$ mm) upward by introducing gas at adjusted and measurable rates into the chamber.

In such a system, the rate of pumping from the test chamber can be calculated from simple kinetic theory for all pressures at which free molecular flow prevails.

A proper expression for this pumping speed, S_a, in liters/sec is:

$$S_a = \left(\frac{1}{\sqrt{2\pi}}\sqrt{\frac{RT}{M}}\ a\right)\left(\frac{A}{A - a}\right)\left(1 - \frac{p_2}{p_1}\right) \quad , \qquad (1)$$

where a = aperture area, A = area of test chamber cross section, and p_2/p_1 = ratio of pressure below to that above the aperture. On the right of this equation, the first factor is the well known expression for aperture conductance under static conditions. The second factor corrects for the dynamic case of constant flow-through. The third factor takes into account the finite speed of pumping away from the aperture. For our system, the speed of pumping air at 25°C from the test chamber has been found to be: $S_a = 192 \pm 1$ liters/sec.

Rates of gas inleakage can be determined with comparable precision, provided accurately calibrated manometers in a range of sizes are used in making the measurements.

If the measured rate of gas inleakage at any time is q mm-liters/sec, and the rate of pumping from the test chamber is S_a liters/sec, the increase in chamber pressure, in mm of Hg, produced by this rate of gas inleakage is:

$$p - p_0 = \Delta p = \frac{q}{S_a} \quad . \qquad (2)$$

Gage calibration is achieved by comparing gage response with a series of pressure increases calculated from the above relation. Direct comparison with a sensitive McLeod gage shows that pressures derived in this way agree with McLeod measurements to within 2% over the 10^{-5} to 10^{-3} mm pressure range. Poorer agreement is observed below 10^{-5} mm, due to poor precision of the McLeod gage in this pressure range. Above 10^{-3} mm agreement is also poor, due to the fact that flow through the aperture is no longer strictly "free molecular."

Comparing the proposed method of establishing standard pressures with use of a sensitive McLeod gage, it appears that:

1. The two methods are in good agreement over the two decades of pressure (10^{-5}–10^{-3} mm) for which both are expected to be accurate.
2. Below 10^{-5} mm the proposed method has the advantage of higher precision.
3. There is no apparent reason why unexpected changes should occur in any of the basic measurements from which pressures are derived in the proposed method, that is, the test system should retain its calibration. This is not true of a standard McLeod gage.
4. The calibration of one or more gages at a number of points over an extended range of pressures can be carried out in a fraction of the time required with a sensitive McLeod gage.
5. An objection to the proposed method, and possibly a valid one, is that all calibrating pressures are equilibrium pressures in a dynamic system. Pressure gradients exist in such a system, and it is possible that the pressure responsible for flow through the aperture is not the same as that seen by the gages under test. The fact that the test chamber is a very high conductance region, and the added fact that agreement with a McLeod gage is found, suggests that no significant error arises from this source.

A dozen or more gages – some new, some old, and of a number of different types – have been calibrated by this method. Although the results of these calibrations have not been fully correlated, several qualitative observations can be made:

1. In general, the ratio of gage readings to standard pressures is almost constant over the calibrating pressure range; and the reciprocal of this ratio, averaged over the pressure range, can be applied as a multiplying correction factor to the gage readings. Also, if the gage operates in the linear portion of its sensitivity curve – and this is usually the case – this same factor, applied to the electron emission setting used during the calibration, gives the proper emission for correct direct reading of the gage.
2. Correction factors for gages of the same type and past history appear to be comparable, but not generally identical.
3. Proportionality of gage pressure to standard pressure is not found in gages that have become defective due to long use and/or excessive contamination.

Typical calibration results for individual gages of a number of types are listed in Table 11.3. Generalization of these results is not justified at this time.

Table 11.3. Typical Gage Calibration Results

Gage	Type	Recommended Emission (ma)	Correction Factor	Corrected Emission (ma)
Veeco RG-75	Bayard-Alpert	10	0.746	7.46
VIC T-34	Bayard-Alpert	6	1.124	7.44
NRC 507	Bayard-Alpert	5	1.438	7.19
CVC VG-1A	External ion collector	5	0.848	4.24
CVC PGH-09	Cold cathode		0.974	

11.6 MASS SPECTROMETRY

The CEC 21-620 mass spectrometer has been operated extensively. The sensitivity and fragmentation patterns of most of the gases commonly encountered in vacuum systems have been determined. The response of the vacuum system and mass analyzer to various operational procedures has been determined and data have been obtained on the operation of an Evapor-Ion pump under a variety of circumstances. The results thus far have confirmed findings previously reported in the literature.

Considerable difficulty has been encountered in obtaining satisfactory operation of the spectrometer when the spectrometer tube is removed from the original installation and is operated as a part of another vacuum system. Some information was obtained, however, by the DCX group during several runs and is reported in Sec 1.4.

Present efforts are directed toward increasing the versatility of the instrument by modifications to permit the reliable use of the spectrometer tube on other vacuum systems and, if possible, to decrease the pickup of electrical noise permitting its operation in electrically noisy environments.

11.7 ZEOLITE TRAPPING OF OIL DIFFUSION PUMPS

A zeolite trap has been constructed and has been serving with a water baffled MCF300 (Consolidated) oil diffusion pump. The zeolite is contained in a removable annular basket designed in such a manner that it can

be baked conveniently. A protracted baking at 400–450°C until the pressure has fallen to below 10^{-6} mm serves to dehydrate and thus activate the material (Linde 13-X). Upon cooling to room temperature, the partial pressure of water in equilibrium with the zeolite falls markedly allowing the material to readily adsorb water and other gaseous species. The baked trap has operated at lower base pressures than are obtained with liquid nitrogen in the same configuration. The system pressure remains in the vicinity of 2×10^{-8} up to 7×10^{-8} mm over a 24-hr period.

11.8 PERMEABILITY AND OUTGASSING

The permeability to helium of samples of Coors AD85 porcelain and samples of glazed and unglazed Lapp electrical porcelain have been measured. The results of these measurements are shown in Table 11.4.

Table 11.4. Permeability of Insulators to Helium

Material	Permeability to Helium $\left(\frac{\text{atm cm}^3 \text{ mm}}{\text{sec cm}^2 \text{ Torr}}\right)$
Coors AD85	6×10^{-14}
Lapp electrical porcelain	
Glazed	5×10^{-13}
Unglazed	9×10^{-13}

12. PRELIMINARY SURVEY ON BALL LIGHTNING OBSERVATIONS

J. R. McNally, Jr.

"Ball lightning," as a possible stable plasma configuration, is receiving increasing emphasis in fusion research especially in the USSR.[1] Kapitza[2] has proposed a model in which electromagnetic energy is fed to the ball or Kugelblitz from an outside source such as very intense high frequency electromagnetic waves which are absorbed in the plasma. This explanation appears to describe appropriately the beaded or "rosary Kugelblitz" in which energy external to the phenomenon is dissipated at the antinodes set up by appropriate interference effects. Kapitza also compares ball lightning with the thermonuclear fireball.

Another possible interpretation of ball lightning types — namely, the individual, luminous, free-floating type — may be that it consists of a circular or ring current in a dynamic pinch type of equilibrium with the pressure of the external atmosphere. Such a model for a thermonuclear plasma of the DCX type has been postulated (pinched ion current ring)[3] and independently Shafranov[4] proposed theories for ring (presumably electron) current pinches in stable equilibrium configurations defined by (a) a gravitational field, (b) an external gas pressure (ball lightning), or (c) an external magnetic field. There appears then to be ample reason for surveying the field of ball lightning for properties related to a plasma system in a static or even dynamic type of equilibrium.

A preliminary survey in the form of a questionnaire has been made of ORNL technical personnel. A total of 110 individuals reported observations on "ball lightning" for a return of 5.6% observers. Table

---

[1]D. J. Ritchie, Missiles and Rockets, Aug. 24, 1959.

[2]P. L. Kapitza, Proc. Acad. Sci. U.S.S.R. 101, 245 (1955); Physikalische Blatter 1 (1958).

[3]J. R. McNally, Jr., unpublished work (December 1957); "On the Energy Dependence of the DCX Type of Sherwood Device," unpublished (August 1958); "The Direct Current Experiment (DCX) and High Temperature Measurements in the Carbon Arc," paper presented at Symposium on Optical Spectrometric Measurements of High Temperatures, University of Chicago (March 1960).

[4]V. D. Shafranov, Soviet Phys. JETP 6, 545 (1958).

12.1 lists a few of the pertinent observations reported. A complete survey of all Union Carbide Corporation personnel in Oak Ridge is presently under way and should result in significant additional information.

The statistics compiled to date agree in general with other observations reported in the literature.[5] There is no doubt that some of them fall into the category of St. Elmo's fire, Jacob's ladder, and other discharges; however, there is a surprisingly high percentage of the airborne or free-floating type to which Kapitza's postulate of standing waves does not appear to apply. (It is also of interest that no reports of beaded or rosary lightning were made.) The fact that five observations of doughnut or ring configurations plus six observations of surface type of glows were reported suggest the possibility of vortex or ring

[5]See, for example, B. L. Goodlet, J. Inst. Elec. Eng. 81, 1 (1937); H. Nauer, Umschau Fortschr. Wiss. u. Tech. 56, 75 (1956); J. C. Jensen, Physics 4, 372 (1933); M. Rodewald, Z. Meteorol. 8, 27 (1954).

Table 12.1. Observations on Ball Lightning (110 Observers)

Observation	Category	Number Reporting
Glow distribution	Unreported or uncertain	24
	Uniform or volume	75
	Surface	6
	Doughnut or ring	5
Size	Unreported or uncertain	26
	Less than 1 in.	2
	From 1 to 12 in.	43
	Greater than 12 in.	39
Type of decay	Unreported or uncertain	30
	Quiet, slow	22
	Sudden, explosive	58
Duration	Unreported or uncertain	21
	Less than 1 sec	12
	From 1 to 10 sec	68
	From 10 to 60 sec	8
	Greater than 60 sec	1
General character	Unreported or uncertain	17
	Attached (ground, conductors, insulators)	42
	Free-floating	51

current motion although it is possible that psychological factors inherent in the question may have led observers to make such reports ("Was it a surface, volume, doughnut or ring type of glow?").

The possible existence of a dynamically stable plasma configuration of the ion current pinch type establishing a completely closed magnetic torus poses certain basic questions:

1. Can the DCX approach lead to such a configuration?
2. If H_2^+ injection energies higher than 600 kev are required, what fraction of charged nuclear reaction products will be trapped?
3. Under what conditions is an ignited thermonuclear plasma configuration of this type controllable?

The response to these questionnaires by Laboratory personnel has been very gratifying (39.3% returned questionnaires). Numerous suggestions and references have been brought out. The writer is indebted to E. Dewan of the Air Force Cambridge Research Center, Bedford, Massachusetts, for suggestions and references.

13. DESIGN AND ENGINEERING

J. F. Potts, Jr.

The activities of the Engineering Design and Construction Group are in support of the Thermonuclear Project with no direct research responsibilities. The group executes or coordinates engineering design, shop fabrication, building operations, and maintenance.

Design Section activities are summarized as follows:

Jobs on hand 2-1-60 on which work had not started	26
New jobs received	123
Total jobs	149
Jobs completed	123
Jobs now in progress	8
Backlog of jobs	18
Total drawings completed for period, not including changes in design and preliminary conceptual layouts for DCX-2 and DCX-EP-B	329

The Design Section lost an electrical design engineer to the DCX-2 Project and two draftsmen who had been on loan from another division. In addition, one engineer from the section is now spending full time as Building Engineer. Overloads brought about by these losses are being relieved by the Y-12 Engineering Division.

Shop fabrication for the period is summarized as follows:

Jobs requiring 16 man-hours or less	243
Jobs requiring up to 1200 man-hours	460
Jobs requiring up to 2000 man-hours	3
Jobs of miscellaneous character in plating, carpenter, electrical, and millwright shops	215
Jobs by outside contractors	3

The average shop manpower to accomplish the above work consisted of 34 machinists, 7 fabricators, and 4 welders in the Y-12 shops and 5 craftmen in the ORNL shops. Consistent with established ORNL practice, outside

equipment fabrication is coordinated by this group through the Engineering and Mechanical Division.

All phases of the Thermonuclear Project relocation to Building 9201-2 are in progress and are proceeding approximately on schedule. Engineering is proceeding but construction has not started on the addition of four laboratories at large experimental sites. Work is proceeding on several changes prompted by operating experience such as: (1) provision of two more large dry rectifier units making a total of 12, so that magnet power to the four vacuum-magnetic tanks[1] (Beta Tank Facility) may be independently varied; (2) changing of cooling water supply to diffusion and mechanical vacuum pumps from the demineralized water system to a separate process water header. Work has not proceeded beyond planning for the addition of a 5-Mw a-c—d-c motor-generator set, additional demineralized-water pumps, and additional electrical distribution centers. These additional facilities will be needed for operation of DCX-2 or DCX-EP-B while other experiments are in progress.

During the interval since the last report the 600-kv 1-amp d-c power supply[1] has been placed in operation. On the basis of the recent experience of the Ion Source Group in testing a new accelerator tube, it was decided to forego installation of a fast shorting device to dump stored energy from the power supply filter capacitors in the event of electrical breakdown in experimental equipment.

---

[1]E. S. Bettis, Thermonuclear Project Semiann. Rep. Jan. 31, 1959, ORNL-2693, p 101–103.

PUBLICATIONS

DIVISIONAL MEMORANDUMS

These memorandums were written for internal use in the Thermonuclear Division and had a very limited distribution. Copies are not available for distribution outside ORNL. Most of the information is covered in less detail either in this progress report or in one of the documents listed under ORNL Reports. The memorandums are listed here to give an indication of what data has been transcribed to a report type form. In most cases it would be possible to obtain information on a particular subject by contacing the author directly.

DCX-1 Technical Memorandums

Authors	Title	No.	Date
C. F. Barnett, J. L. Dunlap, R. S. Edwards, G. R. Haste, A. Kendig, J. A. Ray, R. G. Reinhardt, W. Shill, and E. R. Wells	Recent DCX Experiments in the New High Magnetic Field Geometry	9	2-29-60
	Paddle Experiments in DCX	10	2-29-60
	Gas Arcs in DCX (A Joint Report from EPA, AIPG, and DCX Groups)	11	5-5-60
	Preliminary Energy Loss Measurements	12	5-17-60
	DCX Gas Dissociation and Mass Spectrometer Runs of 7-1-60 and 7-5-60	13	8-29-60

DCX-2 Engineering Design Memorandums

Author	Title	No.	Date
S. M. Decamp	DCX-2 Outside Booster Coil	1	6-14-60
S. M. DeCamp	Electrical Connections for DCX-2 Coils	2	6-23-60
J. S. Culver	Calculations for Thickness of DCX-2 Tank	3	6-23-60
J. C. Ezell	M-G Control and Coil-Current Measurements	4	7-28-60
J. C. Ezell	Vacuum Gauge Positions and Recording	5	8-3-60

DCX-2 Technical Memorandums

Author(s)	Title	No.	Date
R. J. Mackin, Jr.	Liner Bakeout Problem	1	4-27-60
R. J. Mackin, Jr.	Considerations on Arc Length in DCX-2	2	4-29-60
R. J. Mackin, Jr.	Technical Memo No. 3	3	5-2-60
J. N. Luton, Jr.	Physical Coil Connections	4	5-6-60
R. J. Mackin, Jr.	Magnetic Field Variations on Molecular Ion Orbit	5	5-12-60
G. G. Kelly and N. H. Lazar	Accelerator Tube Requirements	6 (revised)	5-19-60
G. G. Kelly and N. H. Lazar	Beam Trajectory Considerations	7	5-13-60
R. A. Dandl	Discussion of DCX-2 Diagnostics	8	5-16-60
C. E. Normand	Functional Evaluation of Ionization Gauge Controls	9	5-19-60
R. V. Neidigh	Titanium Evaporators	10	5-20-60
R. A. Gibbons and R. J. Mackin, Jr.	Effective Reduction of a Tube's Conductance by an Ionizing Arc	11	5-23-60
C. E. Normand	DCX-2 Vacuum Pumping System	12	5-25-60
J. N. Luton, Jr.	Tank Temperature During Liner Bakeout at 450°C	13	5-27-60
G. R. North	Some Characteristics of Infinite, Lumped Solenoids	14 (later issued as ORNL-2975)	6-2-60
N. H. Lazar and G. G. Kelley	Random Notes About Injector Systems	15	6-3-60
C. E. Normand	DCX-2 Vacuum Pumping System — Non Gaseous Arc	16	6-6-60
D. L. Coffey	Influence of External Ferromagnetic Bodies on the Internal and External Magnetic Fields of DCX-2	17	6-10-60

DCX-2 Technical Memorandums (continued)

Author(s)	Title	No.	Date
R. J. Mackin, Jr.	Neutron Shielding Problem	18	6-9-60
R. J. Mackin, Jr.	DCX-2 Problem List	19	6-13-60
M. Rankin	DCX-2 Tech. Memo No. 20	20	6-17-60
R. J. Mackin, Jr.	Field Dip Problems I — Particle Orbits	21	6-29-60
H. Mott	Simulation of the Field of an Axially Symmetric System of Coils	22	7-29-60
M. Rankin	Magnetic Field Calculations	23	8-3-60

ORNL REPORTS

Author(s)	Title	No.	Date
J. W. Flowers*	Electrode Breakdown and Shielding of Intense Discharges Across the Magnetic Field	ORNL-2710	3-30-60
A. Simon and E. G. Harris	Kinetic Equations for Plasma and Radiation	ORNL-2880	1-7-60
T. K. Fowler	Effect of Plasma Potential on DCX Steady State	ORNL-2914	3-7-60
G. R. North	Some Properties of Infinite, Lumped Solenoids	ORNL-2975	8-10-60
A. Simon	Some Comments on the Ioffe Experiment	CF-60-1-72	1-22-60
P. R. Bell, E. S. Bettis, D. L. Coffey, W. F. Gauster, G. G. Kelly, N. H. Lazar, J. N. Luton, R. J. Mackin, Jr., C. E. Normand, E. D. Shipley, A. Simon, and A. H. Snell	Proposal for a Thermonuclear Experiment Involving Injection of Molecular Ions at 600 kev, Dissociation by Multiple Passes Through an Arc, and Exponentiation upon the Resulting Trapped Atomic Ion Population	CF-60-1-73	3-4-60
F. A. Knox	Test Results NRC H-32-P Diffusion Pump, and Type 1259-32 Angle Valve	CF-60-5-94	5-20-60

*Consultant from University of Florida.

ORNL REPORTS (continued)

Author(s)	Title	No.	Date
J. S. Luce	Compilation of Material Presented by the EP Group at Thermonuclear Meeting June 1, 1960	CF-60-6-96	6-21-60
C. W. Blue and H. C. Hoy	Comparison of General Electric and Veeco Leak Detectors	CF-60-7-47	7-12-60
C. F. Barnett, R. E. Clausing, J. L. Dunlap, J. R. McNally, Jr., R. V. Neidigh, C. E. Normand, W. F. Peed, M. Rankin, E. D. Shipley, R. A. Strehlow, G. K. Werner, and O. C. Yonts	DCX-1 Without Arc	CF-60-7-74	7-21-60
E. D. Shipley and T. K. Fowler	Plasma Density in DCX as a Function of Arc Density	CF-60-8-22	8-3-60

OPEN LITERATURE PUBLICATIONS

Author(s)	Title	Journal
R. A. Dandl and F. T. May	Some Interesting Transistor Characteristics in the Millimicroampere Region	Rev. Sci. Instr. 31, 575–76 (1960)
R. A. Gibbons and R. J. Mackin, Jr.	Energetic Deuterium Arc. II	Bull. Am. Phys. Soc. [2]5(5), 371 (1960)
E. G. Harris and A. Simon	Coherent and Incoherent Radiation from a Plasma	Phys. Fluids 3, 255 (1960)
R. J. Mackin, Jr., and R. A. Gibbons	Energetic Deuterium Arc. I	Bull. Am. Phys. Soc. [2]5(5), 370 (1960)
A. Simon and E. G. Harris	Kinetic Equations for Plasma and Radiation	Phys. Fluids 3, 245 (1960)
A. H. Snell	The DCX Approach to the Thermonuclear Problem – Progress Since Geneva	Proc. Intern. Conf. Ionization Phenomena Gases, 4th, Uppsala, 1959 2, 997 (1960)
O. C. Yonts, C. E. Normand, and D. E. Harrison, Jr.	High-Energy Sputtering	J. Appl. Phys. 31, 447–50 (1960)

ORNL-3011
UC-20 – Controlled Thermonuclear Processes
TID-4500 (15th ed.)

INTERNAL DISTRIBUTION

1. I. Alexeff
2. R. G. Alsmiller
3. C. F. Barnett
4. P. R. Bell
5. D. S. Billington
6. E. P. Blizard
7. C. W. Blue
8. R. L. Brown
9. C. E. Center (K-25)
10. R. A. Charpie
11. R. E. Clausing
12. R. S. Cockreham
13. D. L. Coffey
14. F. L. Culler
15. J. S. Culver
16. R. A. Dandl
17. R. C. Davis
18. S. M. DeCamp
19. J. L. Dunlap
20. H. O. Eason
21. R. S. Edwards
22. L. B. Emlet (K-25)
23. A. C. England
24. J. C. Ezell
25. J. L. Fowler
26. T. K. Fowler
27. J. E. Francis
28. J. H. Frye, Jr.
29. W. F. Gauster
30. J. H. Gibbons
31. R. A. Gibbons
32. P. M. Griffin
33. W. R. Grimes
34. E. Guth
35. D. P. Hamblen
36. C. S. Harrill
37. C. C. Harris
38. A. Hollaender
39. A. S. Householder
40. H. C. Hoy
41. R. P. Jernigan, Jr.
42. W. H. Jordan
43. C. P. Keim
44. M. T. Kelley
45. G. G. Kelley
46. R. J. Kerr
47. R. L. Knight
48. F. A. Knox
49. P. Lafyatis
50. J. A. Lane
51. N. H. Lazar
52. G. F. Leichsenring
53. T. A. Lincoln
54. S. C. Lind
55. R. S. Livington
56. J. S. Luce
57. J. R. McNally, Jr.
58. R. J. Mackin
59. W. D. Manly
60. E. R. Mann
61. O. D. Matlock
62. F. T. May
63. K. Z. Morgan
64. O. B. Morgan
65. J. P. Murray (Y-12)
66. R. V. Neidigh
67. J. H. Neiler
68. M. L. Nelson
69. J. Neufeld
70. C. E. Normand
71. G. R. North
72. C. E. Parker
73. W. F. Peed
74. D. Phillips
75. J. F. Potts
76. M. Rankin
77. H. Postma
78. J. D. Redman
79. R. G. Reinhardt
80. P. M. Reyling
81. M. T. Robinson
82. P. W. Rueff
83. W. K. Russell
84. H. E. Seagren
85. E. D. Shipley
86. A. Simon
87. M. R. Skidmore
88. M. J. Skinner

89. A. H. Snell
90. W. L. Stirling
91. R. F. Stratton, Jr.
92. R. A. Strehlow
93. J. A. Swartout
94. E. H. Taylor
95. A. Tell
96. P. A. Thompson
97. R. E. Toucey
98. R. M. Warner
99. H. L. Watts
100. A. M. Weinberg
101. E. R. Wells
102. T. A. Welton
103. G. K. Werner
104. G. C. Williams
105. C. E. Winters
106. W. L. Wright
107. O. C. Yonts
108. W. P. Allis (consultant)
109. D. Alpert (consultant)
110. W. B. Ard, Jr. (consultant)
111. J. F. Bailey (consultant)
112. W. H. Bostick (consultant)
113. W. R. Chambers (consultant)
114. E. Creutz (consultant)
115. J. W. Flowers (consultant)
116. M. W. Garrett (consultant)
117. O. G. Harrold (consultant)
118. E. G. Harris (consultant)
119. R. Hefferlin (consultant)
120. D. E. Harrison (consultant)
121. G. W. Hoffman (consultant)
122. V. W. Hughes (consultant)
123. D. W. Kerst (consultant)
124. E. D. Klema (consultant)
125. H. Lewis (consultant)
126. F. E. Low (consultant)
127. E. W. McDaniel (consultant)
128. M. R. C. McDowell (consultant)
129. H. Mott-Smith (consultant)
130. W. B. Pardo (consultant)
131. H. K. Reynolds (consultant)
132. H. S. Robertson (consultant)
133. D. J. Rose (consultant)
134. L. P. Smith (consultant)
135. H. S. Snyder (consultant)
136. P. M. Stier (consultant)
137. J. D. Trimmer (consultant)
138. C. H. Weaver (consultant)
139. J. D. Tillman (consultant)
140. Thermonuclear Library
141. Sherwood Reading File (V. Glidewell)
142. Biology Library
143. Health Physics Library
144. Reactor Division Library
145-147. Central Research Library
148-167. Laboratory Records Department
168. Laboratory Records, ORNL RC
169-170. ORNL – Y-12 Technical Library, Document Reference Section

EXTERNAL DISTRIBUTION

171. E. P. Gyftopoulos, Massachusetts Institute of Technology
172. S. C. Brown, Massachusetts Institute of Technology
173. M. B. Gottlieb, Princeton University
174. J. M. B. Kellogg, Los Alamos Scientific Laboratory
175. A. C. Kolb, Naval Research Laboratory
176. J. A. Phillips, Los Alamos Scientific Laboratory
177. R. F. Post, University of California, Lawrence Radiation Laboratory
178. Lyman Spitzer, Jr., Princeton University
179. E. Teller, University of California, Lawrence Radiation Laboratory
180. C. M. Van Atta, University of California, Lawrence Radiation Laboratory

181-182. Division of Research and Development, AEC, ORO (1 copy each to H. M. Roth and R. B. Martin)

183-184. Controlled Thermonuclear Branch, AEC, Washington, (1 copy each to A. E. Ruark and H. S. Morton)

185. Oak Ridge Operations Office

186-779. Given distribution as shown in TID-4500 (15th ed.) under Controlled Thermonuclear Processess category (75 copies – OTS)